

Report on Early-Age Cracking: Causes, Measurement, and Mitigation

Reported by ACI Committee 231



American Concrete Institute®



American Concrete Institute®
Advancing concrete knowledge

First Printing
January 2010

Report on Early-Age Cracking: Causes, Measurement, and Mitigation

Copyright by the American Concrete Institute, Farmington Hills, MI. All rights reserved. This material may not be reproduced or copied, in whole or part, in any printed, mechanical, electronic, film, or other distribution and storage media, without the written consent of ACI.

The technical committees responsible for ACI committee reports and standards strive to avoid ambiguities, omissions, and errors in these documents. In spite of these efforts, the users of ACI documents occasionally find information or requirements that may be subject to more than one interpretation or may be incomplete or incorrect. Users who have suggestions for the improvement of ACI documents are requested to contact ACI. Proper use of this document includes periodically checking for errata at www.concrete.org/committees/errata.asp for the most up-to-date revisions.

ACI committee documents are intended for the use of individuals who are competent to evaluate the significance and limitations of its content and recommendations and who will accept responsibility for the application of the material it contains. Individuals who use this publication in any way assume all risk and accept total responsibility for the application and use of this information.

All information in this publication is provided "as is" without warranty of any kind, either express or implied, including but not limited to, the implied warranties of merchantability, fitness for a particular purpose or non-infringement.

ACI and its members disclaim liability for damages of any kind, including any special, indirect, incidental, or consequential damages, including without limitation, lost revenues or lost profits, which may result from the use of this publication.

It is the responsibility of the user of this document to establish health and safety practices appropriate to the specific circumstances involved with its use. ACI does not make any representations with regard to health and safety issues and the use of this document. The user must determine the applicability of all regulatory limitations before applying the document and must comply with all applicable laws and regulations, including but not limited to, United States Occupational Safety and Health Administration (OSHA) health and safety standards.

Order information: ACI documents are available in print, by download, on CD-ROM, through electronic subscription, or reprint and may be obtained by contacting ACI.

Most ACI standards and committee reports are gathered together in the annually revised *ACI Manual of Concrete Practice* (MCP).

American Concrete Institute
38800 Country Club Drive
Farmington Hills, MI 48331
U.S.A.

Phone: **248-848-3700**
Fax: **248-848-3701**

www.concrete.org

Report on Early-Age Cracking: Causes, Measurement, and Mitigation

Reported by ACI Committee 231

Will Hansen
Chair

Anton K. Schindler
Secretary

Akthem A. Al-Manaseer
Emmanuel K. Attiogbe
Dale P. Bentz
Joseph J. Biernacki
Daniel Cusson
Matthew D. D'Ambrosia

Marwan A. Daye
Noel J. Gardner
Zachary C. Grasley
Allen J. Hulshizer
Elin A. Jensen

Mohamed Lachemi
Benjamin J. Mohr
Kamran M. Nemat
Jan Olek
Farro F. Radjy

Jussara Tanesi
Carlos C. Videla
Thomas Voight
W. Jason Weiss
Wayne M. Wilson

Early-age cracking is a challenge for the concrete industry. Materials selection, environmental conditions, and field practices all have considerable influence on the propensity for early-age cracking to occur. This document focuses on thermal- and moisture-related deformations; both are materials-related and contribute to early-age cracking. The document provides detailed reviews on the causes of deformation and cracking, test methods for assessing shrinkage and thermal deformation properties, and mitigation strategies for reducing early-age cracking.

Keywords: autogenous shrinkage; cracking; early-age; heat of hydration; measurement; microstructure; mitigation methods; shrinkage; shrinkage cracking; sustainability; thermal cracking; thermal properties.

ACI Committee Reports, Guides, Manuals, and Commentaries are intended for guidance in planning, designing, executing, and inspecting construction. This document is intended for the use of individuals who are competent to evaluate the significance and limitations of its content and recommendations and who will accept responsibility for the application of the material it contains. The American Concrete Institute disclaims any and all responsibility for the stated principles. The Institute shall not be liable for any loss or damage arising therefrom.

Reference to this document shall not be made in contract documents. If items found in this document are desired by the Architect/Engineer to be a part of the contract documents, they shall be restated in mandatory language for incorporation by the Architect/Engineer.

CONTENTS

Chapter 1—Introduction and scope, p. 231R-2

- 1.1—Introduction
- 1.2—Scope

Chapter 2—Notation and definitions, p. 231R-2

- 2.1—Notation
- 2.2—Definitions

Chapter 3—Causes of early-age deformation and cracking, p. 231R-3

- 3.1—Thermal deformation
- 3.2—Autogenous shrinkage
- 3.3—Drying shrinkage
- 3.4—Creep and stress relaxation from deformation restraint
- 3.5—Mitigation of shrinkage

Chapter 4—Test methods and assessment, p. 231R-10

- 4.1—Introduction
- 4.2—Shrinkage measurements
- 4.3—Ring test

ACI 231R-10 was adopted and published January 2010.
Copyright © 2010, American Concrete Institute.

All rights reserved including rights of reproduction and use in any form or by any means, including the making of copies by any photo process, or by electronic or mechanical device, printed, written, or oral, or recording for sound or visual reproduction or for use in any knowledge or retrieval system or device, unless permission in writing is obtained from the copyright proprietors.

- 4.4—Rigid cracking frames
- 4.5—Coefficient of thermal expansion (α_T) measurement
- 4.6—Analysis tools assessing stresses and cracking

Chapter 5—Shrinkage control, p. 231R-27

- 5.1—Introduction
- 5.2—Expansive additives
- 5.3—Shrinkage-reducing admixtures
- 5.4—Internal curing

Chapter 6—References, p. 231R-39

- 6.1—Referenced standards and reports
- 6.2—Cited references

CHAPTER 1—INTRODUCTION AND SCOPE

1.1—Introduction

ACI Committee 231 defines “early age” as the period after final setting, during which properties are changing rapidly. For a typical Type I portland-cement concrete moist cured at room temperature, this period is approximately 7 days. This document, however, includes discussions of early-age effects beyond 7 days. It is important to understand how concrete properties change with time during early ages and how different properties are interrelated, which may not be the same as for mature concrete. It is also important to understand how these early-age changes influence the properties of concrete at later ages. The temperature history at early ages has a strong effect on whether concrete may develop its potential strength. Poor early-age curing has been demonstrated to detrimentally affect the strength, serviceability, and durability.

Concrete structures change volume due to the thermal- and moisture-related changes. This may be detrimental because substantial stresses may develop when the concrete is restrained from moving freely. This is particularly important at early ages while the concrete has a low tensile strength. Therefore, the assessment and control of early-age cracking should be based on several factors, such as age-dependent material properties, thermal- and moisture-related stresses and strains, material viscoelastic behavior, restraints, and environmental exposure.

Temperature control in concrete during the early stages of hydration is essential for achieving early strength as well as ultimate strength and to eliminate or minimize uncontrolled cracking due to excessive mean peak temperature rise and thermal gradients (ACI 207.1R and 207.2R). Of particular importance in determining the risk of early-age cracking of any concrete member is an assessment of the magnitude of the stresses generated in the concrete as a result of restraint to thermally induced movement. In general, there are two types of restraint: external and internal. External restraints are caused by support conditions, contact with adjacent sections, applied load, reinforcement, and base friction in the case of concrete slabs-on-ground. Internal restraint is a manifestation of the residual stresses that develop as a result of nonlinear thermal and moisture gradients within a cross section.

New methods were developed and older methods rediscovered for evaluating stress and strain development and assessing

cracking risk in concrete mixtures under realistic exposure conditions. Categories of evaluation methods discussed in this document include restrained and unrestrained volume change tests, coefficient of thermal expansion tests, and tools for assessing stress development and cracking potential. Some of these evaluation methods have been standardized.

Mitigation methods have focused mainly on reducing the autogenous (moisture-related) component of the early-age stresses or compensating for the early-age shrinkage by employing expansive cement. In the former case, both shrinkage-reducing admixtures (SRAs) and internal curing have been demonstrated to reduce the magnitude of the early-age shrinkage of specimens cured under sealed, isothermal conditions.

The prevention or mitigation of early-age cracking will improve the long-term durability of concrete structures and, therefore, enhance their sustainability by increasing the service life.

1.2—Scope

This document reviews the causes of early-age deformation and cracking. The test methods for quantifying the early-age stress development and hence the risk of cracking due to thermal and moisture conditions are described. Mitigation methods for stress reduction are also discussed.

CHAPTER 2—NOTATION AND DEFINITIONS

2.1—Notation

C	= cement factor (content) for concrete mixture, lb/yd ³ (kg/m ³)
C_f	= correction factor accounting for the change in length of the measurement apparatus with temperature, $0.56 \times 10^{-6}/^{\circ}\text{F}$ ($1 \times 10^{-6}/^{\circ}\text{C}$)
CS	= chemical shrinkage of cement (mass of water/mass of cement)
D	= moisture diffusion coefficient of concrete
dT/dt	= temperature change
$d\varepsilon_{hygral}/dt$	= rate of nonthermal deformation due to autogenous shrinkage, drying shrinkage, or both
$E(t)$	= Young's modulus at time t , psi (MPa)
E_c	= creep-adjusted modulus of elasticity of concrete, psi (MPa)
$E_c(t)$	= age-dependent elastic modulus of concrete
E_{CON}	= elastic modulus of concrete
E_{steel}	= modulus of elasticity of steel ring, psi (MPa)
$erfc$	= complementary error function
f	= geometry function (Moon and Weiss 2006)
h	= humidity (0 to 1)
G	= coefficient relating stress to steel ring strain 10.44×10^6 psi (72.2 GPa) for the ASTM ring
\hat{K}	= stress amplification factor
K_r	= degree of restraint factor
L	= length
L_o	= measured length of specimen at room temperature, in. (mm)
M_{LWA}	= mass of (dry) fine lightweight aggregate needed per unit volume of concrete, lb/yd ³ (kg/m ³)
R	= degree of restraint

R'	= ideal gas constant [8.314 J/(mol·K)]
R_{IC}	= inner radius of concrete ring
R_{IS}	= inner radius of steel ring
R_{OC}	= outer radius of concrete ring
R_{OS}	= outer radius of steel ring
r	= radius
S	= degree of saturation of aggregate (0 to 1)
T_c	= average concrete temperature °F (°C)
T_{min}	= minimum concrete temperature on a cold night, °F (°C)
$T_{zero-stress}$	= concrete zero-stress temperature, °F (°C)
t_{CR}	= time to cracking
V_W	= molar volume of pore solution
α_{max}	= maximum expected degree of hydration of cement (0 to 1)
α_T	= coefficient of thermal expansion, strain/°F (strain/°C)
β	= coefficient relating shrinkage rate to shrinkage (0.056 day ⁻¹)
$\Delta\epsilon$	= strain increment from autogenous and drying shrinkage
ΔL_a	= actual length change of specimen during temperature change, in. (mm)
ΔL_m	= measured length change of specimen during temperature change, in. (mm) (increase = positive; decrease = negative)
ΔL_f	= length change of the measuring apparatus during temperature change, in. (mm)
ΔT	= measured temperature change (average of the four sensors) °F (°C) (increase = positive; decrease = negative)
$\Delta\sigma$	= stress increment, psi (MPa)
$\varepsilon_c(t)$	= creep strain
$\varepsilon_e(t)$	= elastic strain
$\varepsilon_{sh}(t)$	= free shrinkage strain
ε_{hygral}	= nonthermal deformation due to autogenous or drying shrinkage
ε_{SH}	= free shrinkage at time t
$\varepsilon_{SH-CONST}$	= shrinkage coefficient
ε_{ST}	= deformation of steel
ϕ_{LWA}	= desorption of lightweight aggregate from saturation down to 93% RH (mass water/mass dry lightweight aggregate)
$\phi(t)$	= creep coefficient at time t
γ	= surface tension
θ	= contact angle
v	= Poisson's ratio
v_c and v_s	= Poisson's ratio of concrete and steel
σ	= stress, psi (MPa)
$\sigma_{Elastic-Max}$	= theoretical maximum elastic stress
$\psi(t)$	= relaxation coefficient at time t
$\Omega(t)$	= aging coefficient to account for the reduced creep coefficient due to a gradually increasing load in restrained specimen; 0.6 to 0.9 for ordinary hardened concrete, and 0.9 to 1.0 for young concrete

2.2—Definitions

ACI provides a comprehensive list of definitions through an online resource, "ACI Concrete Terminology," <http://terminology.concrete.org>. Definitions provided herein complement that resource.

early age—the period after final setting, during which properties are changing rapidly. For a typical Type I portland-cement concrete moist cured at room temperature, this period is approximately 7 days.

CHAPTER 3—CAUSES OF EARLY-AGE DEFORMATION AND CRACKING

The two major driving forces for early-age volume change are the thermal deformation due to cement hydration and shrinkage deformation (autogenous shrinkage and drying shrinkage). The hydration reaction leads to a net reduction in the total volume of the hardened paste, which causes self-desiccation of pores and associated shrinkage. The incremental stress development in a hardening concrete structure with thermal and shrinkage deformations being considered is written as

$$\Delta\sigma = (\Delta T \cdot \alpha_T + \Delta\epsilon) \cdot E \cdot \psi \cdot R \quad (3-1)$$

3.1—Thermal deformation

Thermal deformation is a dimensional change resulting from a temperature change in concrete. Thermal deformation depends on the coefficient of thermal expansion (α_T), which is a function of the state of internal moisture. This was first experimentally identified in 1950 by Meyers (1950), later found by Zoldners (1971), and more recently validated by Bjontegaard (1999). Both Meyers and Zoldners found that, while the α_T at fully dried or saturated conditions was approximately the same, there was a dramatic increase in the α_T at intermediate relative humidities (RHs). Meyers hypothesized that in the intermediate RH range, there is additional dilation due to changes in the pore water pressure exerted on the solid skeleton. Powers and Brownyard (1947) noted that with changes in temperature, water expands and undergoes a reduction in surface tension. As the surface tension of water goes down, the negative pressure exerted on the pore system goes down (the pressure pushing the solid nanostructure apart increases), causing additional expansion with increases in temperature.

The development of thermal stresses due to a temperature rise for concrete flatwork may be calculated by the simplified expression presented in Eq. (3-2). The magnitude of the thermal stress is directly proportional to the magnitude of the temperature change to which the flatwork is exposed. For an accurate estimate of the thermal stress, creep effects during early ages and throughout the member's life should be accounted for in Eq. (3-2) (Emborg 1989)

$$\text{thermal stress} = \sigma_T = \Delta T \alpha_T E_c K_r \quad (3-2)$$

It is clear from Eq. (3-2) that the α_T of mixtures is an important factor affecting early-age thermal stress. During early ages, α_T changes very rapidly as the concrete gains

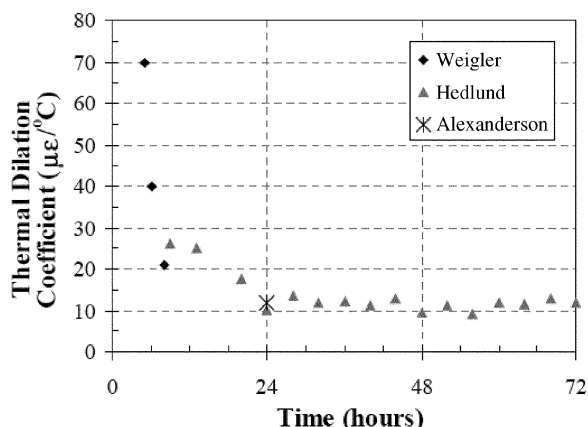


Fig. 3.1—Early-age thermal dilation coefficient for concrete (Hedlund 1996; Byfors 1980). (Note: 0.556 microstrain per °F is equivalent to one microstrain per °C.)

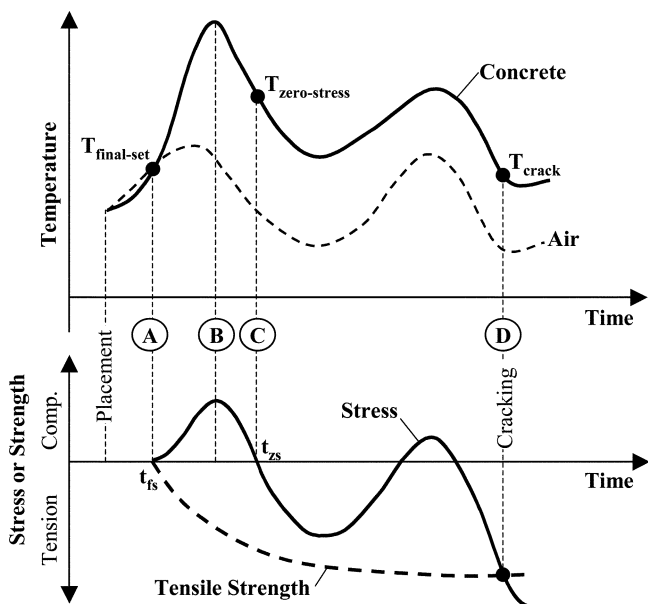


Fig. 3.2—Development of thermal stresses (Schindler and McCullough 2002).

strength. Research by Hedlund (1996) provided thermal dilation coefficients of concrete at early ages, as shown in Fig. 3.1. His test results are supplemented by those of Weigler and Alexanderson (Byfors 1980) that provide even higher values during the first hours. The thermal dilation coefficient reaches a plateau of approximately $6.7 \times 10^{-6}/^{\circ}\text{F}$ ($12 \times 10^{-6}/^{\circ}\text{C}$) after 24 hours. The α_T of hardened concrete depends both on the mixture proportions and its hygral state. There is a general agreement in the literature that the α_T of a given concrete depends strongly on the water content (Meyers 1950; Neville 1981). A fully saturated pore system and an empty (dried) pore system give lower α_T values, around 5.6 to $6.7 \times 10^{-6}/^{\circ}\text{F}$ (10 to $12 \times 10^{-6}/^{\circ}\text{C}$). A partially saturated pore system shows maximum values in the range of $13.9 \times 10^{-6}/^{\circ}\text{F}$ ($25 \times 10^{-6}/^{\circ}\text{C}$).

Figure 3.2 is a typical illustration of early-age temperature and stress development. For summer casting conditions, the

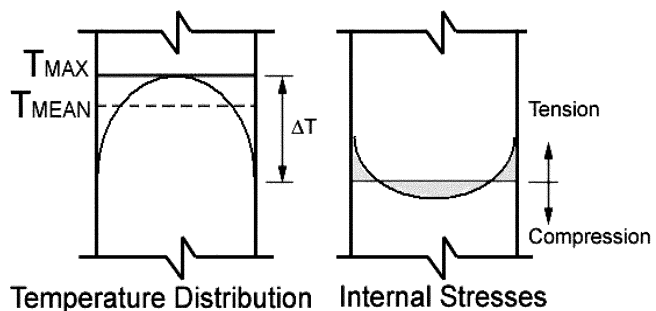


Fig. 3.3—Temperature profile and self-equilibrating stresses in symmetrical cross section at early ages (Emborg 1998).

concrete temperature increases beyond the setting temperature, Line (A). As the expansion of the concrete caused by this temperature rise is restrained, the concrete will be in compression when the peak temperature, Line (B), is reached. During this phase, the hydrating paste is still developing structure, the strength is low, and high amounts of early-age relaxation may occur when the concrete is subjected to high compressive forces (Emborg 1989). When a subsequent decline in concrete temperature starts to occur, the compressive stress will be relieved until the concrete temperature drops below the zero-stress temperature, where the stress condition changes from compression to tension (Line (C)). Due to the effects of relaxation, the zero-stress temperature may be significantly higher than the final-set temperature (Line (A)). If tensile stresses, caused by a further temperature drop, exceed the developing tensile strength of the concrete, cracking will occur (Line (D)).

The zero-stress temperature for the section placed under hot weather conditions (Fig. 3.2) is much higher than the section cast under normal paving temperatures. To improve the performance of concrete pavement placed throughout the year, sections constructed under high air temperature conditions require mitigation techniques to reduce heat development in the concrete (Schindler and McCullough 2002).

Large temperature gradients may develop if concrete surfaces are exposed to large thermal inputs that cannot dissipate quickly; hence, a rather large temperature difference may develop between the center and surface of the structure. Temperature gradients, typically a negative temperature gradient during the curing period, may produce cracks in the finished concrete structure due to the associated thermal strains. With the double-sided heating and cooling conditions seen in Fig. 3.3, the member should maintain a continuous and compatible displacement/strain field. This causes self-equilibrated internal stresses, known as residual stresses, to develop. If external restraint exists, forced thermal deformations create additional stresses.

The difference in surface and interior temperatures may be used to predict the risk of early-age thermal cracking. Based on a comprehensive experimental study, Freiesleben-Hansen and Pedersen (RILEM Committee 42-CEA 1981) suggest that the temperature difference between the middle and surface of a plain wall should be limited to approximately 68°F (20°C) to avoid thermally induced cracks. They found a systematic relationship between the magnitude of the

temperature difference and the occurrence of cracks. Similarly, in cases where a new concrete structure is restrained by a previously placed concrete section (external restraint), it has been suggested that the differentials between the average temperatures of the old and new placements should not exceed 54 to 59°F (12 to 15°C).

Temperature differences generally provide only a first estimate of the risk of thermal cracking. Pioneering work by Emborg (1998) demonstrated that the accuracy of thermal stress analysis depends not only on predicting the early-age temperature profiles, but also the development of concrete properties and degree of restraint. The effects of concrete mixture temperature and composition have a significant influence on thermal cracking.

3.1.1 Influence of placement temperature—As demonstrated previously, the cracking susceptibility of a concrete mixture is highly sensitive to the temperature of fresh concrete. The effect of fresh concrete temperature on cracking sensitivity is shown in Fig. 3.4 and, as expected, lowering the fresh concrete temperature allows the concrete to cool to a lower temperature before cracking initiates, thereby lowering the cracking temperature. These tests were conducted in a room with a temperature that matched the placement temperature using the measurement method described in detail in Chapter 4. Springenschmid and Breitenbücher (1998) found that lowering the fresh concrete temperature from 77 to 54°F (25 to 12°C) decreased the cracking temperature by 21.6 to 34.2°F (12 to 19°C). This vast reduction in cracking temperature may be attributed to a lower concrete setting temperature and an increase in the tensile strength of the hardening concrete (Springenschmid and Breitenbücher 1998).

Low placement temperatures reduce the heat of hydration, thereby reducing the zero-stress temperature. Lowering the zero-stress temperature decreases the subsequent temperature drop during cooling, which in turn reduces tensile stresses (Breitenbücher and Mangold 1994). Springenschmid and Breitenbücher (1998) stated that, as a general rule, increasing the fresh concrete temperature by 18°F (10°C) increases the cracking temperature by 23.4 to 27°F (13 to 15°C).

The increased tensile strength of the hardening concrete may be explained by the bonds formed between the hydration products (Springenschmid and Breitenbücher 1998). At low curing temperatures, the bond formed between the calcium silicate hydrate (C-S-H) gel is stronger than the bond formed at higher temperatures, thus resulting in an increase in tensile strength (Verbeck and Helmuth 1968).

3.1.2 Influence of concrete mixture compositions—To assess the cracking susceptibility of a concrete mixture, the various constituents used to produce the concrete should be investigated on an individual basis. To achieve this, Springenschmid and Breitenbücher (1998) employed an approach that used a standardized concrete mixture. Based on experience, RILEM Technical Committee 119 (1998) specified an appropriate mixture composition to use for a standard:

- Maximum aggregate size: 1.25 in. (32 mm);
- Cement content*: 573 lb/yd³ (340 kg/m³)

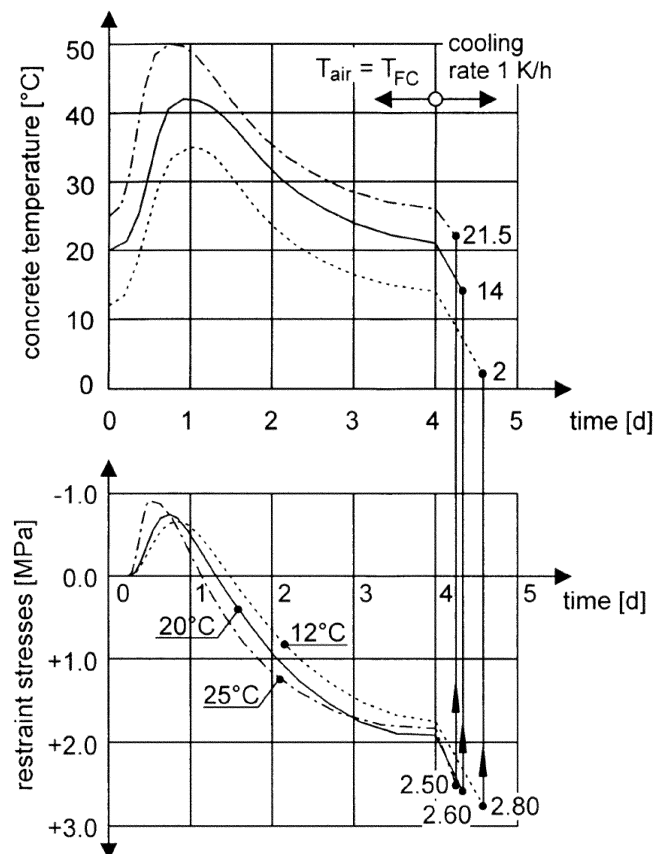


Fig. 3.4—Influence of fresh concrete temperature on cracking sensitivity (Springenschmid and Breitenbücher 1998). (Note: °F = 1.8 × °C + 32; 145 psi = 1 MPa.)

- Water content: 273 lb/yd³ (162 kg/m³)

*The cement content should be appropriately reduced when pozzolanic admixtures are used.

3.1.2.1 Aggregates—Concrete aggregates, especially coarse aggregates, have a substantial effect on cracking tendency. To determine an appropriate coarse aggregate for a given application, consideration should be given to the α_T as well as the aggregate roughness and size. Thermal deformations may be drastically reduced by using aggregates with a low α_T . Breitenbücher and Mangold (1994) reported that concretes composed of quartzite aggregates, which have a 50% higher α_T than limestone, generated approximately 50% higher stresses in the rigid cracking frame (refer to test description in Chapter 4). Although the concretes tested had almost identical temperature profiles, those produced with quartzite aggregates had a cracking temperature 10.8 to 16.2°F (6 to 9°C) higher than those produced with limestone aggregates (Breitenbücher and Mangold 1994).

In addition to their α_T , other thermophysical properties of the aggregates, such as density, heat capacity, and thermal conductivity also influence heat transfer within and through a concrete element and thermal stresses. Literature values indicate that the thermal conductivity of siliceous aggregates (Kim et al. 2003; Horai 1971) is in the range of 2.9 to 4.6 Btu/(ft·hr·°F) (5 to 8 W/(m·K)), approximately double that of the value of 1.7 Btu/(ft·hr·°F) (3 W/(m·K)) for limestone (Kim et al. 2003; Vosteen and Schellschmidt 2003). Conversely, the

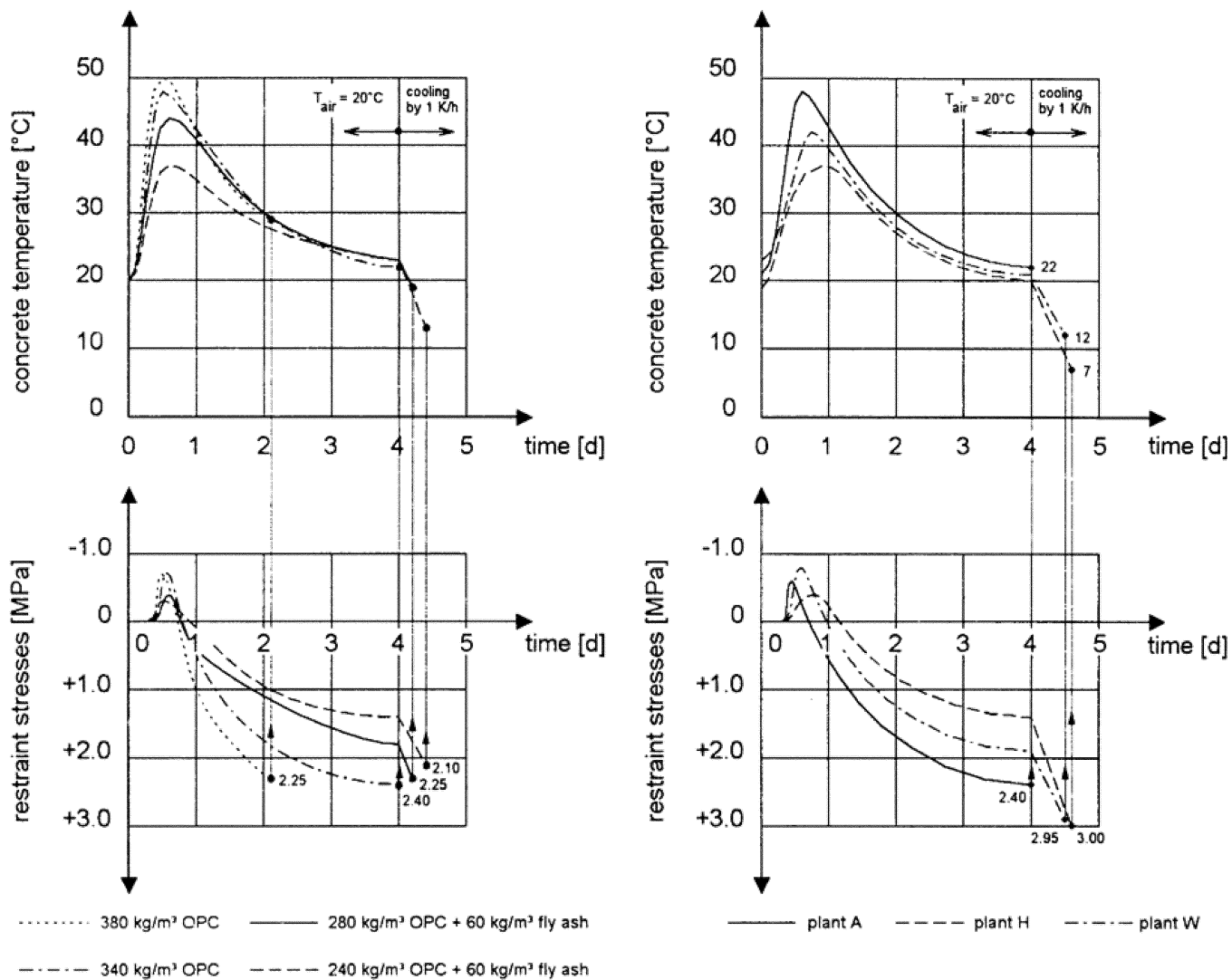


Fig. 3.5—Influence of cement content and cement sources on cracking sensitivity (Breitenbücher and Mangold 1994). (Note: $^{\circ}F = 1.8 \times ^{\circ}C + 32$; 145 psi = 1 MPa; $1.686 \text{ lb}/\text{yd}^3 = 1 \text{ kg}/\text{m}^3$.)

heat capacities of the two most common types of aggregates are similar, with limestone having a value of 0.2 Btu/(lb·°F) (0.84 J/(g·K)), and siliceous aggregates having a value of 0.18 Btu/(lb·°F) (0.75 J/(g·K)) (Waller et al. 1996).

Crushed aggregates with a rough surface are usually advantageous because the tensile strength of the concrete is increased. Furthermore, the use of larger aggregates tends to reduce the cracking susceptibility of a concrete mixture and reduces the amount of cement paste necessary for sufficient workability; lowering the amount of cement paste results in a lower heat of hydration. Larger coarse aggregates, however, tend to reduce the tensile strength of the concrete (Springenschmid and Breitenbücher 1998).

3.1.3 Cement types and sources—Portland cements obtained from different plants displayed very different cracking sensitivities in the rigid cracking frame, as shown in Fig. 3.5. The cements were all of the same specification type; however, each had different chemical compositions, fineness, or both (Springenschmid and Breitenbücher 1998). Tests on 17 concretes made with cements acquired from

different plants yielded cracking temperatures ranging from 43 to 72 °F (6 to 22 °C). Although temperature profiles of these concretes were different, the large range of cracking temperatures may only be partly attributed to the various temperature histories (Breitenbücher and Mangold 1994).

Springenschmid and Breitenbücher (1998) found that portland cements with a low alkali content (K_2O , Na_2O), a high sulfate content in relation to the C_3A content, and that are not too fine, lead to low cracking temperatures. These results indicate that higher sulfate contents (that is, higher additions of gypsum) could decrease the cracking temperature; however, this is true only for cements with low alkali content. In high-alkali cements, an increased sulfate content does not improve the cracking sensitivity (Breitenbücher and Mangold 1994).

3.1.3.1 Cement content and fly ash—The effect of cement content and fly ash on the cracking temperature is also shown in Fig. 3.5. In the normal range of water-cementitious material ratios ($0.4 \leq w/cm \leq 0.7$), the cracking temperatures decrease as the cement content decreases.

Breitenbürger and Mangold (1994) found that once the w/cm exceeds 0.7, the tensile strength of the concrete lowers, resulting in increased cracking temperatures.

To maintain sufficient workability, Breitenbürger and Mangold (1994) added fly ash when the cement content of the concrete was lower than 573 lb/yd³ (340 kg/m³). Breitenbürger and Mangold (1994) stated that during the testing period in the first 4 to 5 days, the fly ash itself did not significantly influence the cracking tendency of the concrete, and could be considered as an inert material. As shown in Fig. 3.5, the addition of fly ash as a replacement of portland cement may reduce the cracking temperature.

3.1.3.2 Slag cement—Slag cements are normally used as low-heat cements for mass concrete applications because they are effective in reducing the rate of heat development in the concrete (Breitenbürger 1990). In some concretes with slag cements, however, a higher cracking temperature was found than in concretes using ordinary portland cement (OPC) from a plant with the same clinker (Springenschmid et al. 1987). The increased cracking temperatures are related to the slow strength development of the slag concrete. Although slag cements are effective in reducing thermal deformations, the benefits are offset by the lack of tensile strength at early ages (Thomas and Mukherjee 1994).

3.1.3.3 Air-entraining admixtures—Air-entrained concrete has two important properties that affect cracking susceptibility. First, the ultimate tensile strain capacity of air-entrained concrete is approximately 20% higher than normal concrete (Springenschmid and Breitenbürger 1998). Second, air-entrained concretes have a lower modulus of elasticity, which in turn leads to lower restraint stresses. Breitenbürger and Mangold (1994) found that adding air-entraining agents (air content of approximately 3 to 6% by volume) reduced the cracking temperature by approximately 9°F (5°C).

3.2—Autogenous shrinkage

The internal volume reduction associated with the hydration reactions in a cementitious material is typically 1.66 to 1.94 in.³/lb (6 to 7 mL/100 g) of fully hydrated cement (Jensen and Hansen 1996). The basic reactions of cement clinker are well understood and generally defined in terms of four ideal clinker phases, namely, C₃S, C₂S, C₃A, and C₄AF. Each of these clinker minerals requires water for reaction, and results in a decreased volume of the reaction products. Chemical shrinkage is like a molecular-level volume change, and creates the underlying driving force for the occurrence of autogenous shrinkage that is the macroscopic bulk deformation of a closed, isothermal, cementitious material system not subjected to external forces.

Autogenous shrinkage has been shown to be equal to chemical shrinkage as long as the paste is liquid. Around the time of setting, however, a solid skeleton is formed that allows empty pores to form, and the resulting autogenous shrinkage becomes much smaller than the underlying chemical shrinkage. Figure 3.6 shows such behavior for a $w/cm = 0.3$ portland-cement paste mixture. The chemical and autogenous shrinkage are initially identical within the first 4 hours when

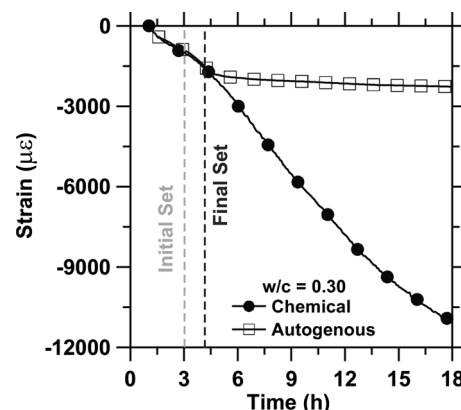


Fig. 3.6—Development of chemical shrinkage and autogenous shrinkage, $w/cm = 0.3$ (Sant et al. 2009).

the paste is in a liquid condition; thereafter, the autogenous shrinkage is substantially reduced due to the formation of a solid skeleton. The part of the autogenous shrinkage that occurs after setting is self-desiccation shrinkage. Autogenous shrinkage due to self-desiccation typically increases with decreasing w/cm . When external curing water is not readily available, self-desiccation will occur, and a set of empty pores will be created within the microstructure. This will produce capillary stresses that result in a measurable physical shrinkage of the material.

There is a general agreement on the existence of a relationship between autogenous shrinkage and relative humidity changes in the pores of the hardening cement paste (Lura 2003). Autogenous shrinkage may be thought of as a special class of drying shrinkage where the moisture is removed from the pore structure through internal chemical and physical reactions rather than external drying. The hydration reaction that occurs when portland cement comes in contact with water leads to an overall volume reduction such that the volume of the products is less than the volume of the reactants. Once percolation of the solid phase (initial setting) occurs, the volume reduction leads to the formation of vapor-filled porosity as water is further consumed in the hydration reaction. Moisture will tend to be consumed from larger pores first, followed by successively smaller pores. Unlike later-age drying that may occur from the outside of the specimen inward, internal drying occurs uniformly throughout the concrete microstructure.

3.2.1 Influence of water-cementitious material ratio—High-performance concrete (HPC) (relative to conventional concrete) and concrete with a low water-cementitious material ratio (w/cm) are expected to have increased autogenous shrinkage due to higher cement content, and the pozzolanic mineral admixtures that consume additional water in a reaction to form secondary C-S-H (Jensen and Hansen 1996). From linear measurements of autogenous shrinkage, a low w/cm produces higher autogenous shrinkage for both cement paste and concrete, as shown in Fig. 3.7. For concrete, autogenous shrinkage differences are pronounced within the first days, and a low w/cm gives high autogenous shrinkage. At the same time, autogenous expansions are observed in cement paste with w/cm above 0.4, resulting in lower net tensile stresses.

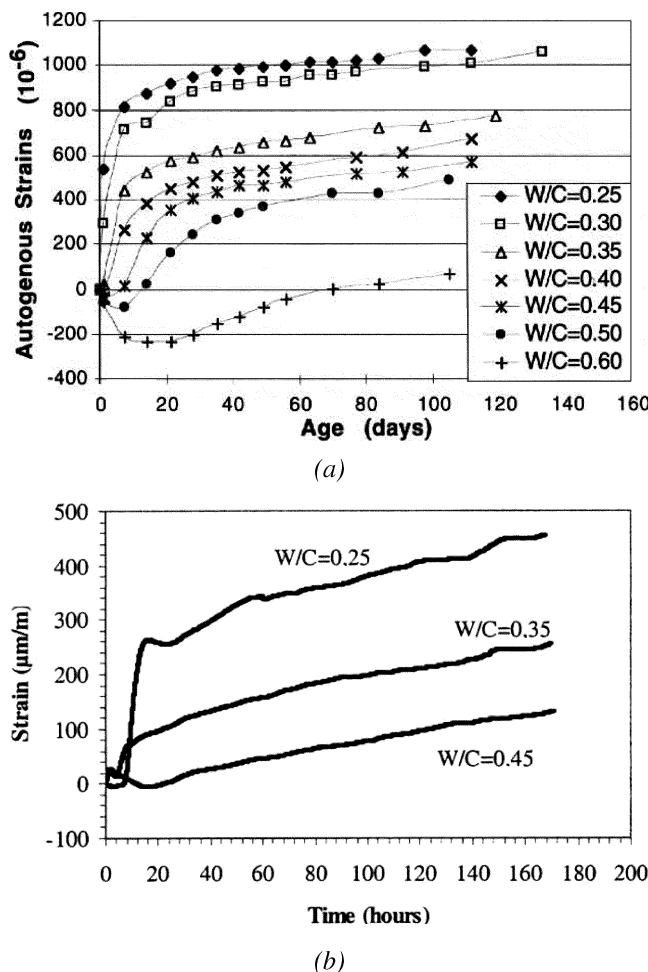


Fig. 3.7—Effect of w/cm on autogenous deformation (+ is shrinkage) in: (a) cement paste (Baroghel-Bouny 1996); and (b) concrete (Toma et al. 1999) (both with ordinary portland cement) during 68°F (20°C) isothermal tests. The measurements were started at the time of initial set in (a), and from $t = 0$ in. (b). (Note: $1 \times 10^{-6} \text{ in./in.} = 1 \mu\text{m/m.}$)

The correlation between w/cm and autogenous shrinkage may be explained by the self-desiccation process that dominates the autogenous shrinkage after the formation of a solid skeleton of the cement paste. The self-desiccation process is assumed to be based on a capillary tension mechanism such that a finer initial pore structure will generate a lower-equilibrium, internal RH and will create higher tension in the pore water. This is in agreement with experimental observations that have indicated autogenous shrinkage is increased by a reduction in w/cm , an increase in the fineness of the cement (Bentz et al. 2001a), or an addition of silica fume (Jensen and Hansen 1996).

3.2.2 Influence of aggregate—An increase in aggregate volume fraction (reduction in paste content) or an increase in maximum aggregate size will generally reduce autogenous shrinkage. Holt's experimental results show that paste has approximately 1.7 times greater shrinkage as compared with mortar (Holt 2002). Test results reported by Tazawa et al. (1995) also show that an increase in the aggregate content leads to a decrease of autogenous shrinkage.

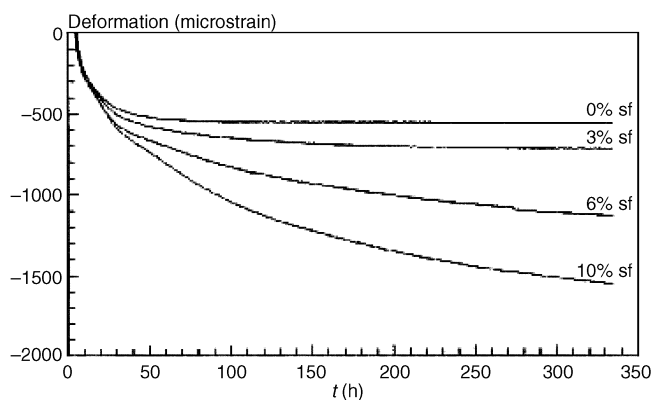


Fig. 3.8—Autogenous deformation after setting of cement pastes with $w/cm = 0.35$ and 0 to 10% silica fume addition: silica fume addition marked on curves; time measured from water addition; deformation fixed to 0 at time of setting, temperature 86°F (30°C) (Jensen and Hansen 1996).

3.2.3 Influence of supplementary cementitious materials

Supplementary cementing materials, such as fly ash, silica fume, and slag cement, are increasingly used for the production of low w/cm mixtures.

Jensen and Hansen (1996) measured the linear autogenous shrinkage of cement pastes containing 0 to 10% silica fume. All mixtures had a w/cm of 0.35. Their experiments indicated that the silica fume dosage has a dominating influence, as shown in Fig. 3.8. A 10% silica fume addition could increase the autogenous deformation after 2 weeks by 1000 microstrains. By way of comparison, a change of the w/cm from 0.40 to 0.25 for cement pastes containing 10% silica fume only increased the autogenous deformation after 2 weeks by approximately 200 microstrains. A mechanism was proposed by Jensen and Hansen (1996) to explain the considerable increase of autogenous shrinkage by the addition of silica fume. It is because of the disappearance of restraining components (silica fume, calcium hydroxide, or both), as the pozzolanic reaction of the silica fume involves a consumption of calcium hydroxide. The addition of silica fume may also lead to a finer pore structure of the cement paste, thereby increasing self-desiccation. Furthermore, the pozzolanic reaction increases the chemical shrinkage and, thus, the autogenous shrinkage of the blended cement. In concrete practice, silica fume addition has frequently been linked with cracking during hardening. This might be a consequence of the highly increased autogenous deformation due to silica fume additions.

Autogenous shrinkage depends both on the slag cement content and its fineness (Tazawa and Miyazawa 1995) (Fig. 3.9). Fly ash was found to have a variable influence in the literature. An investigation by Setter and Roy (1978) showed that fly ash has no significant effects on the autogenous shrinkage. In a study by Justnes et al. (1998), however, it was found that the addition of Class F fly ash significantly increases the autogenous shrinkage of cement paste. Note that this research was based on the measurement of chemical shrinkage.

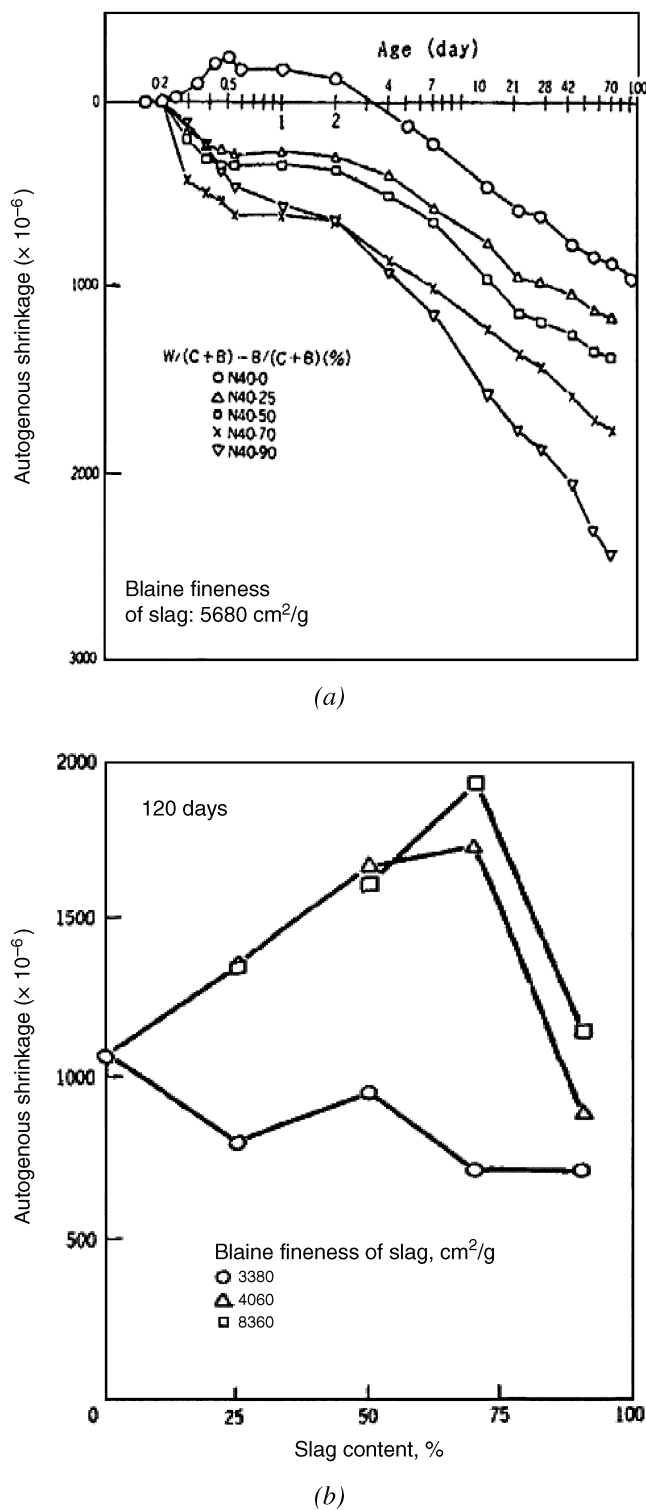


Fig. 3.9—(a) Influence of slag cement on autogenous shrinkage; and (b) influence of Blaine fineness of slag cement (Tazawa and Miyazawa 1995).

3.3—Drying shrinkage

Drying shrinkage may produce cracks in concrete if the shrinkage is restrained internally, externally, or both. As drying progresses from the concrete surface inward, pore humidity and the corresponding free drying shrinkage are generally distributed nonuniformly along the structure's

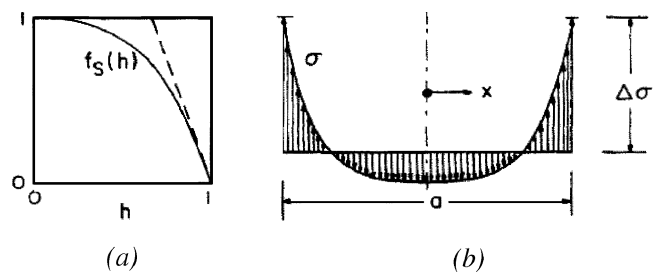


Fig. 3.10—(a) Variation of free shrinkage with RH h in pores; and (b) typical distribution of stresses throughout a wall (Bažant and Raftshol 1982).

thickness, with the largest strain at surface and decreasing as the distance from the free surface increases. Bažant and Panula (1978) established a function for determining the free drying shrinkage of a small element of concrete from the pore RH, as shown in Fig. 3.10(a). For the case of drying from both sides, the drying shrinkage stress is obtained through the consideration of internal restraint, and the strain should be uniform over the cross section. Bažant and Panula (1978) calculated the drying shrinkage stress by multiplying free drying shrinkage with an effective modulus that is Young's modulus E reduced to consider creep effects. Calculated shrinkage stress is illustrated in Fig. 3.10(b), which shows maximum tensile stress is reached at the drying surfaces. Many researchers found that peak tensile stress in the surface layer occurs in the beginning or during the first day of drying, and surface microcracking was observed in concrete and cement paste (Hwang and Young 1984; Higgins and Bailey 1976). Higgins and Bailey (1976) even observed microcracking in cement paste within 1 minute after exposure to drying.

The structural responses to drying may be different from other types of shrinkage deformations, such as autogenous shrinkage and thermal contraction, because drying often occurs differentially throughout the member thickness. For the case of a concrete slab resting on the ground, drying proceeds from the top surface only (humidity at the bottom is fairly constant due to contact with the ground) will cause a nonlinear distributed shrinkage profile along slab depth. Two visible deformations develop as a result of the differential shrinkage: 1) the axial movement, which is conventionally treated as drying shrinkage; and 2) warping. If restrained, these two deformations may cause axial stress and bending stress, respectively, as shown in Fig. 3.11. Another stress component is also generated during the drying, and is described as the residual stress that is due to the internal restraint from the surrounding small elements to satisfy translational symmetry in concrete cross sections.

3.4—Creep and stress relaxation from deformation restraint

Concrete undergoes time-dependent deformations during the application of internal or external stresses. Aggregate in concrete serves to restrain these deformations, which are a function of the volume of cement paste. The mechanisms of creep are not completely understood, as they depend on the composition and microstructure of cement hydration products.

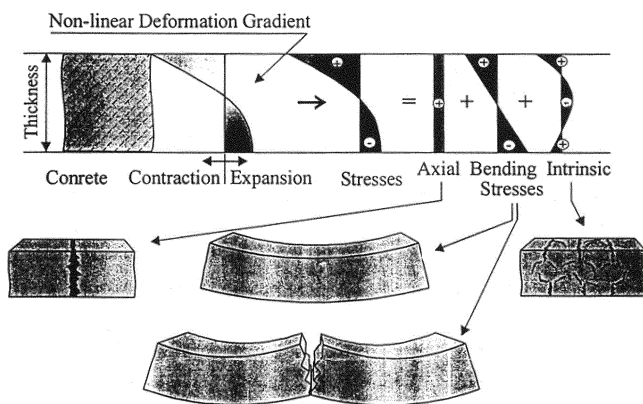


Fig. 3.11—Deformations and stresses caused by a nonlinear drying-shrinkage gradient (Springenschmid and Plannerer 2001).

Creep in concrete is the viscoelastic deformation of the porous cement hydration products due to applied stress. Several mechanisms are thought to be responsible for time-dependent deformation (ACI 209R; Acker 2004; Altoubat and Lange 2003):

- Redistribution of capillary water or interlayer water movement;
- Sliding or shearing of gel particles lubricated by adsorbed water (viscous flow);
- Sliding or shearing movement of the crystalline lattice (plastic flow);
- Diffusion of solid material; and
- Permanent plastic deformation caused by micro-cracking, recrystallization, or the formation of new physical bonds in the hydration products.

At early ages, creep may be viewed as a beneficial relaxation mechanism because it reduces tensile stress development that leads to cracking. In some instances, a reduced creep capacity could have a negative impact on a restrained structure in terms of cracking and durability. Creep deformation, however, leads to larger deflections in structural elements and loss of prestressing force, so it may be unfavorable for structural serviceability requirements.

Many of the same concrete properties that affect shrinkage also affect creep, such as internal moisture content, drying rate, and temperature. In fact, shrinkage of concrete may be analyzed as a viscoelastic response to internal stresses (Acker 2004; Grasley et al. 2006b; Lura et al. 2005). Creep is often divided into separate mechanisms for drying creep and basic creep. Basic creep occurs in sealed specimens; however, deformations at an early age may also be due to autogenous shrinkage (Altoubat 2000). Drying creep was first observed by Pickett, and is often referred to as the Pickett effect (Pickett 1942). Although several mechanisms for drying creep have been proposed, none are universally accepted (Neville 1981). The two components have been separated by experimental methods using superposition analysis (Kovler 1994; Altoubat 2000). Pickett observed that the creep deformation of a specimen loaded in compression during drying was greater than creep measured in a sealed specimen and shrinkage added together from separate

specimens. The Pickett effect, also referred to as stress-induced shrinkage, describes the additional creep not explained with superposition.

3.5—Mitigation of shrinkage

The simplest way of mitigating shrinkage is to reduce the cement paste content in concrete, because cement paste undergoes autogenous and drying shrinkage. Research by Bisschop (2002) indicates that the amount of drying shrinkage is approximately six to eight times smaller for concrete compared with cement paste. This mitigating method, however, may not be feasible as in cases where specific concrete properties are to be maintained. The advance of technology, therefore, has resulted in alternatives for mitigating shrinkage, such as adding chemical admixtures (SRAs) and incorporating internal curing agents (internal curing). These topics are covered in more detail in [Chapter 5](#).

CHAPTER 4—TEST METHODS AND ASSESSMENT

4.1—Introduction

Often, it is the superposition of shrinkage (autogenous plus drying shrinkage) and thermal stresses that, combined, lead to early-age cracking. As the two effects are difficult to separate experimentally for realistic size concrete replicas, their combined influence on a measurement is instead assessed in Chapter 4.

Several test methods have been proposed to assess the shrinkage cracking potential of concrete mixtures (Grzybowski and Shah 1990; Weiss and Shah 1997) including ring specimens (Carlson 1942; Shah et al. 1992; Bentur 2003; AASHTO 2004; ASTM C1581) and linear specimens (Paillere et al. 1989; Springenschmid et al. 1985; Kovler et al. 1993; Toma et al. 1999; Altoubat and Lange 2002). Ring tests evaluate the performance of concrete or mortar mixtures when they are restrained from shrinking freely. In the ring test, a concrete (or cement paste) annulus is cast around a steel ring. If unrestrained (that is, no steel ring), the concrete would shrink freely; however, the steel ring prevents (restrains) this movement, resulting in the development of tensile stresses. Due to its simplicity and economy, the ring test has been developed into both AASHTO (2004) and ASTM C1581. Linear specimens have the advantage of a relatively straightforward data interpretation; however, these test methods are generally not used for quality-control procedures, partially due to difficulties associated with providing sufficient end restraint (Weiss and Shah 1997; Altoubat and Lange 2002). Due to the complexity of a concrete member, finite element analysis becomes a useful tool for assessing the restraint stress development. A few commercially available finite element programs and their features are introduced in this chapter.

4.2—Shrinkage measurements

4.2.1 Drying shrinkage—Drying shrinkage is an unavoidable phenomenon when concrete members are exposed to the environment. As mentioned previously, uniaxial shrinkage and warping may be caused by a drying process in concrete.



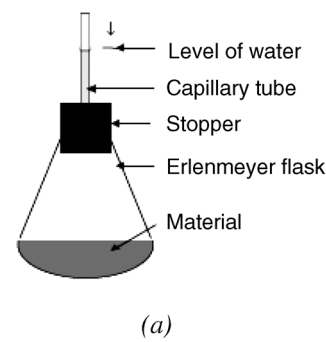
Fig. 4.1—Conventional shrinkage test (Springenschmid and Plannerer 2001).

Typically, only uniaxial drying shrinkage is measured to assess the potential effects of drying shrinkage.

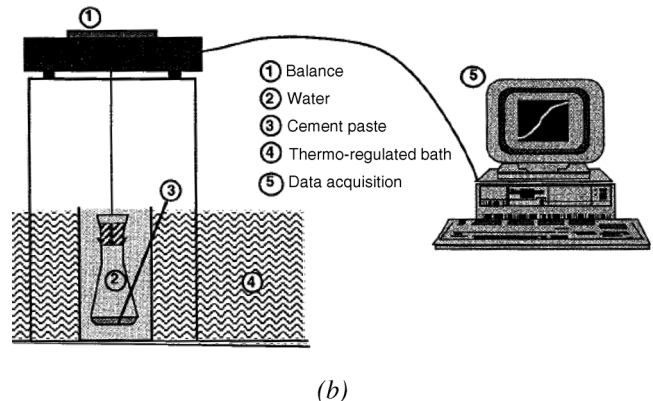
The uniaxial drying shrinkage is a time-dependent longitudinal contraction of a prismatic or cylindrical specimen under drying conditions (Springenschmid and Plannerer 2001) as shown in Fig. 4.1. The magnitude of uniaxial drying shrinkage depends on the size of concrete members because the drying process is limited to a surface region of a few centimeters thickness. A part of the drying shrinkage is irreversible. As concrete dries and then wet again, it will not fully resume its original dimensions (Neville 1981). The shrinkage strain of concrete that is dried for the first time is usually significantly greater than if the concrete is rewetted and dried again.

4.2.2 Autogenous shrinkage—As a result of cement hydration, chemical shrinkage is quantified through measurements of the volume contraction of paste in a glass beaker connected to a water-filled tube (LeChatelier 1904). There have been two methods used to directly measure chemical shrinkage: dilatometry and weighing reduced buoyancy. Both of these methods include an external water source in contact with the cement paste sample. The dilatometry test procedure follows LeChatelier's principle where an Erlenmeyer flask or small glass vial containing a cement paste sample is connected to a pipette in which the dropping water level is monitored (Fig. 4.2). It is a simple and commonly used test procedure (Tazawa 1999), but requires manual reading of the pipette. Typically a cement paste with a w/cm in the range of 0.4 is used. The technique was standardized as ASTM C1608. There is always the risk of faulty readings from the fit of the pipette through a rubber stopper in the top of the vial or flask.

The mass method (reduced buoyancy) is easier in the sense that it may be continuously measured and logged by a computer. It was developed based on Archimedes principle that a water-submerged sample will register a volume reduction by a mass increase. The mass of the submerged cement paste or mortar sample increases as the cement hydration proceeds. This method has been applied by many researchers, and is shown in Fig. 4.2 (Boivin et al. 1999; Geiker and Knudsen 1982; Paulini 1992). An excellent



(a)



(b)

Fig. 4.2—(a) Dilatometry test of chemical shrinkage; and (b) reduced buoyancy test arrangement.

correlation between the two chemical shrinkage measuring methods was shown in tests by Boivin et al. (1999).

The major difference between the environments used for chemical shrinkage and autogenous shrinkage measurements is that in chemical shrinkage, an external water source provides the additional water absorbed by the cementitious material. In an autogenous shrinkage test, the sample is sealed, and there is no moisture exchange between the sample and the environment.

Autogenous shrinkage may be measured in terms of either volume change or length change. Volumetric measurements are done by taking the mass of a submerged sample sealed in a thin rubber membrane, as shown in Fig. 4.3 (Bjontegaard 1999). The procedure consists of filling the rubber membrane with fresh cement paste or mortar and placing it in a rigid tube. This tube is then immersed in a temperature-controlled water bath and continuously rotated to avoid bleeding. The creation of empty spaces leads to a modification of the buoyancy, making it possible to obtain variations in volume of the sample by simple mass measurements (Justnes et al. 1996).

Reabsorption of the bleeding water, however, may be an important factor affecting the autogenous shrinkage measured using the volumetric method. The autogenous shrinkage of a static sample is always smaller than that of a rotated sample. This is caused by the reabsorption of the bleeding water, which significantly reduces the self-desiccation in the static sample. This effect increases with the increase of w/cm , as higher w/cm samples are more susceptible to bleeding. Even more importantly, it was found that the impermeable membranes commonly used are actually quite

permeable to water over the course of the testing period (Lura and Jensen 2005).

Linear measurements are usually carried out by placing the sample in a rigid mold with low friction. The length change of the cement paste is recorded by a displacement transducer at the end of the specimen (Fig. 4.4). There are, however, a few limitations in the linear measurements. For example, the geometry of the sample, the friction between the sample and mold, and the measurement might not be carried out before the sample has set.

Jensen and Hansen (1995) developed a method for measuring the autogenous shrinkage from the linear length change of the sample, as shown in Fig. 4.5. Cement paste or mortar may be cast into the sealed soft plastic tubes that are corrugated to minimize restraint on the paste. The tubes are 11.8 in. (300 mm) in length, and 1.18 in. (30 mm) in diameter. The techniques allow measurements to start 30 minutes after casting, and a transducer monitors the change in tube length over time. This corrugated mold transforms volumetric deformations into linear deformations when the paste is in a fluid state; the ratio between the length and volume change was found to be 2.15 in./fl oz (1.85 mm/mL). This measurement technique is being standardized within the ASTM C09-68 subcommittee on volume change.

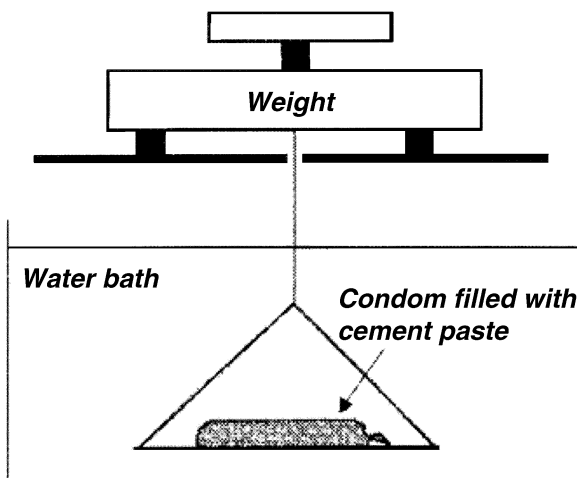


Fig. 4.3—Rubber membrane test for measuring autogenous shrinkage (Bjontegaard 1999).

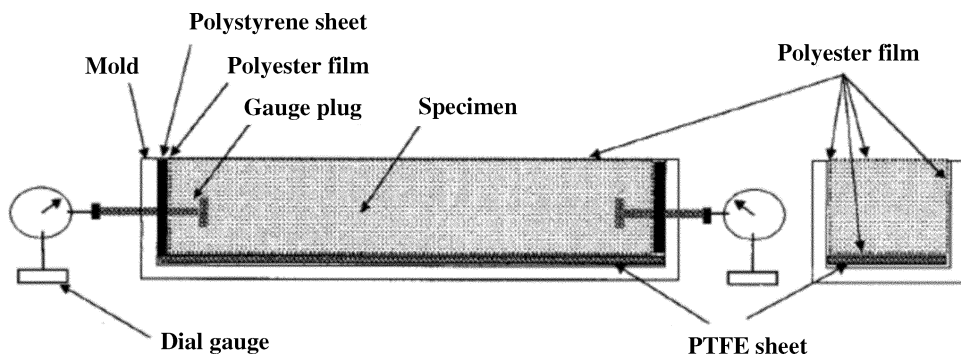


Fig. 4.4—Linear measurement of autogenous shrinkage (Tazawa 1999).

4.3—Ring test

The ring test is a practical tool for assessing time-of-cracking and cracking sensitivity in cementitious materials. The following sections provide an overview of the qualitative use of the restrained ring test, the use of the ring for quantitative analysis of stress development, and emerging developments that may account for materials that expand at early ages.

4.3.1 Quantitative restrained ring tests—The ring test has been used by many researchers over the last century. The most common use of the ring test is where the inner (steel) ring provides passive restraint (through its stiffness) to the concrete ring specimen. For example, Carlson (1942, 1988) and Coutinho (1959) used the ring test to assess the cracking of restrained concrete elements. Brewer and Burrows (1951) used a smaller ring geometry to assess cracking in the cement paste. Swamy and Stavarides (1979) and Krenchel and Shah (1987) used the ring test for fiber-reinforced materials. The restrained ring test has also been used to examine the influence of new materials (for example, SRAs) (Shah et al. 1992, 1998; Folliard and Berke 1997) and mixture proportions on the cracking potential of concrete (Krauss et al. 1996).

Grzybowski and Shah (1989, 1990) used a model to calculate the stresses that could be expected to develop in a ring specimen (assuming the tangential stress is uniform along the radius) and predicted the cracking potential using a damage-based model. Weiss (1999) and Weiss et al. (2000) computed the nonlinear stress distribution that develops in the ring and used a nonlinear fracture mechanics model to predict cracking for various ring geometries. Other researchers used the ring geometry with a more active inner core. Malhotra (1970) used a pressurized ring to determine tensile strength of concrete, Kovler et al. (1993) used an inner ring made of poly(methyl) methacrylate that expanded on heating, and Weiss (1999) used a pressurized inner ring to monitor creep. Figure 4.6 is a schematic illustration of the restraint stress distribution in typical ring tests for ring specimens that experience drying from top and sides, respectively.

4.3.2 Stress development—Over the last few decades, ring tests have been instrumented with strain gauges and used to quantify the stress development inside concrete. Figure 4.7 illustrates the geometry of the ring specimens, with the inner radius of the steel ring given as R_{IS} , the outer radius of the steel and the inner radius of the concrete ring given as $R_{OS} = R_{IC}$, and the outer radius of the concrete ring given as R_{OC} .

In general, strain is measured using four strain gauges mounted on the inner surface of the steel ring (that is, at R_{IS}) at midheight along the z-direction (however, a greater or lesser number of strain gauges may be used). The average strain measured on the inner surface of the steel ring, ε_{ST} , is used in the stress calculations. Figure 4.7(b) shows the

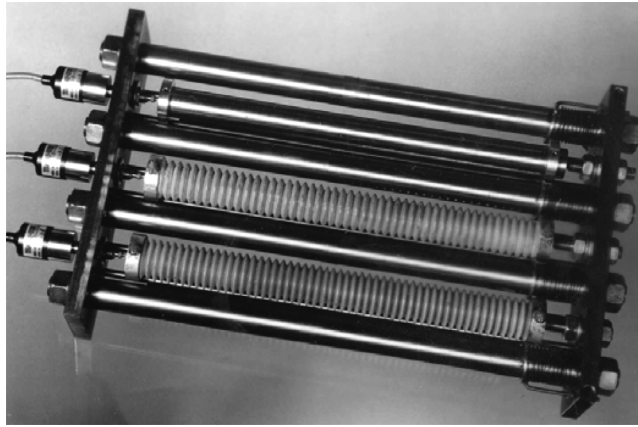


Fig. 4.5—Dilatometer with corrugated modulus for measurement of linear autogenous shrinkage of cement paste (Jensen and Hansen 1995).

geometry and dimensions of the ASTM C1581 ring setup. In this setup, two strain gauges are mounted on diametrically opposite inner surfaces of the steel ring. The specimens are dried from the outer circumference of the ring.

Swamy and Stavarides (1979) used the strain gauges to obtain an indication of the magnitude of the stress (average stress) that develops in the concrete (E_{Steel} is the elastic modulus of the steel ring)

$$\sigma|_{Ave} = -\varepsilon_{ST} \cdot E_{Steel} \cdot \frac{(R_{IC} - R_{IS})}{2(R_{OC} - R_{IC})} \left(1 + \frac{R_{IC}^2 - R_{OC}^2}{2R_{OC}} \right) \quad (4-1)$$

Equation (4-1) was derived assuming a linear stress distribution throughout the steel ring. Equilibrium concepts were then applied, setting the compressive force in the steel ring equal to the tensile force in the concrete ring. This enabled the determination of the average tensile stress in the concrete ring.

Attiogbe et al. (2001), See et al. (2003), and Weiss and Ferguson (2001) independently proposed solutions that use the strain measured in the steel ring to compute the maximum stresses in the concrete ring. Attiogbe et al. (2001) and See et al. (2003) considered a thin-wall approximation to

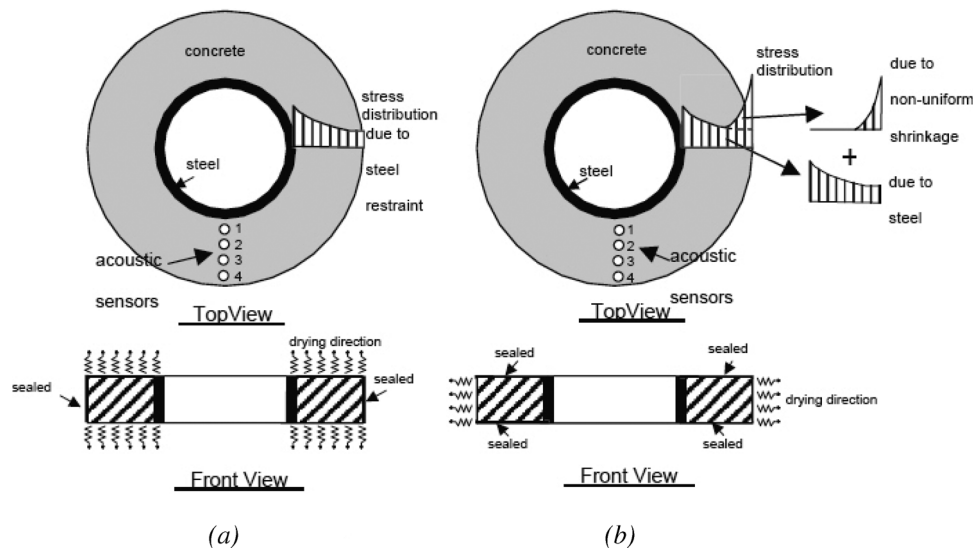


Fig. 4.6—Schematic illustration of restraint stresses generated in ring test (Weiss et al. 2000).

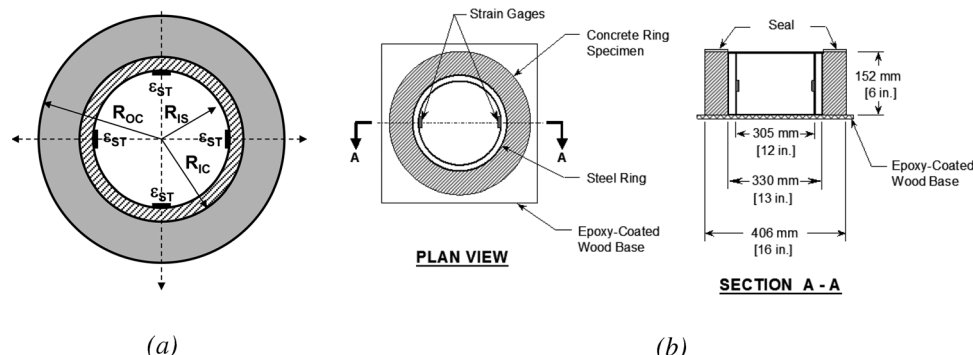


Fig. 4.7—(a) Ring geometry; and (b) ASTM C1581 ring setup.

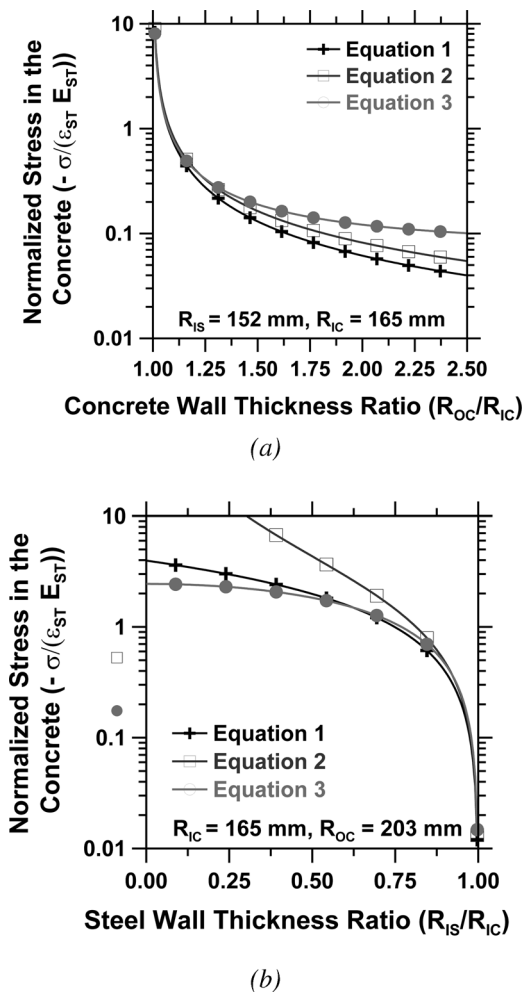


Fig. 4.8—Comparison of Eq. (4-1), (4-2), and (4-3): (a) varying concrete wall thickness; and (b) varying steel wall thickness (Attigobe et al. 2004). (Note: 1 in. = 25.4 mm.)

determine the maximum stress in the concrete ring using Eq. (4-2) (that is, circumferential stress for $r = R_{IC}$)

$$\sigma_{max}|_{r=R_{IC}} = -\varepsilon_{ST} \cdot E_{Steel} \cdot \frac{R_{IC} \cdot (R_{IC} - R_{IS})}{R_{IS} \cdot (R_{OC} - R_{IC})} \quad (4-2)$$

Weiss et al. (2001) and Hossain and Weiss (2004) performed a similar analysis using a thick-walled solution that resulted in Eq. (4-3) for the maximum tensile stress (that is, circumferential stress for $r = R_{IC}$)

$$\sigma_{max}|_{r=R_{IC}} = -\varepsilon_{ST} \cdot E_{Steel} \cdot \frac{R_{IC}^2 - R_{IS}^2(R_{OC}^2 + R_{IC}^2)}{2R_{IC}^2(R_{OC}^2 - R_{IC}^2)} \quad (4-3)$$

Weiss and Ferguson (2001) and Hossain and Weiss (2004) obtained Eq. (4-4a) and (4-4b) as general solutions to calculate the circumferential (σ_θ in Eq. (4-4a)) and radial (σ_r in Eq. (4-4b)) stresses in the concrete ring at a radius r . Equations (4-1) to (4-4) show that the stress is simply a product of the steel ring strain and a constant term G , which reflects steel stiffness and the geometry of the ring setup.

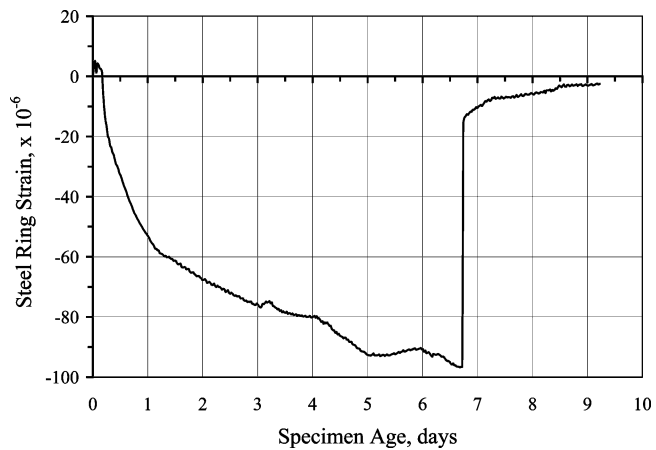


Fig. 4.9—Steel ring strain versus specimen age (Attigobe et al. 2003).

$$\sigma_\theta(r) = -\varepsilon_{ST} \cdot E_{Steel} \cdot \frac{R_{IC}^2 - R_{IS}^2}{2(R_{OC}^2 - R_{IC}^2)} \left(1 + \frac{R_{OC}^2}{r^2} \right) \quad (4-4a)$$

$$\sigma_r(r) = -\varepsilon_{ST} \cdot E_{Steel} \cdot \frac{R_{IC}^2 - R_{IS}^2}{2(R_{OC}^2 - R_{IC}^2)} \left(1 - \frac{R_{OC}^2}{r^2} \right) \quad (4-4b)$$

Attigobe et al. (2004) compared the results from Eq. (4-2) and (4-3) and observed good agreement for thinner rings, such as the ASTM C1581 ring, which are the geometries that are commonly used. The results, however, differ as R_{OC}/R_{IC} increases. Figure 4.8 shows a comparison of Eq. (4-1), (4-2), and (4-3) for specimens with geometries similar to the ASTM C1581 ring: $R_{IS} = 5.98$ in. (152 mm), $R_{IC} = 6.5$ in. (165 mm), and $R_{OC} = 7.99$ in. (203 mm). Both the AASHTO (2004) and ASTM C1581 rings have a similar R_{IS}/R_{IC} (0.92); however, the R_{OC}/R_{IC} is greater for the AASHTO ring (1.5) than the ASTM ring (1.23). It has been suggested that, for most practical geometries, R_{IS}/R_{IC} should be approximately 0.8 to 0.95 because thicker steel rings have difficulty in resolving strain measurements, and thinner rings may bend along the z-axis (Shah and Weiss 2006).

Typical steel ring strain versus time data, starting from the time after casting the test specimen, is shown in Fig. 4.9. The sudden decrease in compressive strain in the steel ring indicates the point of cracking. For the ASTM C1581 test, the steel ring strain data are converted to stress values over time using Eq. (3-2).

A plot of the stress rate versus time-to-cracking obtained from the ASTM ring setup for a broad range of test mixtures (concrete and mortar) is shown in Fig. 4.10 (Attigobe et al. 2003; See et al. 2004). Time-to-cracking is inversely related to the stress rate.

4.3.3 Quantifying effect of stress relaxation (creep) using ring—In addition to computing the actual stress level that develops inside the concrete ring (as described in the previous section), procedures were developed to assess the extent of creep or relaxation that occurs in the concrete ring. Hossain and Weiss (2004) formulated an equation for the

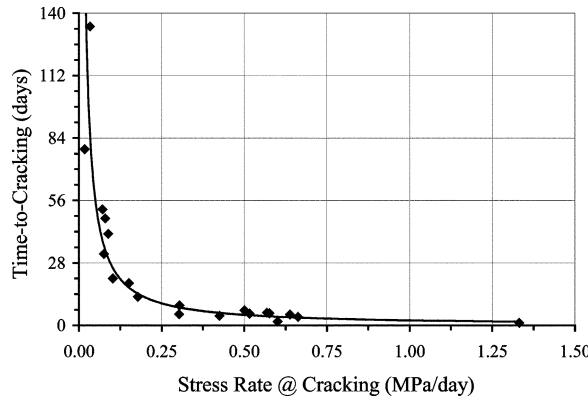


Fig. 4.10—Relationship between time-to-cracking and stress rate at cracking (Attiogbe et al. 2003). (Note: 145 psi = 1 MPa.)

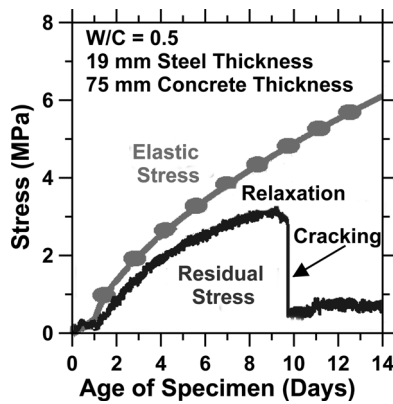


Fig. 4.11—Elastic stress and residual stress that develops in a concrete ring (Hossain and Weiss 2004). (Note: 145 psi = 1 MPa; w/c = w/cm.)

theoretical elastic stress that develops if creep (or relaxation) is not considered (Eq. (4-5))

$$\sigma_{Elastic-Max}(t) = \frac{\varepsilon_{SH}(t) \cdot E_C(t) \cdot \frac{[(1 - v_s)R_{IS}^2 + (1 - v_c)R_{IC}^2]}{(R_{IC}^2 - R_{IS}^2)}}{\frac{E_C(R_{OC}^2 + R_{IC}^2)}{E_s(R_{OC}^2 - R_{IS}^2)} + \frac{[(1 - v_c)R_{IC}^2 + (1 - v_s)R_{OC}^2]}{(R_{OC}^2 - R_{IS}^2)}} \quad (4-5)$$

where $\sigma_{Elastic-Max}$ is the theoretical maximum elastic stress; $\varepsilon_{SH}(t)$ is the free shrinkage at time t ; $E_C(t)$ is the age-dependant elastic modulus of concrete, and v_c and v_s are the Poisson's ratio of concrete and steel, respectively. The elastic stress from Eq. (4-5) may be compared with the actual stress from Eq. (4-2) or (4-3) to determine the magnitude of stress relaxation experienced by the material as shown in Fig. 4.11 (after Hossain and Weiss [2004]).

Attiogbe et al. (2001, 2003) and See et al. (2003) analyzed the case of a thin-walled ring, such as the ASTM C1581 ring, and formulated an equation to calculate tensile creep coefficients based on measured values of shrinkage and steel ring strain. The tensile creep coefficients under restrained shrinkage are smaller than the coefficients under constant stress (See et al. 2003). A similar result was reported by Kovler et al. (1999).

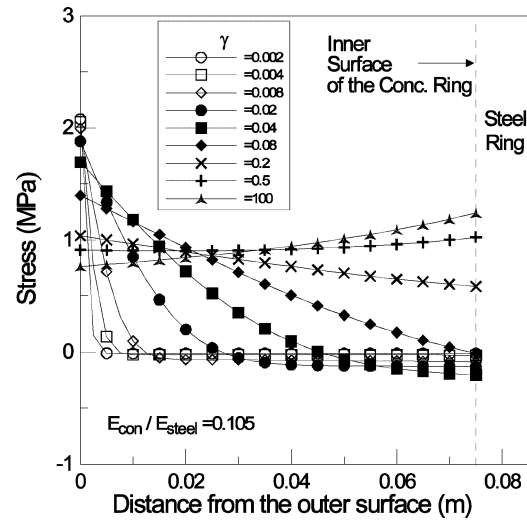


Fig. 4.12—Influence of moisture gradients on residual stress distribution (Attiogbe et al. 2004). (Note: 145 psi = 1 MPa; 39.37 in. = 1 m.)

4.3.4 Influence of moisture gradients—Weiss (1999), Weiss and Shah (2002), and Hossain and Weiss (2004) showed that the stress that develops in the ring depends on whether the ring dries from the top and bottom surfaces or from the outer circumference. While drying from the top and bottom may be described using Eq. (4-3), Moon et al. (2004) and Moon and Weiss (2006) showed that, in addition to the restraint from the steel, residual stress may develop due to circumferential drying because the concrete near the outer radius shrinks more rapidly than the inner concrete. The total stress development was expressed as the sum of the restraint that comes from the inner steel ring and the differential shrinkage in the concrete using Eq. (4-6)

$$\sigma_0(r, \gamma) = -\varepsilon_{steel}(t) \cdot E_s \cdot \frac{R_{OS}^2 - R_{IS}^2}{2(R_{OC}^2 - R_{OS}^2)} \left(1 + \frac{R_{OC}^2}{r^2} \right) + \frac{\varepsilon_{SH-const} \cdot E_{con}}{r^2} \quad (4-6)$$

$$\left[\frac{r^2 + R_{IC}^2}{R_{OC}^2 - R_{IS}^2} (f(R_{OC}) - f(R_{IC})) + f(r) - f(R_{IC}) - erfc\left(\frac{R_{OC} - r}{\gamma}\right) r^2 \right]$$

where $\varepsilon_{SH-const}$ is a shrinkage coefficient; f is a geometry function given in Moon and Weiss (2006); E_{con} is the elastic modulus of the concrete; $erfc$ is the complementary error function; and $\gamma = 2(Dt)^{0.5}$ when D is the moisture diffusion coefficient of concrete.

The impact of external drying may be seen in the simulation shown in Fig. 4.12 (Attiogbe et al. 2004). When drying is initiated (low values of γ), stresses develop along the outer circumference of the concrete ring. Over time (as γ increases), the stresses become better distributed throughout the concrete until the stress distribution matches the stresses predicted by Eq. (4-2) and (4-3) (when γ approaches 100).

An approximate analysis carried out by Attiogbe et al. (2004) indicated that the inverse relationship between stress rate and the time-to-cracking, as shown in Fig. 4.12, arises from moisture gradient effects because the concrete ring is

dried from the outer circumferential surface. Equation (4-7) shows that the average rate of residual stress is inversely proportional to the square root of time-to-cracking t_{cr} , where R is the degree of restraint, E'_C is the effective modulus of elasticity of concrete, ε_{shu} is the ultimate drying shrinkage of the concrete, D is the moisture diffusion coefficient, and K is a constant. Moisture gradient effects have been shown to control the fracture behavior by causing the crack to start on the outside of the ring (Hossain and Weiss 2004; Weiss and Shah 2002; Hossain et al. 2003)

$$\frac{d\sigma}{dt} \Big|_{AVE} = \left[\frac{1}{4} R E'_C \varepsilon_{shu} \frac{K \sqrt{D}}{(R_{OC} - R_{IC})} \right] \frac{1}{\sqrt{t_{cr}}} \quad (4-7)$$

4.3.5 Influence of degree of restraint R—The degree of restraint provided by the steel ring is important to consider in interpreting test results. Hossain and Weiss (2004) provided an expression for the degree of restraint. Moon and Weiss (2006) and Moon (2006) rewrote this expression in terms of free shrinkage of the concrete ε_{SH} and the measured steel strain ε_{ST} (Eq. (4-8a))

$$R = \left[1 - \frac{1}{2} \frac{\varepsilon_{ST}(t)}{\varepsilon_{SH}(t)} \left[\frac{R_{IS}^2}{R_{OS}^2} (1 + v_s) + (1 - v_s) \right] \right] 100\% \quad (4-8a)$$

For thin-walled rings, such as the ASTM C1581 ring, Eq. (4-8a) may be approximated by Eq. (4-8b), which was reported by Attiogbe et al. (2003) and See et al. (2004)

$$R = \left[1 - \frac{\varepsilon_{ST}(t)}{\varepsilon_{SH}(t)} \right] 100\% \quad (4-8b)$$

In the aforementioned equations, the strain in the steel is only known after the test is performed. To overcome this limitation, Moon et al. (2006) and Moon (2006) developed an approach (Eq. (4-9)) to estimate the degree of restraint before the test is performed so that the geometry of the ring may be properly tailored to match a particular field application of the concrete (E'_C is the effective elastic modulus of concrete)

$$R = 100\% - 100\% \frac{E'_C}{E_{ST}} \frac{1}{\left(\frac{E'_C}{E_{ST}} - \frac{1 - \left(\frac{R_{IS}^2}{R_{IC}^2} \right) \left[(1 + v_e) \left(\frac{R_{OC}^2}{R_{IC}^2} \right) + (1 - v_e) \right]}{1 - \left(\frac{R_{OC}^2}{R_{IC}^2} \right) \left[(1 + v_s) \left(\frac{R_{IS}^2}{R_{IC}^2} \right) + (1 - v_s) \right]} \right)} \quad (4-9)$$

4.3.6 Influence of specimen geometry and bond between the concrete and steel—Moon et al. (2004) and Moon (2006) used finite element analysis to assess the influence of specimen height (z-direction), steel ring thickness, and the appropriateness of the shrink fit solutions, while Hossain and Weiss (2006) studied these factors experimentally. Moon observed that very thin steel rings ($R_{IC} - R_{IS} = 0.12$ in. [3 mm]) may be susceptible to bending along the z-direction. More

realistically sized steel rings ($R_{IC} - R_{IS}$ of 0.35 in. [9 mm]), however, do not show substantial deformations along the z-direction. Moon (2006) and Moon et al. (2005) also demonstrated that the bond conditions between the steel and concrete need to be modeled properly.

In both experiments and simulations, only the transfer of compressive stresses is considered (that is, no tensile or shear stresses are transferred between the steel and concrete rings). In experiments, the surface of the steel ring is typically coated with a form-release agent or a plastic separation sheet to provide this unbonded boundary condition. The results of the finite element simulation compared well with the closed-form analytical simulations (Eq. (4-3) and (4-4)) (Moon et al. 2004, 2005; Moon 2006; Hossain and Weiss 2006). Other bond conditions provide additional restraint that does not represent the actual experimental conditions properly. Note that if other bond conditions are assumed between the ring and the concrete, they may result in stress distributions that do not accurately describe the stresses that develop in the ring. Specifically, if complete bonding is assumed, the tensile stresses that are calculated are too low on the inner surface of the ring.

4.3.7 Effect of variable concrete wall thickness (eccentricity)—A potential area where errors may arise in the interpretation of the ring test is if the wall thickness of the concrete ring is not uniform (Fig. 4.13(a)). Equation (4-3) may be modified to form Eq. (4-10), which illustrates the amplification that may be expected to occur due to the eccentricity of the inner ring using an approach that follows the derivation of Jeffery (1921) and Timoshenko and Goodier (1987)

$$\sigma_{max} \Big|_{r=R_{IC}} = -\varepsilon_{ST} \cdot E_{Steel} \cdot \frac{R_{IC}^2 - R_{IS}^2 (R_{OC}^2 + R_{IC}^2)}{2R_{IC}^2 (R_{OC}^2 - R_{IC}^2)} \hat{K} \quad (4-10)$$

where the stress amplification factor \hat{K} accounts for the eccentric placement of the inner steel ring that may be computed using Eq. (4-11) (e is the eccentricity shown in Fig. 4.13). Figure 4.8(b) shows that thinner-walled rings are more sensitive to eccentricity

$$\hat{K} = \frac{R_{OC}^2 - R_{IC}^2}{R_{OC}^2 + R_{IC}^2} \left[\frac{2R_{OC}^2 (R_{OC}^2 + R_{IC}^2 - 2R_{IC} \cdot e - e^2)}{(R_{OC}^2 + R_{IC}^2)(R_{OC}^2 - R_{IC}^2 - 2R_{IC} \cdot e - e^2)} - 1 \right] \quad (4-11)$$

4.3.8 Cracking potential classification—Four zones of performance were identified for the results of the ASTM C1581 test method (Attiogbe et al. 2003; See et al. 2004), as shown in Fig. 4.14. These zones are: 1) a zone of high potential for cracking with stress rates exceeding 50 psi/day (0.34 MPa/day) and cracking occurring within 7 days after initiation of drying; 2) a zone of moderate-high potential for cracking with stress rates between 25 and 50 psi/day (0.17 and 0.34 MPa/day) and cracking occurring between 7 and 14 days; 3) a zone of moderate-low potential for cracking with stress rates between 15 and 25 psi/day (0.10 and 0.17 MPa/day) and cracking occurring between 14 and 28 days; and 4) a zone of low potential for cracking with stress rates lower than 15 psi/day

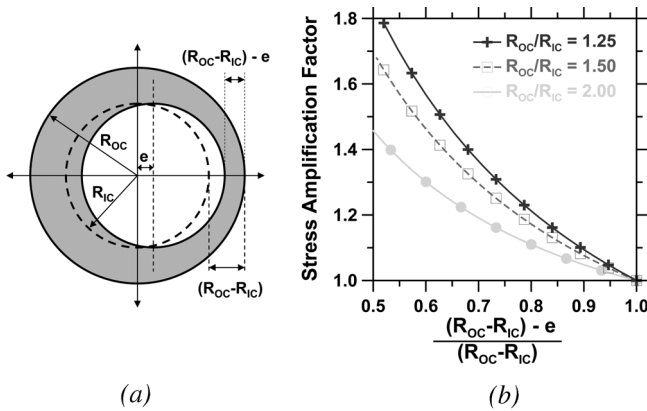


Fig. 4.13—(a) Eccentric ring geometry; and (b) effect of eccentricity on maximum stress (Attigbe et al. 2003).

(0.10 MPa/day) and either no cracking or cracking occurring beyond 28 days after initiation of drying. Materials that last beyond 14 days (moderate-low or low) have the potential for excellent resistance to cracking under restrained shrinkage.

4.3.9 Cracking potential envelopes—An analysis was performed by See et al. (2004) to develop cracking potential envelopes based on the stress rate versus time-to-cracking relationship and the zones of cracking potential shown in Fig. 4.15. The envelopes shown in Fig. 4.15 for modulus of elasticity and drying shrinkage values obtained at 7 days after initiation of drying provide a rapid means of determining the cracking potential of a given concrete mixture. For a given modulus of elasticity, these envelopes give the maximum drying shrinkage target at 7 days of drying so as not to exceed a given level of cracking potential, such as low or moderate-low potential for cracking. As stated previously, to minimize the probability of restrained cracking of concrete elements, the concrete mixture should have a low potential for cracking. The envelopes in Fig. 4.15 are obtained from Eq. (4-12)

$$\varepsilon_{sh} = \frac{\left(\frac{d\sigma_t}{dt}\right)_{limit}}{G\beta(1-R)} \quad (4-12)$$

where $(d\sigma_t/dt)_{limit}$ is the maximum value of stress rate at 7 days for a given zone of cracking potential (24.65, 40.6, or 59.5 psi/day [0.17, 0.28, or 0.41 MPa/day] for low, moderate-low, or moderate-high, respectively); G relates stress to steel ring strain and reflects the stiffness and geometry terms in Eq. (4-1) to (4-4) (10.44×10^6 psi [equal to 72.2 GPa] in Eq. (4-2) for the ASTM ring); β relates shrinkage rate to shrinkage (equal to 0.056 day^{-1}); and the degree of restraint R is a function of the modulus of elasticity of the concrete.

4.3.10 Developments for advancement of restrained ring analysis

4.3.10.1 Measurement variability—Experimental results are typically reported as average values of the time-to-cracking, strain in the steel, or residual stress; however, material variability may significantly alter the time of cracking. Monte Carlo simulations and statistical analysis have been used to assess the influence of material variability or specimen

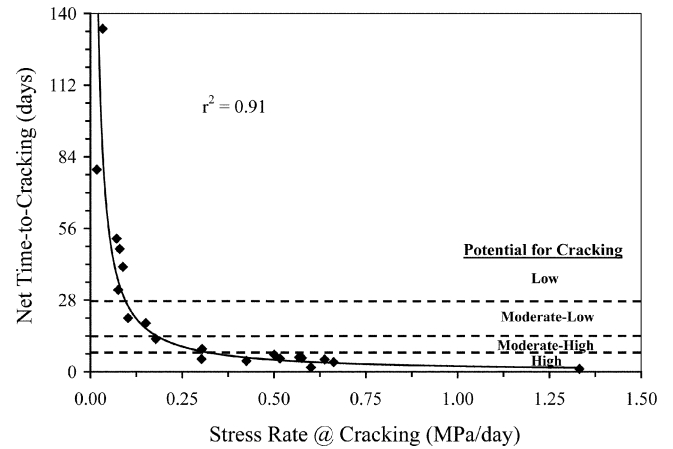


Fig. 4.14—Time-to-cracking versus stress rate and zones of cracking potential (See et al. 2004). (Note: 145 psi = 1 MPa.)

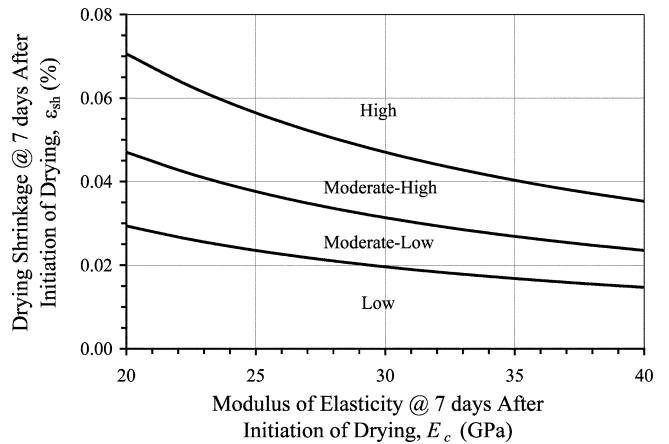


Fig. 4.15—Cracking potential envelopes (See et al. 2004). (Note: 145,038 psi = 1 GPa.)

geometry on cracking prediction (Radlinska et al. 2007). This work has been extended to the ring test to assess the anticipated confidence level for the results of restrained ring specimens. Further, ASTM developed a working group of North American laboratories that will perform a series of tests to determine the repeatability, precision, and bias of the ASTM C1581 restrained ring test.

4.3.10.2 Dual ring—One difficulty that may develop in using the restrained ring test is if the concrete expands. This may occur when an SRA is used (Pease et al. 2005) or when specific repair materials with expansive agents are used (Barde et al. 2006). When the concrete ring expands, it may come out of contact with the steel ring and, as a result, stresses will not be generated in the steel ring until the concrete shrinks back to its original position. This difficulty may be overcome by using a dual-ring approach with inner and outer restraining rings as shown in Fig. 4.16. The inner ring would behave similarly as in the previous ring tests; however, the outer ring would be used to restrain and quantify the expansion.

Preliminary tests were carried out by Moon et al. (2006) using a dual-ring apparatus with rings made of nickel steel

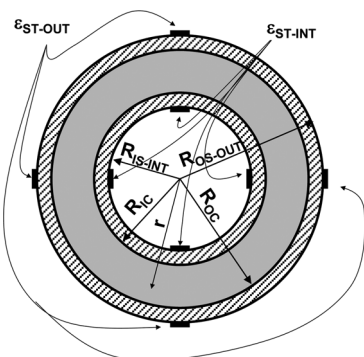


Fig. 4.16—Dual ring (Radlinska et al. 2006).

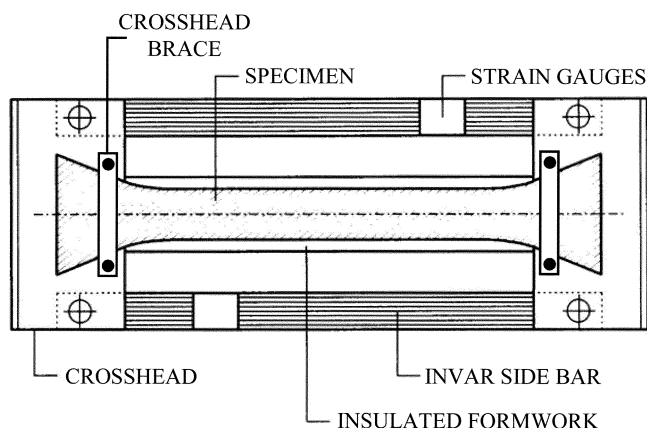


Fig. 4.17—Rigid cracking frame developed at Technical University of Munich (based on Mangold [1998]).

alloy (nickel steel alloy was chosen to minimize the effects of temperature change on the level of restraint that is provided). If the temperature of the nickel steel alloy and concrete are decreased, the nickel steel alloy will have negligible temperature-induced deformation, while the concrete will shrink. If the reduction in temperature that causes cracking is known, the residual strength of concrete may be computed. An approach was developed, and further research is ongoing, to determine the circumferential stresses in the concrete ring with the dual-ring setup.

4.3.11 Summary of developments on ring test—Developments on the restrained ring test have been reviewed. Although the ring test has been used for over a century, it has only recently been used in a more quantitative fashion. Equations (4-1) to (4-3) enable the strain that is measured in the steel ring to be used to compute the residual stress in the concrete. A solution for the elastic stress was developed (Eq. (4-5)). Subtracting the residual stress (Eq. (4-2) or (4-3)) from the elastic stress (Eq. (4-5)) provides a measure of creep or relaxation. Solutions were developed to account for moisture gradients (Eq. (4-6) and (4-7)). Cracking potential classifications were developed to characterize materials using the ASTM C1581 test method. Envelope curves were proposed for a rapid assessment of the potential for cracking under restrained drying shrinkage. Equations (4-8) and (4-9) may be used to quantify the degree of restraint provided by a ring of a

specific geometry. The effects of fiber reinforcement may be quantified in terms of the reduction in crack width that occurs and the stress that is transferred across the crack (Eq. (4-10)). Ongoing research is focused on areas for advancement. These areas include the use of a dual ring to capture early-age expansions, the quantification of variability in results from the ASTM C1581 ring test, and further development of procedures, such as cracking potential envelope curves, to facilitate assessment of the potential for restrained shrinkage cracking.

4.4—Rigid cracking frames

4.4.1 Test setup—The first generation of the uniaxial stress testing machine is a rigid cracking frame as shown in Fig. 4.17, which is composed of two mild-steel crossheads connected by two rigid nickel steel alloy side bars. For the rigid side bars to provide the proper restraint, it is critical that the concrete specimen be fixed at both ends. This is accomplished by placing the fresh concrete directly into the dovetails in each crosshead. The dovetails contain teeth that grip the concrete specimen. To ensure that the test specimen does not slip in the dovetails, crossbars are bolted on the top and bottom of each crosshead. The crossbars prevent the dovetails from opening during the tensile phase of a test, reducing any slippage deformations to a negligible value (Mangold 1998).

To minimize the effect a change in temperature would have on the length change of the restraining side bars, nickel steel alloy steel is used. Nickel steel alloy has a very low $\alpha_t = 0.55 \times 10^{-6}/^{\circ}\text{F}$ ($1.0 \times 10^{-6}/^{\circ}\text{C}$), compared with mild steel, $\alpha_t = 6.67 \times 10^{-6}/^{\circ}\text{F}$ ($12 \times 10^{-6}/^{\circ}\text{C}$). Each bar is equipped with strain gauges capable of measuring the very small axial strains produced by the combined effects of thermal and autogenous shrinkage (Breitenbücher 1990). In the central portion of the beam specimen, the stresses are uniaxial; therefore, a uniform stress distribution may be assumed. By assuming a uniform stress distribution, the measured strains in the nickel steel alloy side bars may be used to compute the corresponding stress development in the restrained concrete specimen (Mangold 1998).

To control the temperature of the test specimen, the cracking frame is equipped with thermally insulated formwork. The formwork is designed to insulate the test specimen, producing a heat of hydration approximately equal to that of a concrete element 19.7 in. (500 mm) thick (Breitenbücher 1990). Not only does the formwork provide a means to control the concrete temperature, it also allows restraint measurements to begin immediately after the fresh concrete has been placed.

Figure 4.18 displays the five stages that Breitenbücher (1990) used to describe the behavior of concrete in the rigid cracking frame. Stage I occurs immediately after placement of the concrete during which the temperature of the fresh concrete remains constant. Stage II begins with the onset of hydration and the corresponding heat development. During this stage, the concrete behaves plastically; therefore, no compressive stresses are produced. Stage III begins once the concrete specimen has achieved final setting. The concrete begins to gain strength and compressive stresses are developed

due to the increased temperature associated with the continued hydration of the concrete. The relatively high relaxation of the young concrete produces a maximum compressive stress that occurs a few hours before the concrete reaches its maximum temperature. During Stage IV, the concrete temperature begins to fall, and the remaining compressive stresses are rapidly reduced. The rapid reduction of compressive stresses is a result of an increased modulus of elasticity as well as the high relaxation of the young concrete. The specimen then reverts back to a stress-free state at a temperature well above the fresh concrete placement temperature and only a few degrees below the maximum. The concrete temperature corresponding to the stress-free state is referred to as the zero-stress temperature T_{zs} . In Stage V, the concrete temperature continues to decrease, producing tensile stresses. An increased modulus of elasticity and an increasingly smaller relaxation produce large tensile stresses. Finally, cracking occurs when the tensile stresses exceed the tensile strength of the concrete. The temperature of the concrete when cracking transpires is referred to as the cracking temperature T_{cr} .

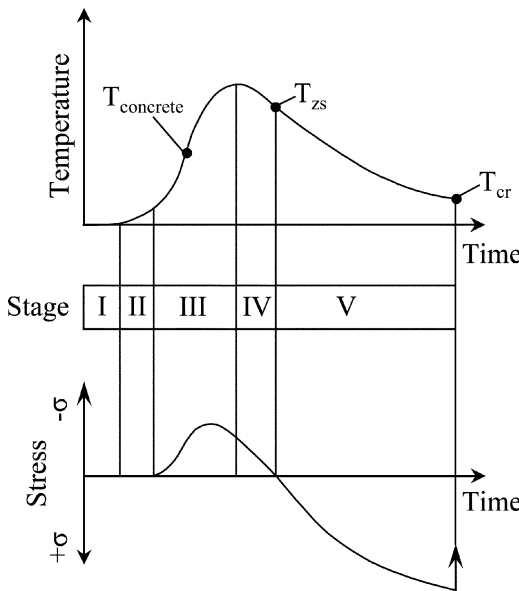


Fig. 4.18—Behavior of restrained specimens in rigid cracking frame (Breitenbücher 1990).

The rigid cracking frame (RCF) provides 100% restraint for fresh concrete and approximately 80% restraint for hardened concrete (Mangold 1998). Due to the inability to easily change the amount of restraint provided by the RCF, Mangold (1994) developed a model to compute the stress response at various restraint levels based on the stress response measured in the RCF. It has been reported that the stress responses computed with the model correlate well with results obtained from the temperature-stress testing machine (TSTM) (Springenschmid et al. 1994). If needed, therefore, the results from the RCF may be used to determine behavior at different restraint levels.

The RCF is a tool that may be used to directly measure restraint stresses and assess the cracking tendency of various concrete mixtures. The cracking temperature obtained from the RCF is a global indicator of all the factors that influence cracking under restrained conditions; the lower the cracking temperature, the lower the cracking sensitivity of a concrete mixture. Results from the RCF test may thus provide valuable insight toward the early-age behavior of concrete due to autogenous and thermal shrinkage (Burrows et al. 2004).

Using the same principle, Springenschmid and Adam (1980) and Springenschmid et al. (1985) developed a TSTM, as shown in Fig. 4.19, to measure the thermal- and shrinkage-induced stresses for the evaluation of the cracking risk of mass concrete and the influences of different contributing factors.

The TSTM is characterized by a fully automated closed-loop control as well as high accuracy of measurements, soft and regular loading. A temperature-stress testing machine was designed to make it possible to evaluate the effect of creep and stress relaxation in early-age concrete and to determine a variety of mechanical characteristics of concrete (Kovler 1994).

The TSTM uses an active control to control the strain in the specimen to the degree of restraint desired. When the concrete strain reaches a threshold value (usually 1 microstrain or smaller), a motor on the frame activates to load the specimen until the desired strain is again reached. A key point is that the concrete strain should be measured between points attached to the concrete, not between the two frame cross-heads. Otherwise, any slippage between the grip and the concrete specimen would then erroneously be recorded as

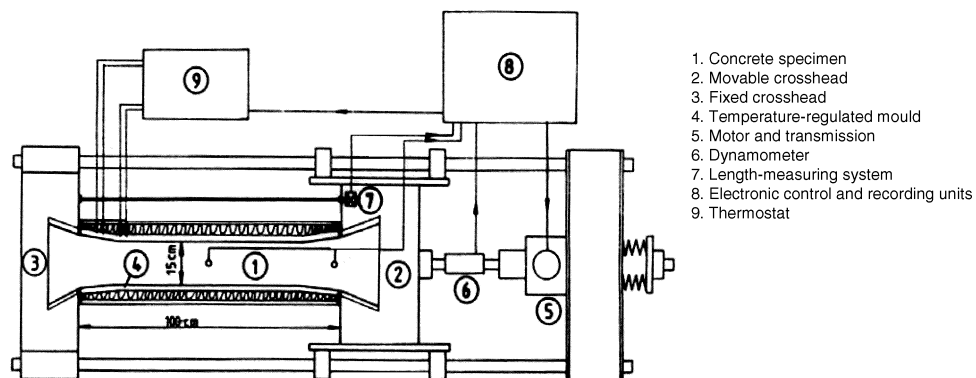


Fig. 4.19—Temperature-stress testing machine (Springenschmid and Adam 1980; Springenschmid et al. 1985).

strain in the concrete, producing less than the desired restraint. The stress in the concrete is measured using a load cell that is between the motor and the specimen (Mangold 1998). The temperature in the concrete is controlled using either tempered water that flows through pipes embedded in the formwork (Bjøntegaard 1999), or by heated air that is circulated around the sealed specimen (Westman 1999). In a TSTM specimen, therefore, it is possible to simulate a temperature profile occurred in a field structure of any thickness.

The TSTM is capable of assessing the total stress development in young concrete as a result of a complex interaction among growth of strength, development of thermal deformation, hygral deformation (autogenous shrinkage and drying shrinkage), and creep deformation. Under a fully restrained condition, the total strain at any time t should be zero. Hence, the measured restraint stress including the nonthermal effects may be defined by (Schoppe 1994)

$$\sigma(t)_{TSTM} = \int \left(\alpha_T \cdot \frac{dT}{dt} + \frac{d\epsilon_{hygral}}{dt} \right) E(t)(1 - \psi(t)) dt \quad (4-13)$$

where

- α_T = coefficient of thermal expansion;
- dT/dt = temperature change;
- $d\epsilon_{hygral}/dt$ = rate of nonthermal deformation due to autogenous shrinkage, drying shrinkage, or both;
- $E(t)$ = Young's modulus at time t ; and
- $\psi(t)$ = relaxation at time t .

It is, however, not exactly a creep or relaxation case as the stress develops gradually over time in the restrained concrete specimen. The creep in a restrained specimen therefore progresses more slowly than under a constant stress applied at the beginning of the test (Bažant 1972).

4.4.2 Thermal stresses—Development of thermal stress in hardening concrete may be determined using TSTM by casting in the temperature-controlled mold to realize prescribed thermal conditions.

It was demonstrated that a slag-based cement mixture is less susceptible to early-age thermal cracking than an ordinary portland cement (OPC) concrete mixture (Van Breugel et al. 2002). Figure 4.20 shows the temperature and stress development in these two concrete mixtures. The degree of restraint was 100% for all tests. The characteristic positions in the stress curve of BFS-cement concrete, such as maximum compressive stress or the change of stress from compression to tension, are shifted toward later times as compared with those for OPC concrete due to the slower reaction rates in BFS concrete. The OPC concrete cracked in the cooling phase at approximately 96 hours after casting, and no cracking was observed in BFS concrete until it was deliberately brought to failure after 120 hours.

Experimental results by Van Breugel et al. (2002) show that the w/cm affects both stress magnitude and the rate of stress development. As shown in Fig. 4.21, both compressive stress during the heating phase and tensile stress during the cooling phase are higher for a lower w/cm . The rate of stress

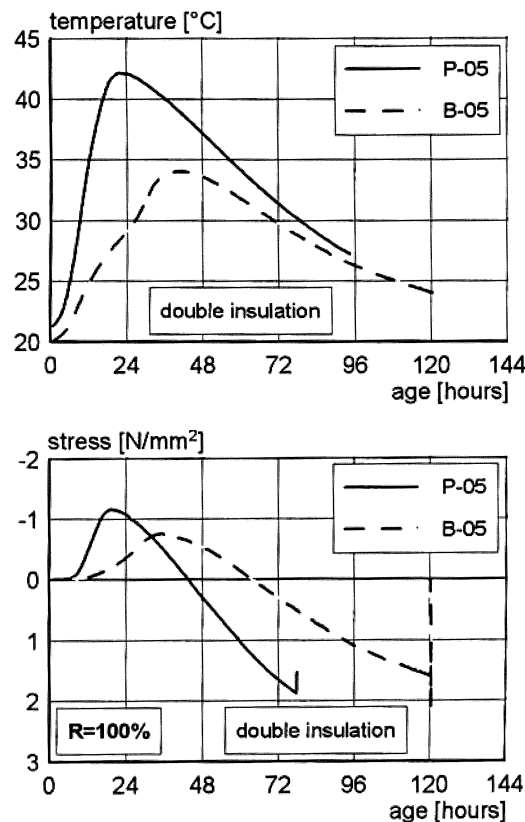


Fig. 4.20—Effect of cement types. (Note: $1^{\circ}\text{F} = 1.8 \times ^{\circ}\text{C} + 32$; $145 \text{ psi} = 1 \text{ N/mm}^2$.)

development is also higher in low w/cm concretes due to the fact that higher autogenous shrinkage and rapid growth of stiffness develop in these mixtures. As expected, cracking occurs earlier in the low w/cm mixtures.

4.4.3 Shrinkage deformation and stresses—Autogenous shrinkage may lead to, or at least contribute to, early-age cracking in concrete, which has been experimentally proven (Paillere et al. 1989; Bloom and Bentur 1995; Kovler 1994; Lura 2003). The development of autogenous shrinkage stress depends on factors such as autogenous strain development, degree of restraint, and the viscoelastic behavior of the material. As shown in Fig. 4.22, the development of self-induced stress follows closely with the autogenous shrinkage development, and the increase in stress of all three mixtures is roughly proportional to the autogenous shrinkage. Cracking occurs in the low w/cm mixtures of 0.26 and 0.3 after 4 and 15 days, respectively. Significant stress is generated in w/cm mixtures of 0.44 even though no cracking occurred.

By applying an isothermal temperature profile, the influence of nonthermal effects due to autogenous shrinkage may be estimated if the specimen is sealed curing during the test. To evaluate the stress development in a mass concrete member, a semi-adiabatic temperature condition, either determined by using a semi-adiabatic calorimeter or from a field measurement, should be used in the TSTM specimen.

Figure 4.23 shows measured restraint stresses due to semi-adiabatic and isothermal temperature conditions for the same mixture. It is clear that tensile stress generated during the cooling phase of a semi-adiabatic temperature condition is

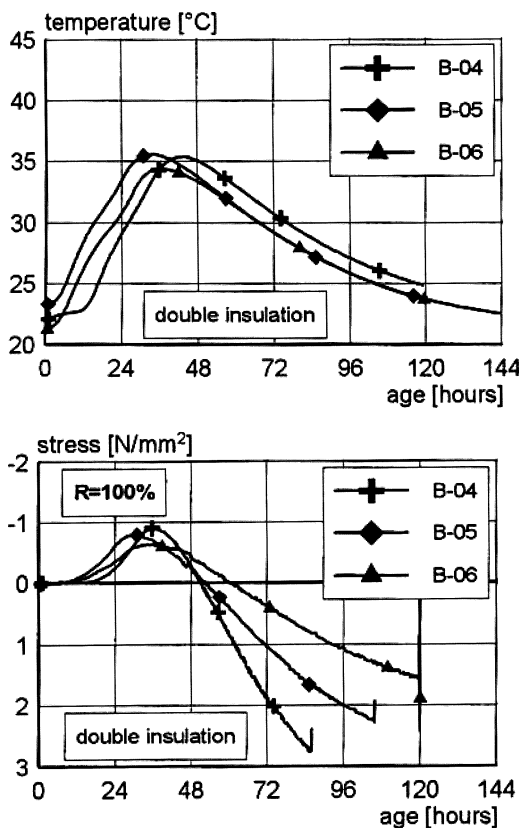


Fig. 4.21—Effect of w/cm. (Note: $1^{\circ}\text{F} = 1.8 \times ^{\circ}\text{C} + 32$; $145 \text{ psi} = 1 \text{ N/mm}^2$.)

substantially higher than that of an isothermal condition; the autogenous shrinkage deformation is much lower than the thermal contraction at early ages.

According to Toma et al. (1999), the level of tensile stress generated by self-desiccation in restrained normal portland cement concrete specimens increases as the w/cm decreases. This level was observed to be 36% of ultimate strength for a w/cm of 0.25, 29% for 0.35, and still quite significant at 23% for 0.45.

The autogenous shrinkage and the restraint stress developments at different temperatures are shown in Fig. 4.24 and 4.25 (Bjontegaard 1999). Note that the temperature has an unsystematic effect on the autogenous shrinkage development. The stress buildup at 41, 55, and 68°F (5, 13, and 20°C) is similar during the first 3 days, indicating a low E-modulus development in the low-temperature specimens. The high rate of autogenous shrinkage at 113°F (45°C) causes a rapid buildup of tensile stresses, and the specimen cracked after 1 week at approximately 363 psi (2.5 MPa). This low cracking stress indicates a reduced tensile strength due to the high curing temperature. For the 68°F (20°C) curing temperature, the specimen cracked at 450 psi (3.1 MPa) after 1 month. No cracking occurred in the 41 and 55°F (5 and 13°C) tests; instead, a stress reduction was observed in the 41°F (5°C) test due to the fact that no autogenous shrinkage develops after 3 days and the induced stress was relaxed.

4.4.4 Creep and stress relaxation—A temperature-stress testing machine may be used to quantify the effect of creep

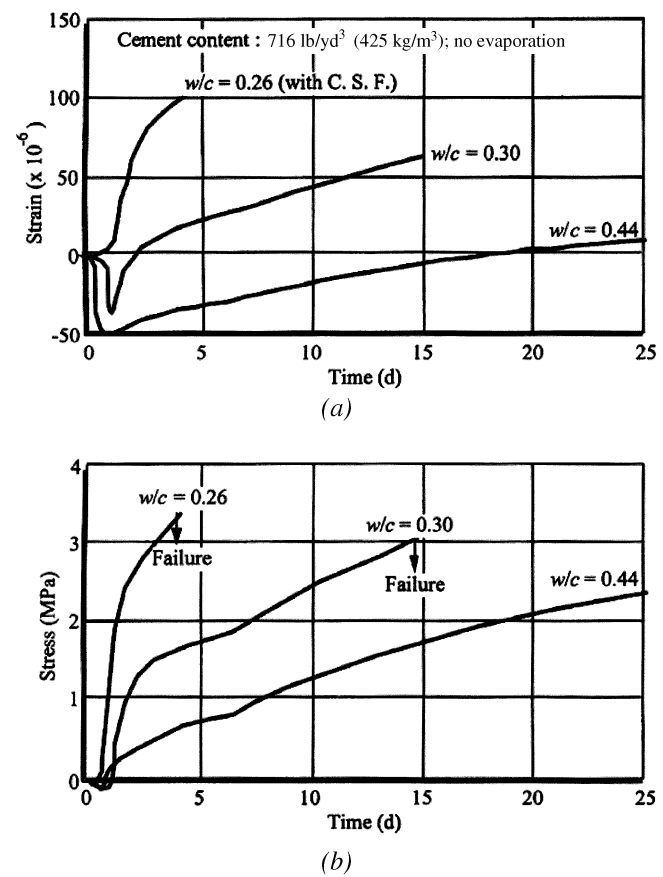


Fig. 4.22—Results of: (a) free; and (b) restrained shrinkage in the self-cracking test apparatus on different HPC mixtures (Pailiere et al. 1989). (Note: $^{\circ}\text{F} = 1.8 \times ^{\circ}\text{C} + 32$; $145 \text{ psi} = 1 \text{ N/mm}^2$; w/c = w/cm.)

and stress relaxation in an early-age concrete. The creep coefficient is obtained from deformation data on restrained and free-shrinkage twin specimens.

The test consists of a setup to measure the free autogenous shrinkage from the setting time, together with a TSTM with a movable head to determine the increase in load due to autogenous shrinkage starting from the same time. In both cases, the specimens are cast directly into the mold after mixing, and are then sealed using a special film. In the equipment with a movable head, the specimen is allowed to contract or expand freely until it reaches a threshold strain, at which time a load is applied to pull (or push) the specimen back to its original position. The load is then kept constant until the threshold strain is once again reached. The load is increased to once again to pull (or push) the specimen back to its original position. This procedure continues until the end of the test. Such a procedure allows the determination of the stress buildup in the specimen as well as creep deformation. The creep deformation is determined in the restrained shrinkage specimen by subtracting the cumulative sum of the strains in the restrained shrinkage specimen from the free shrinkage in the companion specimen (Kovler 1994; Toma et al. 1999).

Figure 4.26 demonstrates the method of creep strain calculation from a uniaxial shrinkage test conducted on restrained and free companion specimens (Kovler 1994). For the

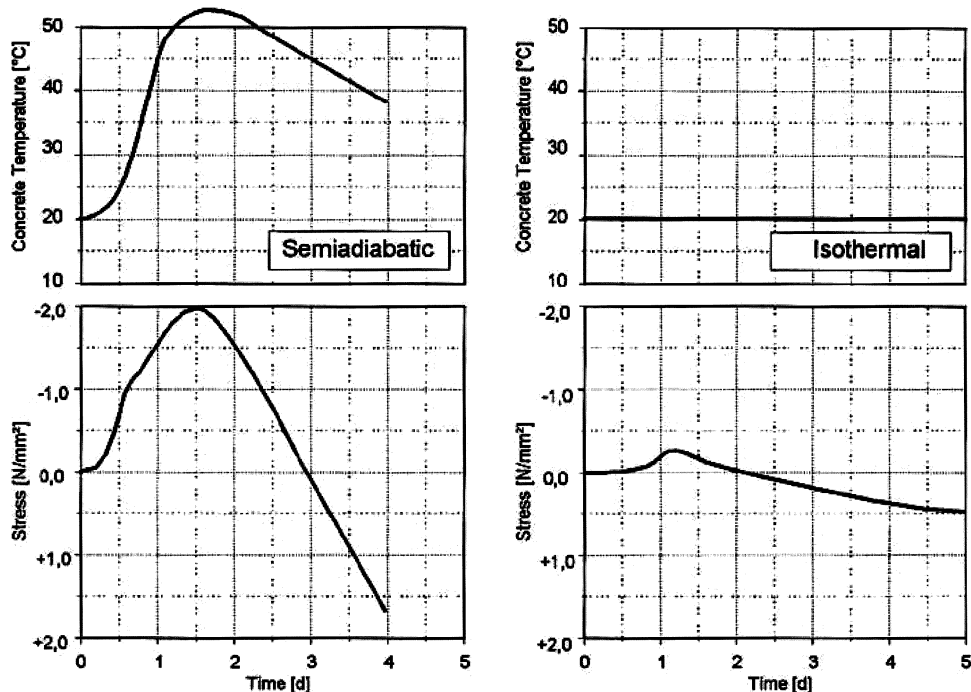


Fig. 4.23—Temperature-stress testing machine results under semiadiabatic and isothermal conditions for one concrete mixture (Schoppel 1994). (Note: $^{\circ}\text{F} = 1.8 \times ^{\circ}\text{C} + 32$; $145 \text{ psi} = 1 \text{ N/mm}^2$.)

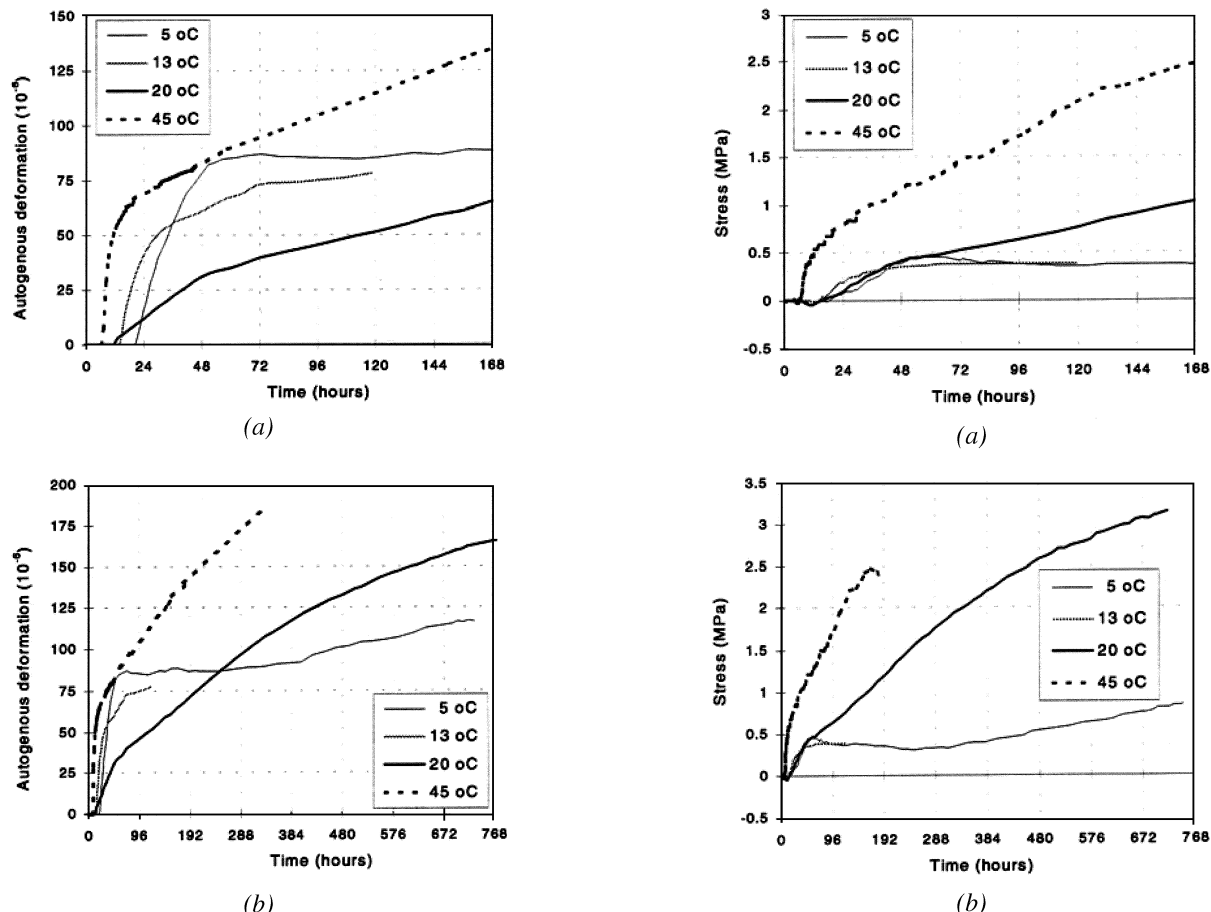


Fig. 4.24—Autogenous deformation during isothermal tests at different temperatures: (a) first week; and (b) up to 1 month (Bjontegaard 1999). (Note: $^{\circ}\text{F} = 1.8 \times ^{\circ}\text{C} + 32$.)

Fig. 4.25—Restraint stresses during isothermal tests at different temperatures: (a) first week; and (b) up to 1 month (Bjontegaard 1999). (Note: $^{\circ}\text{F} = 1.8 \times ^{\circ}\text{C} + 32$.)

restrained shrinkage test, a compensation cycle shown in Fig. 4.26 represents the process during which the motor will bring the specimen back to its original position if the strain exceeds the threshold value. Each compensation cycle consists of shrinkage and creep strain that is compensated by instantaneous elastic strain. Thus, the sum of elastic strains at any time is equal to the cumulative strain that is the sum of shrinkage and creep strain. Creep strain is easily obtained by subtracting cumulative strain from the free shrinkage measured from the companion specimen.

The creep strain is determined as (Kovler 1994)

$$\Omega(t)\phi(t) = \frac{\varepsilon_c(t)}{\varepsilon_e(t)} = \frac{\varepsilon_{sh}(t)}{\varepsilon_{sh}(t) + \varepsilon_c(t)} - 1 \quad (4-14)$$

where

- $\Omega(t)$ = aging coefficient to account for the reduced creep coefficient due to a gradually increasing load in restrained specimen; 0.6 to 0.9 for ordinary hardened concrete, 0.9 to 1.0 for young concrete;
- $\phi(t)$ = creep coefficient;
- $\varepsilon_c(t)$ = creep strain;
- $\varepsilon_e(t)$ = elastic strain; and
- $\varepsilon_{sh}(t)$ = free shrinkage strain.

It was observed that stress relaxation has a very significant influence on the stress development in a restrained specimen (Springenschmid et al. 1994; Kovler 1994; Toma et al. 1999). Calculations indicate the stress measured in the 0.25 w/cm concrete was 32% of that observed in a purely elastic material, that is, with no relaxation capacity (Toma et al. 1999). The stress relaxation may be calculated on the basis of the stress that would be generated if there was no creep. As may be seen in Fig. 4.27, the relaxation phenomenon is more significant for the 0.35 w/cm concrete (363 psi [2.5 MPa] at 7 days) and particularly for the 0.25 w/cm mixture (479 psi [3.3 MPa] at 7 days). The calculation is based on the assumption that restrained shrinkage has not damaged the material and that the elastic modulus is determined on a nonrestrained specimen. The result indicates that relaxation should be considered in assessing the risk of early-age cracking (Toma et al. 1999).

4.4.5 Degree of restraint—Schoppe (1994) stated that when using a variable degree of restraint in the TSTM, the stresses generated in concrete specimens may be determined realistically. The restraint strain is defined as free strain minus measured strain of the restrained specimen. The degree of restraint is determined as the ratio of restraint strain over the free strain, as shown in Fig. 4.28. For instance, the degree of restraint of 0.3 represents such a case that 30% of the free strain is restrained and only 70% of the free strain is allowed to develop. In TSTM testing, the degree of restraint may be set arbitrarily from free deformation (degree of restraint = 0) to fully restraint (degree of restraint = 1) condition by presetting threshold strain at which the actuator will be placed back to its original position (Mizobuchi et al. 2000).

The development of autogenous shrinkage stress may be affected considerably by the restraint level. Figure 4.29

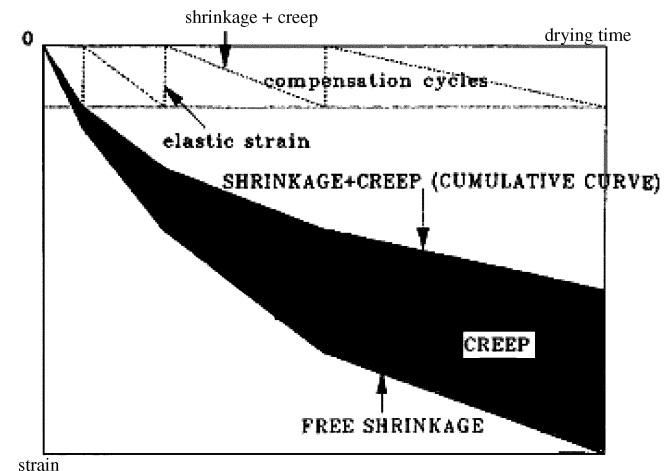


Fig. 4.26—Creep strain calculated from data of restrained and free shrinkage tests (Kovler 1994).

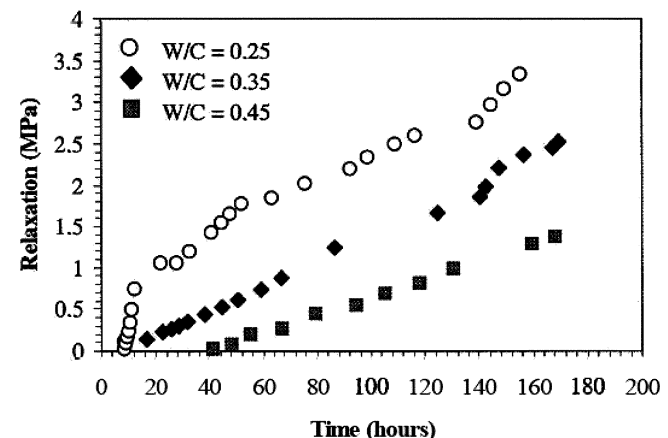


Fig. 4.27—Relaxation in fully restrained concrete shrinkage test (Toma et al. 1999). (Note: 145 psi = 1 MPa; w/c = w/cm.)

shows the temperature history and corresponding stress development in TSTM specimens when the degree of restraint was varied from 0.2 to 1.0 for the same mixture (Mizobuchi et al. 2000). Cracking occurred in the specimen with a degree of restraint of 1.0 at the age of 4 days, where it was still in the cooling phase. No cracking, however, was observed at a lower degree of restraint levels (0.5 and 0.2) during the entire testing period. The stresses at the end of testing were 247 psi (1.7 MPa) for 0.5 restraint level and 94 psi (0.65 MPa) for 0.2 restraint level.

4.4.6 Summary of cracking frame test—The cracking frame and TSTM are useful tools for studying the mechanical behavior of young concrete subjected to uniaxial free or restrained shrinkage. Through the test on companion specimens under free and restrained conditions, mechanical characteristics of early-age concrete such as free shrinkage, creep strain, restrained shrinkage stress, creep coefficient, and tensile strength may be determined. The measuring method of self-induced stress is independent of specimen geometry and restraint conditions. In addition to quantifying restrained shrinkage stresses, it may be used for the determination of stress-strain relationships and modulus of elasticity (Kovler 1994).

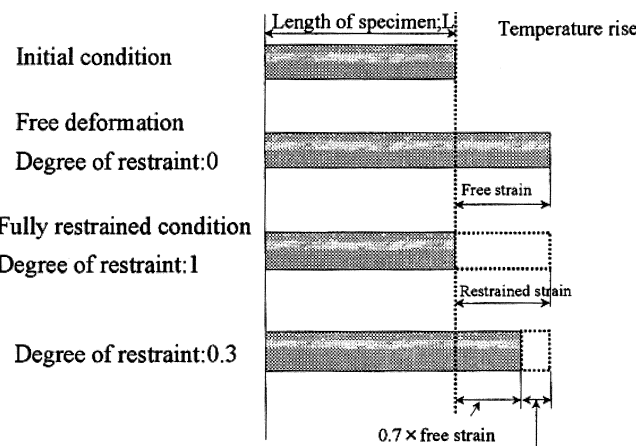


Fig. 4.28—Definition of degree of restraint (Mizobuchi *et al.* 2000).

4.5—Coefficient of thermal expansion (α_T) measurement

The concrete α_T may be either estimated or measured. Nevertheless, Hossain *et al.* (2003) showed that the values of calculated α_T and measured α_T may diverge significantly. This property is particularly difficult to measure at early ages due to the confounding influences of the ongoing hydration (Bjontegaard 1999).

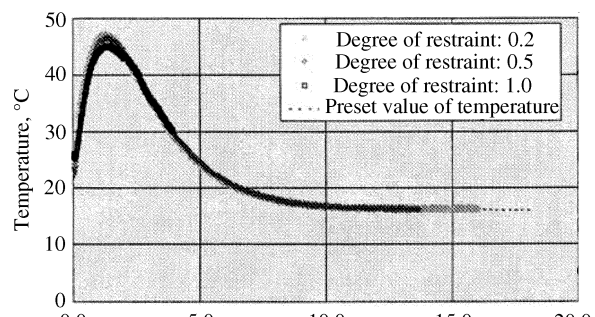
The estimation may be a result of typical values reported in the literature for concretes with a certain type of aggregate or may be calculated as proposed by Neville (1996). In this case, the α_T of concrete is calculated by taking into account the mixture proportions and the α of the individual materials and assuming a series arrangement for the three materials (Eq. (4-15))

$$\alpha_T = \alpha_{FA} \cdot V_{FA} + \alpha_{CA} \cdot V_{CA} + \alpha_{paste} \cdot V_{paste} \quad (4-15)$$

where the α is coefficient of thermal expansion of every individual material; V is the relative volume of every material; FA stands for fine aggregate; and CA stands for coarse aggregate.

The aggregate α may be measured by different methods. Mukhopadhyay *et al.* (2004) proposed a method based on a mineralogical approach where the volume percentage of each constituent mineral phase and its α and elastic modulus are taken into account. Willis and DeReus (1939) described a method to determine the α of coarse aggregate with the use of an optical lever over a considerable range of temperature. The U.S. Army Corps of Engineers method measures the α of coarse aggregate particles that have a strain gauge bonded to them (Lamond and Pielert 2006). Methods that use extensometers to determine α of aggregates and concrete were also reported (Lamond and Pielert 2006).

Until 2000, there was no standard test method available to determine the α of concrete. Currently, the concrete α test method is still a provisional method (AASHTO 2007), and not many laboratories are equipped to run the test. AASHTO TP 60-00 (AASHTO 2007) is based on the test method developed at Turner Fairbank Highway Research Center (TFHRC) as part of a long-term performance pavement



(a)

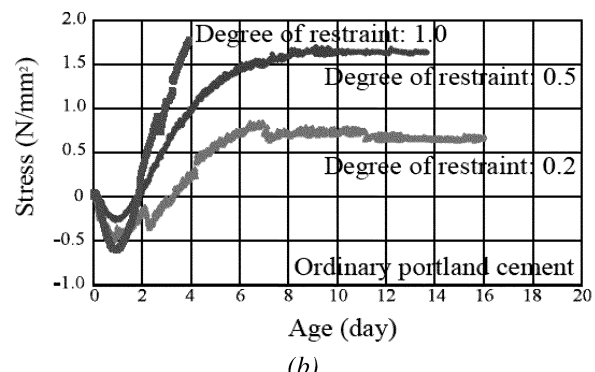


Fig. 4.29—(a) Temperature histories; and (b) corresponding shrinkage stress at different restraint levels (Mizobuchi *et al.* 2000). (Note: 1°F = 1.8 × °C + 32; 145 psi = 1 N/mm².)

(LTPP) test protocol. The research conducted at TFHRC resulted in a simple test method that was easy to run and relatively inexpensive.

The test consists of subjecting a saturated concrete core or cylinder to temperature cycles (called segments) from 50 to 122°F (10 to 50°C) and from 122 to 50°F (50 to 10°C), and measuring the change in length using a linear variable differential transformer (LVDT) attached to a readout (Fig. 4.30). Figure 4.31 shows the water bath setup for the α_T testing. Segments are repeated until the difference between the α_T of two consecutive segments is less than $0.17 \times 10^{-6}/^{\circ}\text{F}$ ($0.3 \times 10^{-6}/^{\circ}\text{C}$). The final α_T is the average of the α_T obtained from two consecutive segments that comply with this requirement. α_T is calculated according to Eq. (4-16). The U.S. Army Corps of Engineers (1981) developed a similar test method (CRD C 39-81) to measure the concrete α_T

$$CTE = (\Delta L_a / L_o) / \Delta T \quad (4-16)$$

where

ΔL_a = actual length change of specimen during temperature change, mm (Eq. (4-17));

L_o = measured length of specimen at room temperature, in. (mm); and

ΔT = measured temperature change (average of the four sensors), °F (°C) (increase = positive; decrease = negative)

$$\Delta L_a = \Delta L_m + \Delta L_f \quad (4-17)$$

where

- ΔL_m = measured length change of specimen during temperature change, in. (mm) (increase = positive; decrease = negative); and
- ΔL_f = length change of the measuring apparatus during temperature change, in. (mm)

$$\Delta L_f = C_f \times L_o \times \Delta T \quad (4-18)$$

where

- C_f = correction factor accounting for the change in length of the measurement apparatus with temperature, $0.56 \times 10^{-6}/^{\circ}\text{F}$ ($1 \times 10^{-6}/^{\circ}\text{C}$).

The influence of the moisture condition on the α_T may be significant. To eliminate the effect of the moisture condition, AASHTO TP 60-00 (2007) is performed in a water bath and the specimens are maintained in the saturated condition. The α_T obtained in the saturated condition is considered to represent the true α_T (Neville 1996).

Won (2005) suggested changes to the AASHTO TP 60-00 (2007). The test would be basically the same, but the α_T would be determined from a regression analysis of temperature and displacement measurements. The modified test method was adopted by the Texas Department of Transportation as TEX 428-A (2001).

In-place α_T measurements were proposed by Burnham and Koubaa (2001) that use vibrating wire strain sensors, and by Li et al. (2002) and Brown et al. (2004) that use optic sensors.

Cusson and Hoogeveen (2007) proposed a new experimental approach to determine the α_T of concrete at very early age, in which sealed concrete prisms (3 x 3 x 12 in. [75 x 75 x 295 mm]) are subjected to temperature cycles from 77 to 86°F (25 to 30°C) in an environmental chamber from the time of setting to 7 days or longer. The entire test apparatus (Fig. 4.32), including molds, frame, and sensors, is exposed to temperature change. The authors performed careful temperature calibration of the assembly during a temperature change to enable them to obtain accurate measurements.

A new calculation method was also proposed to eliminate autogenous shrinkage from the measurements before the α_T is determined from the thermal deformation obtained over time (Fig. 4.33). For the HPC tested in their study, it was found that the α_T decreased toward a minimum value 1 day after the setting of concrete, and increased gradually up to a final value near 7 days. This phenomenon may be due to hydration process and chemical reaction that resulted in dimensional changes.

4.6—Analysis tools assessing stresses and cracking

The time-dependent behavior of structural elements made of cementitious materials is generally modeled numerically with finite element programs. These programs make it possible to take into account thermal, hygral, and chemical effects occurring at the material level to establish the resulting deformations and crack formation at a structural

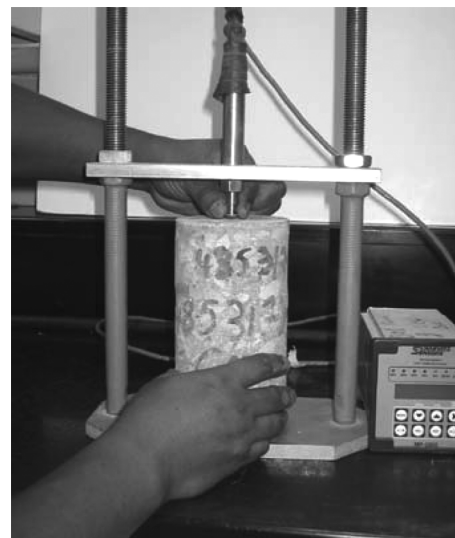


Fig. 4.30—Nickel steel alloy frame, LVDT for length change measurements, and readout. Specimen may be core or cylinder (TFHRC).

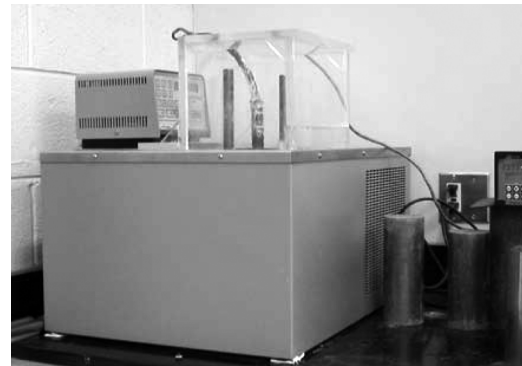


Fig. 4.31—Manual unit built at TFHRC.

level. The options of the programs and their degree of couplings between the phenomena vary from one program to another. Commercially available finite element programs, such as 4C-Temp&Stress, HIPERPAV, and MLS, may predict the early-age stress development and cracking sensitivity in a concrete member. A few finite element programs are detailed as follows.

Note: ACI does not endorse this technology or warrant that the use of this technology will meet code requirements. The selection of any design methodology or use of any patented technology is at the option of the user.

4.6.1 4C-Temp&Stress software—This commercially available finite element program may predict the early-age stress development in a concrete member (Nielsen and Berrig 2005). The temperature calculations performed by 4C-Temp&Stress may include consideration of the: initial temperature of fresh concrete; casting rate; heat of hydration of concrete; ambient wind and temperature effects; type of formwork; type of insulation; time of stripping; and use of cooling pipes, heating wires, and heating mats. Calculations convert the time and temperature history to an equivalent time by applying the maturity concept based on the Arrhenius

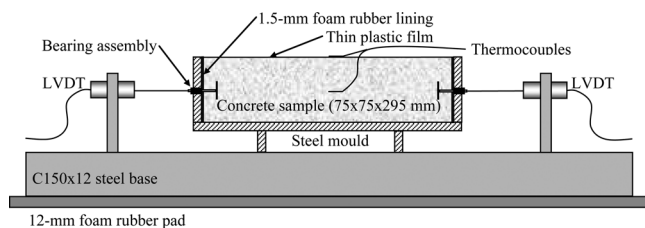


Fig. 4.32— α_T testing apparatus developed at National Research Council Canada (NRCC)⁴ (Cusson and Hoogeveen 2007). (Note: 1 in. = 25.4 mm.)

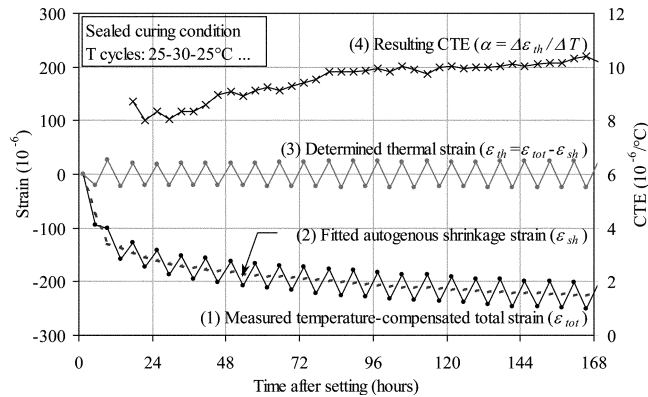


Fig. 4.33—Typical results obtained with NRCC apparatus (Cusson and Hoogeveen 2007). (Note: $^{\circ}\text{F} = 1.8 \times ^{\circ}\text{C} + 32$; 0.556 microstrain per $^{\circ}\text{F}$ is equivalent to one microstrain per $^{\circ}\text{C}$.)

equation. Figure 4.34 provides an overview of the program facilities.

4.6.2 High Performance Concrete Paving (HIPERPAV) software—HIPERPAV software was developed as a tool for predicting the early-age behavior of both jointed plain concrete pavement (JPCP) and continuously reinforced concrete pavement (CRCP). The predictive capabilities of HIPERPAV helps designers, contractors, and concrete suppliers identify factors that may contribute to achieving good-performing pavements. The model parameters required in HIPERPAV II are: slab geometry, concrete properties (strength and α_T), environmental conditions (ambient temperature), and construction conditions (paving time, initial concrete temperature, and curing method). Figure 4.35 shows the predicted relation between tensile stress development and the tensile strength gain in a JPCP project. According to predictions, tensile stresses exceed tensile strength at 15 hours after paving, which is the end of the sawing window; saw-cutting should be performed before this point, otherwise, early-age cracking may occur.

4.6.3 MLS software—MLS (FEMMASSE), a two-dimensional finite element model is capable of computing the physical (temperature, hydration, and moisture content) and structural (tensile and compressive strength, displacement, and evolution of the crack width) behavior of a composed structure and taking varying environmental conditions into account. The preprocessor in MLS gathers the input data for the computation, provides a user-friendly interface to draw objects such as concrete slabs and cooling pipes, and defines

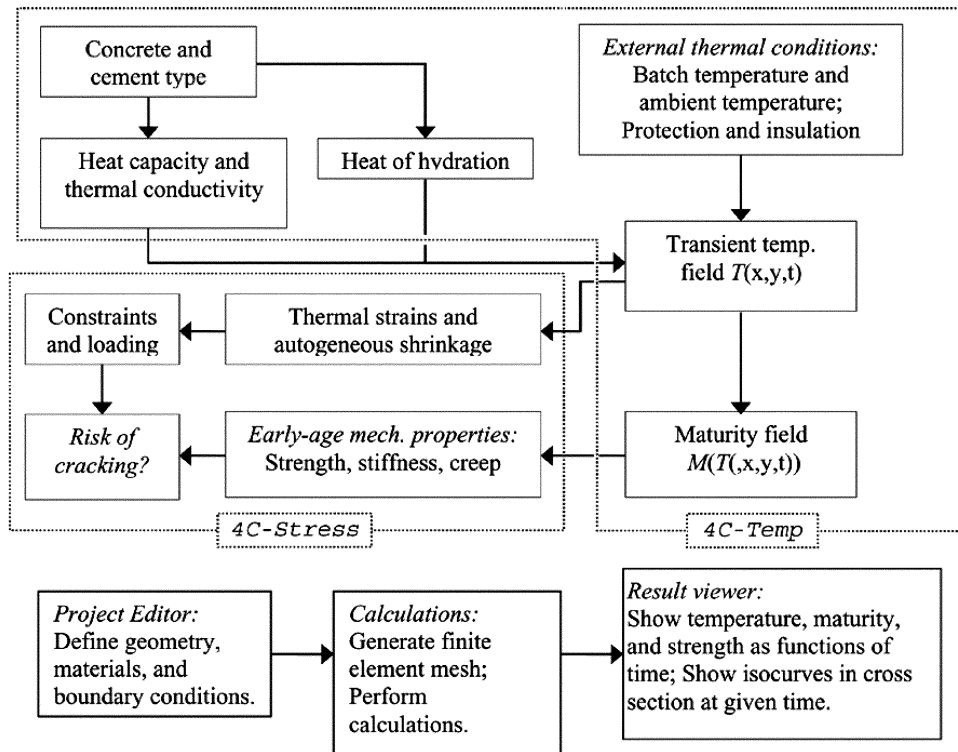


Fig. 4.34—Schematic overview of 4C-Temp&Stress. Risk of cracking is assessed on the basis of calculated tensile stress/strength ratio as a function of maturity (Nielsen and Berrig 2005).

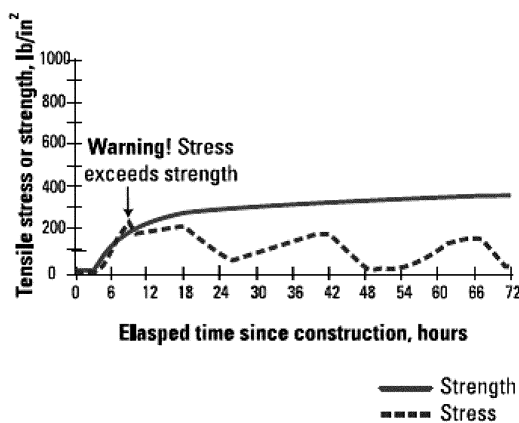


Fig. 4.35—Predicted cracking sensitivity of a concrete pavement using HIPERPAV software. (Note: 145 psi = 1 MPa.)

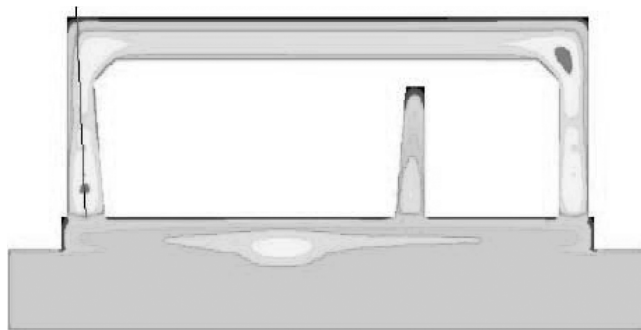


Fig. 4.36—Temperature and stress contour in concrete member simulated by using MLS.

how temperature varies at the boundaries of the drawn structures. The possibility to include reinforcement, cooling circuits, and interfaces between different materials make the program particularly suitable to deal with the building practice. Figure 4.36 (Koenders and van Breugel 2004) shows an example for modeling temperature and stress development in a hardening concrete structure with thermal and autogenous shrinkage being considered in the simulation.

CHAPTER 5—SHRINKAGE CONTROL

5.1—Introduction

Chapter 5 focuses on describing methods to reduce the potential for cracking through material modifications. Shrinkage cracking may be reduced through five main material modifications, including:

1. Increasing the volume of aggregate. It is well known that it is the paste volume that shrinks (L’Hermite 1960); as such, increasing the volume of aggregate generally reduces the shrinkage and potential for shrinkage cracking;
2. Modifying the characteristics of the binder system, namely the cement and supplementary cementitious materials. For example, minimizing the C₃S content for a cement may reduce the chemical shrinkage and, consequently, the autogenous shrinkage (Tazawa and Miyazawa 1995). Other researchers suggested that cracking may be reduced by modifying the size of the particles that will alter the rate of reaction and resulting pore structure (Burrows 1998; Chariton and Weiss 2002; Bentz et al. 2001a);

3. Using expansive additives. Commonly referred to as shrinkage-compensated concrete, these systems use an expansion of the concrete (that is, expansion in the matrix) rather than reduction of shrinkage. These expansions may be obtained mainly through ettringite formation (calcium sulfoaluminate or calcium aluminate-based system) or calcium hydroxide formation (lime based system);

4. Using SRAs. Shrinkage-reducing chemical admixtures are chemical admixtures that primarily reduce shrinkage by reducing the surface tension of the fluid in the pore system. These admixtures may be integrally mixed with the concrete or added topically; and

5. Using internal curing through water-saturated porous inclusions. There is a growing trend of using internal curing to mitigate shrinkage. Internal curing is achieved through placing a material within the concrete that will release water to compensate for the water consumed by cement hydration (chemical shrinkage). The media used for water compensation is usually lightweight aggregates, superabsorbent polymers (SAPs), or cellulose products.

While the first two methods have been described in greater detail in Chapter 3, approaches described in Chapter 5 have experienced dramatic advances and, as such, are described in greater detail in this chapter.

5.2—Expansive additives

One method to reduce the potential for cracking is to use a material that expands during the early stages of hydration to offset the effects of shrinkage (Polivka and Wilson 1973).

Figure 5.1 illustrates the behavior of an expansive component in a conventional low w/cm ($w/cm = 0.30$) cement paste as measured using the dilatometer described in Chapter 4 (Jensen and Hansen 1995). It may be seen that the conventional cement paste experiences little, if any, expansion at early ages. This expansion would be attributed mainly to the absorption of water during hydration. The paste containing the expansive admixture (4 and 10% of a calcined inorganic powder in this case) demonstrates a substantial expansion.

This early expansion, if restrained, may result in the development of a compressive prestress that may counteract the tensile stresses caused by shrinkage. This may be seen in **Fig. 5.1(b)** using the dual ring described in Chapter 4 (Sant et al. 2007b). In **Fig. 5.1(b)**, the compressive prestress delays the development of residual stresses that may allow the concrete to gain strength, thereby better enabling it to resist cracking.

This compressive prestress may also prevent the development of a crack. Breitenbücher and Mangold (1994) found that the high compressive stresses could minimize or fully compensate for the tensile stresses (**Fig. 5.2**) in concrete.

Although such expansive additives are effective in reducing cracking sensitivity, they are sensitive to many parameters, including temperature, moisture, dosage, cement, and mixture composition. If the dosage of the additive is not optimized on an individual basis, either very little expansion or too much expansion may occur; therefore, expansive additives are not licensed in many countries (Breitenbücher and Mangold 1994). One problem associated with the use of an expansive cement (or an expansive additive in cement) is

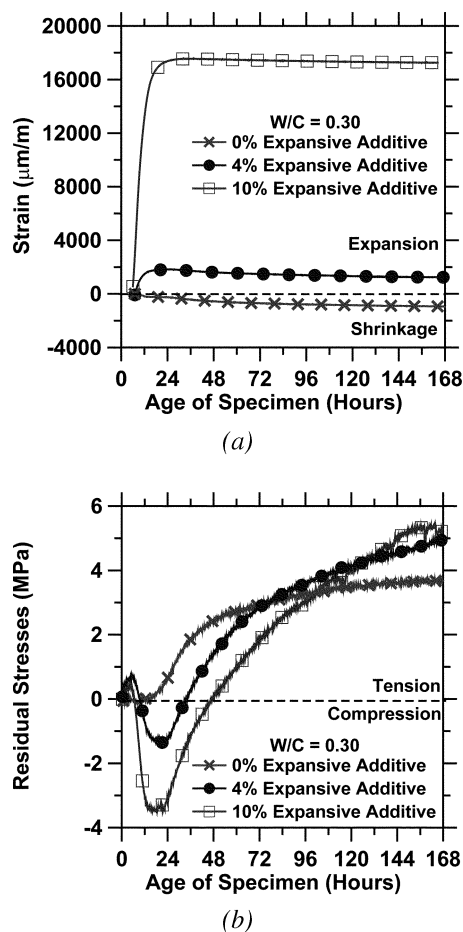


Fig. 5.1—Influence of expansive additives on: (a) volume change; and (b) resulting residual stress development in cement paste (Sant et al. 2007b). (Note: w/c = w/cm; $1 \times 10^{-6} \text{ in./in.} = 1 \mu\text{m}/\text{m}$; 145 psi = 1 MPa.)

that it is difficult to control the chemical reaction in the field due to its strong dependence on environmental conditions. Rapid slump loss is often observed due to the abundance of the formation of ettringite during the early ages. Special precautions should be exercised to ensure the proper supply of moisture to trigger the expansive reactions.

5.3—Shrinkage-reducing admixtures

5.3.1 How SRAs work—Concrete is generally observed to shrink (that is, reduce its volume) in response to the loss of water that is held in the pore space of the concrete. This loss of water results in the development of a meniscus and capillary pressure in pores. The radius of the meniscus (approximately the radius of the pore being emptied) may be directly related to the extent of capillary pressure that is formed using the Young-Laplace equation (Eq. (5-1))

$$\sigma_{cap} = \frac{2\gamma \cdot \cos\theta}{r} \quad (5-1)$$

where γ in lb/in. (N/m) is the surface tension of the pore fluid; θ (rad) is the contact angle between pore fluid and solids; and r , in inches (meters), is the radius of the menisci

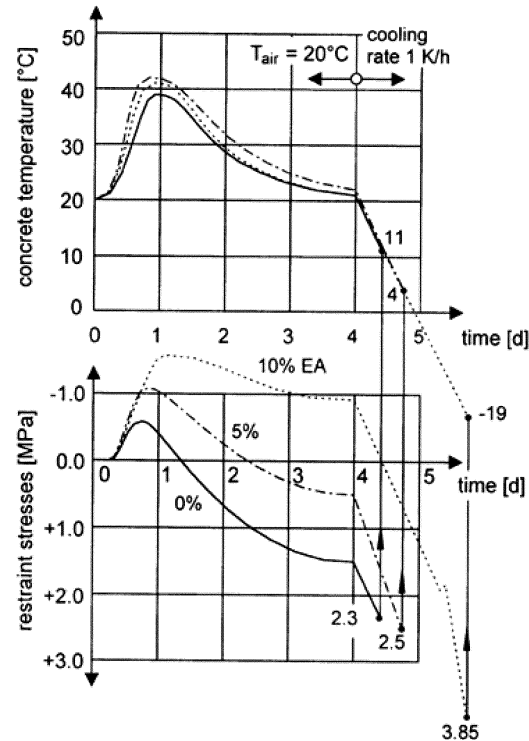


Fig. 5.2—Influence of expansive additives on cracking sensitivity (Breitenbücher and Mangold 1994). (Note: $^{\circ}\text{F} = 1.8 \times ^{\circ}\text{C} + 32$; 145 psi = 1 MPa.)

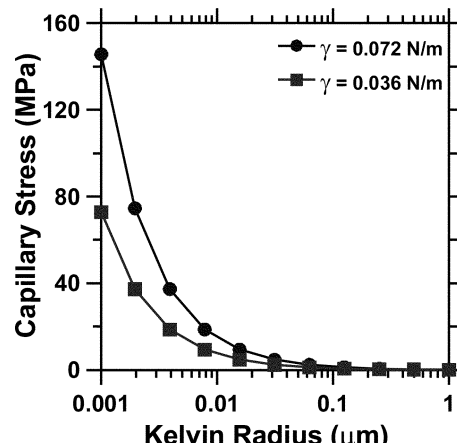


Fig. 5.3—Relationship between capillary pressure and Kelvin radius. (Note: 145 psi = 1 MPa.)

(Kelvin radius). Figure 5.3 illustrates that the capillary pressure increases as smaller and smaller menisci (that is, smaller values of r) are generated. This pressure pulls on the pore walls, which results in the volume reduction that is referred to as shrinkage. By reducing the surface tension of the fluid in the pore (that is, reducing γ), it is possible to reduce the pressure that is generated, corresponding to a reduction in shrinkage. The reduction in capillary pressure is directly proportional to the reduction in the surface tension of the pore fluid. Shrinkage-reducing chemical admixtures work by reducing the surface tension (Ai and Young 1997), as shown in Fig. 5.4 for a series of commercially available admixtures in water. A dramatic reduction in surface tension

occurs when the SRA is initially added, and this reduction slows as the SRA reaches a critical concentration* level of approximately 10 to 15% (Pease et al. 2005). It should be noted that a similar relationship has also been observed for solutions of SRA and pore solution; however, the plateau is reached at a slightly lower concentration due to the presence of ions in the pore solution (Rajabipour et al. 2008).

The capillary pressure may also be related to the RH (partial vapor pressure in the pores) using Kelvin's equations (Eq. (5-2))

$$RH = \exp\left(\frac{\sigma_{cap} V_w}{R'T}\right) = \exp\left(-\frac{2\gamma \cos\theta V_w}{rR'T}\right) \quad (5-2)$$

where V_w is the molar volume of the pore fluid (assumed equal to the molar volume of water (636×10^{-6} ft 3 /mol [18.02×10^{-6} m 3 /mol]); R' is the ideal gas constant, 1545 ft-lbf·R $^{-1}$ ·lb $^{-1}$ ·mol $^{-1}$ (8.314 J/[mol·K]); and $T[K,R]$ is the absolute temperature. At lower RHs, an increased amount of water is lost from smaller capillary pores, and a higher capillary pressure results. Kelvin's equation is used later in this chapter to describe the autogenous and drying shrinkage behavior because it relates the relative humidity, the capillary pressure, and surface tension.

Note that capillary stress is not the only mechanism responsible for shrinkage and disjoining pressure, and surface energy may also contribute to shrinkage (Mindess and Young 1981; Weiss and Berke 2002). Despite this, capillary stress is discussed primarily herein, as it is generally believed to be the mechanism that is most influenced by the addition of shrinkage-reducing chemical admixtures (SRAs).

5.3.2 Brief history of development of SRAs—Shrinkage-reducing chemical admixtures were introduced in Japan in 1983 (Sato et al. 1983; Tomita et al. 1986). Sato et al. (1983) described how SRAs could reduce the surface tension of the pore fluid, resulting in a reduction in capillary stresses and a reduction in drying shrinkage. Shah et al. (1992) demonstrated that in addition to reducing free shrinkage, SRAs could reduce the occurrence of cracking that is caused by the restraint of shrinkage. Nmai et al. (1998) provided a review of the developments of SRAs, including information on the first commercial patents.

5.3.3 Shrinkage-reducing chemical admixture materials—Shrinkage-reducing chemical admixture materials belong to a class of organic chemicals known as surfactants. At a molecular level, surfactants are amphiphilic; that is, each surfactant molecule is composed of a hydrophilic (that is, polar) head that is covalently bonded to a hydrophobic (that is, nonpolar) tail (Israelachvili 1991). Shrinkage-reducing chemical admixtures are generally organic admixtures based on polyalkylethers. Admixtures are commonly reported as commercial glycol ether blends (Berke et al. 1997), propylene glycol ether mixtures (Brooks and Jiang 1994), or polyoxyalkylene ether, a lower alcohol alkyleneoxide adduct (Nmai et al. 1998). Wax-based SRAs are also occasionally

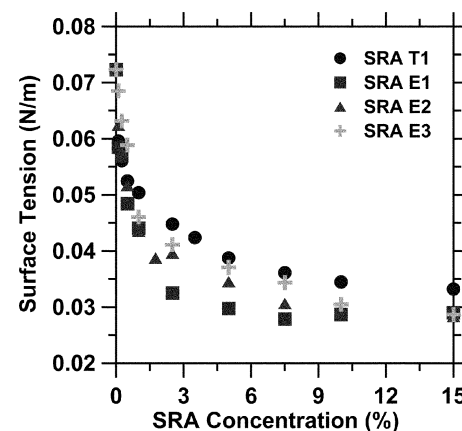


Fig. 5.4—Influence of SRA concentration on surface tension (Pease 2005). (Note: 0.0057 lb/in. = 1 N/m.)

discussed; however, not much information exists in the literature about these materials.

5.3.4 Application of SRAs—The most common method of using SRAs has been through integral mixing; however, Tomita et al. (1986) showed that SRAs may be applied through topical application (that is, impregnation).

When SRAs are mixed, they are reported either by mass of cement or as a percentage of the fluid portion of the system. In this report, the information is reported as a percentage of the fluid in the system, unless noted otherwise, because this enables one to see the level of surface tension reduction that may be expected using Fig. 5.4. It is common to see commercial applications using between 1 and 5% SRA concentrations (by replacement of water), with little additional benefit being observed for additions above 5%. Note that because SRAs generally increase the workability of concrete, they are generally used as a replacement for water (Weiss 1999; Folliard and Berke 1997), thereby keeping the fluid-cement ratio as constant as opposed to the w/cm per se (Weiss 1999; Shah et al. 1998).

Shrinkage-reducing chemical admixtures may be added topically by brushing or spraying, and is generally done immediately before final setting (Nmai et al. 1998). Typical application rates vary between 2.6 to 3.9 fl oz/yd 2 (200 and 300 mL/m 2) (Nmai et al. 1998). Bentz (2005a) showed a reduction in evaporative water loss with the application of an SRA solution to a fresh mortar exposed to drying conditions. Tomita et al. (1986) observed that topical applications lead to substantially higher SRA concentrations in the 0.25 in. (5 mm) of the concrete nearest the surface for most applications (up to 0.39 in. [10 mm] for more severe applications). This is particularly effective for drying shrinkage gradients. Note, however, that application around the time of set may delay the development of surface hardness.

5.3.5 Shrinkage-reducing chemical admixtures and their impact on shrinkage and cracking—The main advantage of using an SRA is its ability to reduce shrinkage. As such, the influence of SRA on shrinkage reduction is described in Section 5.3.5.1, focusing specifically on autogenous shrinkage, plastic shrinkage, and drying shrinkage. The influence of reduced shrinkage on a reduced potential for

*Concentration herein is the ratio of the mass of SRA to the mass of the sum of initial mixture water and SRA.

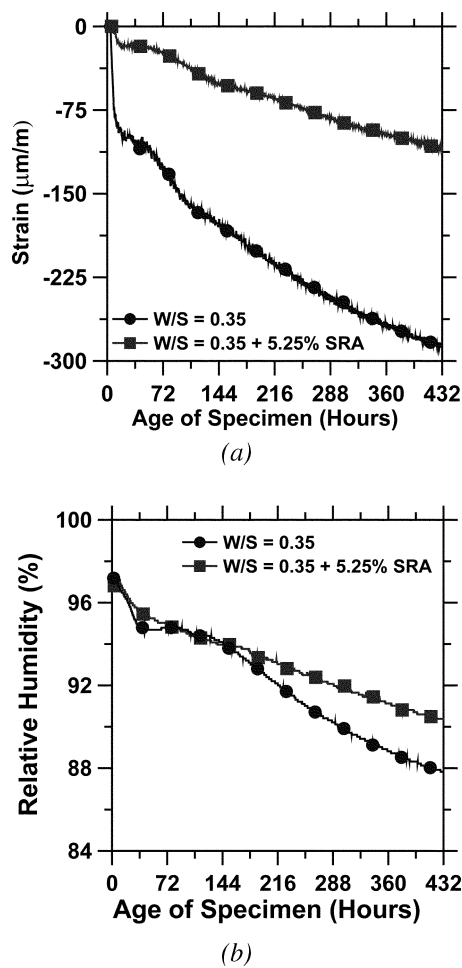


Fig. 5.5—(a) Autogenous deformation; and (b) internal relative humidity for cement mortars ($w/cm = 0.35$) with and without SRA, cured under sealed conditions at $86^{\circ}F$ ($30^{\circ}C$) (Bentz et al. 2001b). (Note: 1×10^{-6} in/in. = $1 \mu\text{m}/\text{m}$.)

cracking is also discussed, and typical results and predictions are provided as a general reference. In addition to the influence on shrinkage-related properties, it is important to understand the influence on mechanical and durability properties, which are also discussed briefly. Note, however, that practices leading to durable concrete will be the same in concretes with SRAs.

5.3.5.1 Influence of SRAs on autogenous shrinkage—Autogenous shrinkage is the shrinkage measured in a paste, mortar, or concrete sample under sealed conditions at a constant temperature. The driving force of autogenous shrinkage is similar to that of drying shrinkage (Baroghel-Bouny 1997) in that a reduction of the RH that occurs in the fine pores causes capillary stresses leading to bulk shrinkage. Note, however, that the mechanisms responsible for the reduction of RH in the case of autogenous shrinkage are different from those responsible for drying. Autogenous shrinkage occurs as a result of internal self-desiccation and chemical shrinkage. As such, it is the consumption of water through hydration that creates the menisci and vapor-filled space.

Weiss et al. (1999a,b) demonstrated that HPC containing an SRA showed a dramatic reduction in shrinkage (and even a slight expansion) when measurements were started at the

time of set. A more substantial reduction in shrinkage was observed at early ages for the HPC with an SRA with approximately 90% of the shrinkage reduced at 24 hours, 30% at 3 days, 40% at 28 days, and 50% at 90 days (Weiss et al. 1999a). Bentz et al. (2001b) measured the autogenous shrinkage of a mortar system with a w/cm of 0.35 containing 8% silica fume (Fig. 5.5), and found that the SRA reduces the autogenous shrinkage by more than a factor of 2, which should translate to a lower susceptibility to early-age cracking for SRA mixtures. Rongbing and Jian (2005) also noticed similar results. Sant et al. (2007a,b) demonstrated that some pastes containing SRA show an expansion shortly after set (Fig. 5.6). The difference in the expansion observed between Fig. 5.5(a) and 5.6(a) appears to be due to the difference in the chemistry of cement, specifically the tricalcium aluminate and sulfate phases; however, research is being conducted to understand this completely. In either case, the general behavior is similar after approximately 24 hours.

In addition to the measurements of length change, the internal RH may provide insight on the behavior of systems containing SRAs. Figures 5.5(b) and 5.6(b) show that the RH in the system containing the SRA remains higher than that in the plain system.

It has been argued that measurements of chemical shrinkage and nonevaporable water show that for the sealed specimens, the volume of water that is consumed by the hydration reaction is similar for both the plain and SRA specimens (assuming that the influence of the SRA on retardation is negligible) (Bentz et al. 2001b; Sant et al. 2006a,b; Weiss 1999). The implication of both systems losing the same volume of water to hydration or chemical shrinkage is that the specimen containing the SRA would maintain a higher internal RH. This is illustrated in Fig. 5.6(c) (Sant et al. 2007a) using the Kelvin equation (Eq. (5-2)). For example, if pores having a radius up to 2.0×10^{-7} in. (5 nm) are emptied, the plain mixture would have an RH of 85%, whereas the SRA mixture would display an RH of 95%. This explains why SRA specimens in Fig. 5.5(b) and 5.6(b) show a higher internal RH and a lower autogenous shrinkage (Fig. 5.5(a) and 5.6(a)).

Finally, note that the residual stress that develops when a sealed system is restrained (as obtained from the dual ring described in Chapter 4) is shown in Fig. 5.6(d). The system containing SRA develops a compressive stress (corresponding with the expansion) between 8 and 24 hours. The effect of this expansion remains throughout the life of the specimen.

5.3.5.2 Influence of SRA on plastic shrinkage—Bentz et al. (2001b) examined the role of SRA in pastes and mortars in fresh concrete using X-ray absorption. They found that SRAs significantly affect drying profiles, drying rates, internal RH, viscosity of the pore solution, and freezable water contents of a fresh cementitious system (Bentz 2006).

Bentz et al. (2001b) observed a lower evaporation from mixtures with SRA and a change in the drying profile and hypothesized that the initial drying causes the formation of a concentrated solution of SRA at the surface, which hinders further evaporation of water. This outer layer, which dries first, protects the inner layer from drying due to its lower

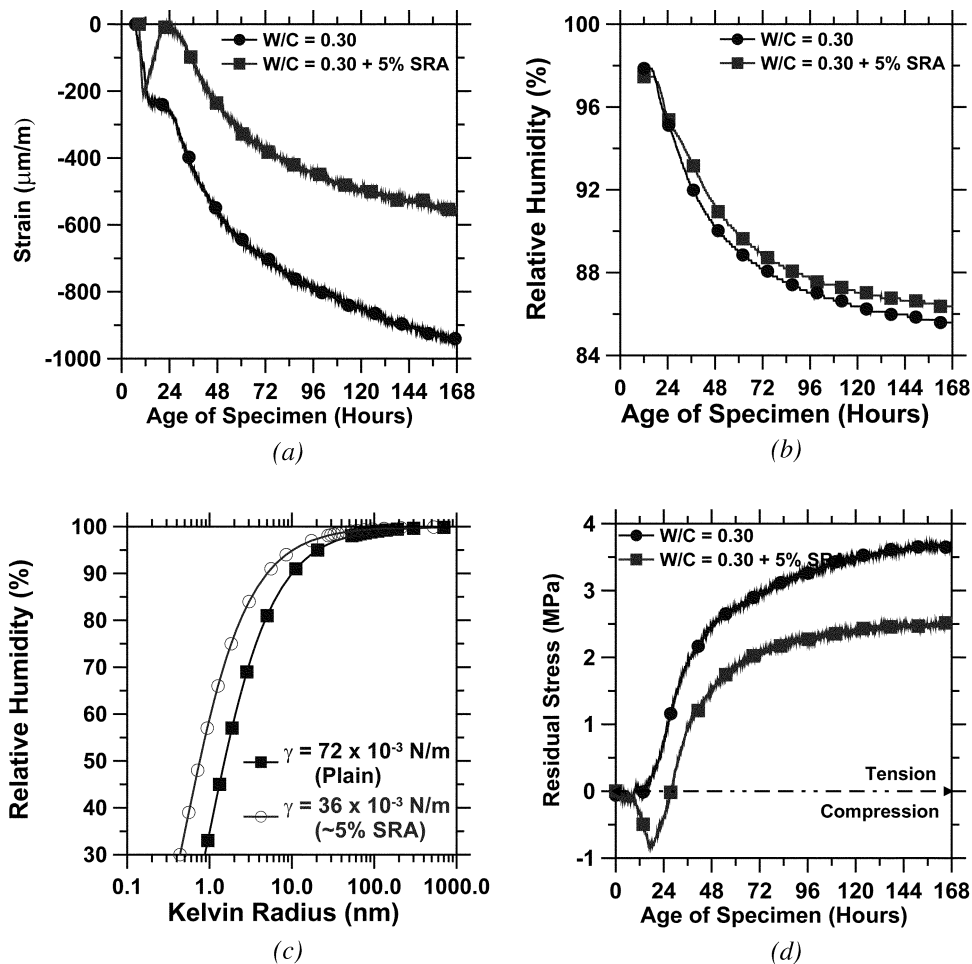


Fig. 5.6—(a) Autogenous deformation; (b) internal relative humidity; (c) Kelvin equation for system with and without SRA; and (d) residual stress for cement paste ($w/cm = 0.30$) with and without SRA, cured under sealed conditions at 73°F (23°C) (Sant et al. 2007b). $1 \times 10^{-6} \text{ in./in.} = 1 \mu\text{m}/\text{m}$; $0.0057 \text{ lb/in.} = 1 \text{ N/m}$; $145 \text{ psi} = 1 \text{ MPa}$; $w/c = w/cm$.

surface tension, associated with the higher content of SRA. The lower surface tension pore solution at the surface of the specimen is unable to pull the higher surface tension pore solution below it to the surface, thus reducing the evaporation rate (Bentz 2005a). With regard to the pore solution movement within a specimen during early-age bleeding and evaporation, it is also worth mentioning that the measured viscosity of a typical 10% SRA solution in distilled water is approximately 50% higher than that of distilled water alone (Bentz 2006), implying a slower internal flow rate under equivalent capillary pressures.

The influence of SRA on plastic shrinkage cracking was also studied by Lura et al. (2005, 2007). Figure 5.7 illustrates the rate of evaporation from solutions containing SRA as well as mortars ($w/cm = 0.50$) containing SRA. It may be noticed from Fig. 5.7(a) that the SRA does not substantially influence the rate of evaporation from a solution (Lura et al. 2005). Figure 5.7(b) shows that during the first 60 to 90 minutes, the total water lost from the mortars with and without SRA is similar. Once the layer of bleed water at the surface is consumed by evaporation (this occurs at approximately 90 minutes for the data in Fig. 5.7(b)), air-liquid

menisci are formed in the liquid between the solid particles on the surface. These menisci cause tensile stresses to develop in the pore fluid, leading to shrinkage. At early ages, the tensile stress in the pore fluid causes the majority of the shrinkage to occur in the vertical direction. As the system shrinks, the pore fluid is brought to the surface, and this pore fluid evaporates.

When menisci form at the surface, the pore fluid is subjected to tensile stresses (capillary pressure) that may be computed from the Young-Laplace equation. In mortars with SRA, the surface tension of the pore fluid is substantially reduced. Because the capillary pressure is proportional to the surface tension, a proportional reduction of the capillary pressure developing upon drying is expected in mortars with SRA. The capillary pressure produced by the menisci on the surface compresses the mortar, forcing fluid out of the porous network. Lura et al. (2005, 2007) proposed that the lower surface tension of the pore fluid in the mortars containing SRA results in less fluid being forced out of the porous network. This is evident in less total evaporation, reduced settlement, reduced capillary tension, and lower crack-inducing stresses at the topmost layer of the mortar.

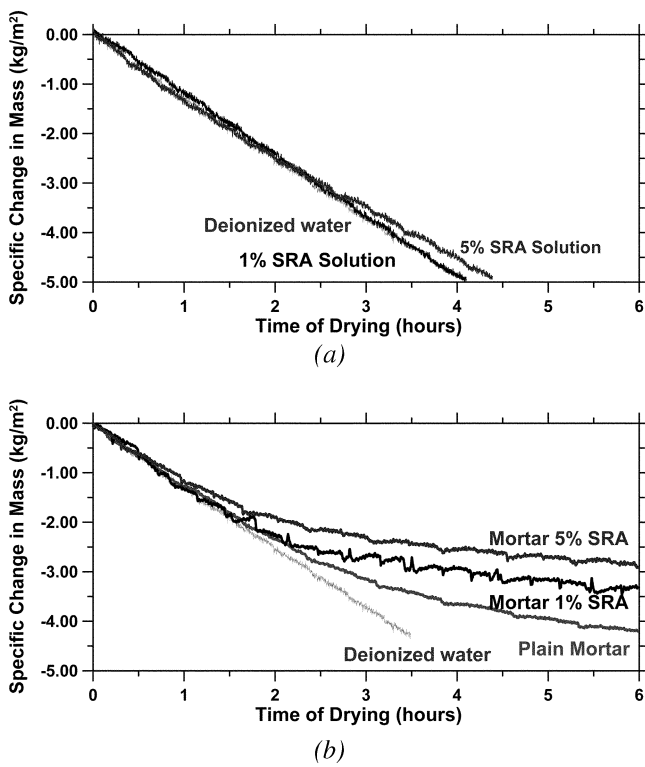


Fig. 5.7—(a) Mass change due to evaporation of solutions at 86°F (30°C) and 30% RH; and (b) mass change due to evaporation of mortars at 86°F (30°C), 50% RH, and 15 mph (24 km/h) wind speed (Lura et al. 2005). (Note: 0.205 lb/ft² = 1 kg/m².)

A high rate of evaporation causes a steep gradient of the capillary pressure at the surface of the mortar or concrete; therefore, a high tensile stress at the surface would induce plastic shrinkage cracks. The lower rate of evaporation obtained by addition of SRA should therefore reduce the tensile stress at the surface and ultimately reduce the probability of plastic shrinkage cracking, as shown in Fig. 5.8.

5.3.5.3 Influence of SRA on drying shrinkage—Concrete is generally observed to shrink (that is, reduce its volume) in response to the loss of water that is held in the pore space of the concrete. When concrete is not sealed, it attempts to equilibrate with the humidity of the air surrounding the concrete. This causes water to be lost from the pores, resulting in the generation of capillary stresses (Eq. (5-1)). Water will be lost until the size of the menisci is in equilibrium with the surrounding RH (Eq. (5-2)). The lower the external RH, the more water that is lost from the concrete and greater range of pore sizes being emptied, with the largest pores being emptied first until Eq. (5-2) is satisfied for the connected pores (Fig. 5.6(c)).

Figure 5.9 illustrates the mass change due to water loss and shrinkage strain for a cement paste system. Figure 5.9(a) indicates that addition of an SRA does not appear to substantially alter the total amount of water that is lost (calculated as a mass change) from the specimens (though the water lost from the SRA system may be slightly higher in the higher RH ranges, for example, between 65 and 85% RH). This is consistent with previous observations (Weiss 1999; Shah et

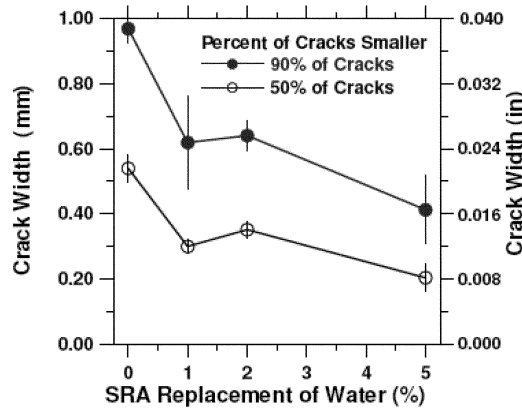


Fig. 5.8—Influence of SRAs on width of plastic shrinkage cracks measured at 24 hours (Lura et al. 2007).

al. 1998). The SRA, however, appears to alter the rate of moisture loss (mass change) from the samples. Figure 5.9(b) shows the shrinkage of the same samples, demonstrating that despite the same loss of water, the specimens with SRA show substantially lower shrinkage at a low RH (70, 50, and 30%). These values, however, are more similar for a higher RH (87 and 95%). This appears to be related with the concept that SRAs may actually alter the range of humidities where the capillary stresses dominate the shrinkage behavior (Weiss et al. 2006, 2007). Due to geometric limitations, capillaries will not be able to exist below approximately 50% RH for the plain system and 75% RH for a system with 5% SRA (assuming a Kelvin radius of 5.9×10^{-8} in. [1.5 nm] is the smallest possible radius at which a menisci may exist) (Sant et al. 2007a; Weiss et al. 2007).

5.3.5.4 Overall shrinkage measurements for concrete containing SRA—While previous sections described the shrinkage behavior of concrete under sealed conditions (5.3.5.1), shrinkage before setting (5.3.5.2), and shrinkage under only drying (5.3.5.3), most practitioners are interested in overall shrinkage of concrete containing SRA. The following describes these general observations.

Most researchers indicate that use of SRA (typically 2 to 5% by mass of water) results in a substantial reduction in overall shrinkage. While this reduction in shrinkage (shown as overall shrinkage) depends on the concentration of SRA used (Fig. 5.10(a)), the reduction in drying shrinkage (after subtracting autogenous shrinkage) appears to be relatively independent of the w/cm (assuming constant aggregate volume and type) as shown in Fig. 5.10(b) (Shah and Weiss 2000). Nmai et al. (1998) report reductions of 50 to 60% at 28 days, and 40 to 50% at 12 weeks. Gettu et al. (2007) also conducted a series of experiments using different types of glycol-based SRAs and observed that the long-term shrinkage was reduced by 50 to 56% when compared with the overall shrinkage of the control specimens. Similar tests conducted using a wax-based SRA showed a much less significant reduction in shrinkage (~13%). Berke et al. (1997) measured the shrinkage for a wider range of mixtures (Fig. 5.11). They also observed that the shrinkage reduction

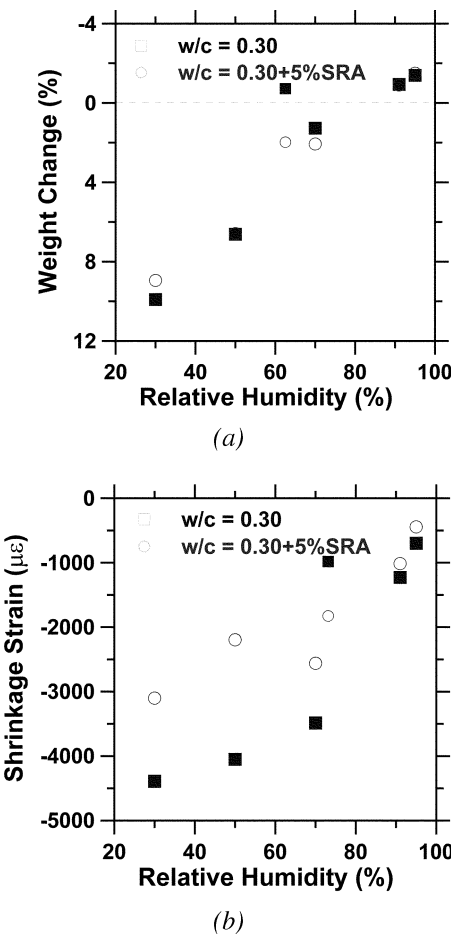


Fig. 5.9—Mass change and shrinkage measured in specimens exposed to drying after 7 days: $w/cm = 0.30$ and $w/cm = 0.30 + 5\%$ SRA (Sant et al. 2007a). (Note: $w/c = w/cm$.)

was relatively independent of the w/cm except for the case of long drying times under poor curing conditions.

Concrete slabs do not shrink uniformly throughout the cross section; greater shrinkage occurs near the surface. It was shown that SRA does not substantially alter the moisture gradient throughout the cross section (Schießl et al. 2000). This corresponds to reduced warping in concrete slabs that contain SRA.

5.3.6 Influence of SRA on shrinkage cracking—Restrained shrinkage tests performed in numerous studies have illustrated that concrete shows an increase in the resistance to early-age cracking if an SRA is used. Brooks and Jiang (1994) found that under 100% restraint, tensile-loaded dog-bone specimens showed a lower stress level at the time of failure when they contained SRA (from 305 to 203 psi [2.1 to 1.4 MPa]) and the age of cracking was delayed from 4.8 to 12.0 days. Bentur et al. (2001) observed similar behavior, as shown in Fig. 5.12(b), although less stress reduction was observed. Delays or prevention in the age of cracking in ring specimens has also been reported for a wide range of concrete mixtures (Shah et al. 1992; Nmai et al. 1998; Weiss 1999; See et al. 2003; Folliard and Berke 1997; Weiss et al. 1998a). Weiss et al. (1998b) demonstrated that the results of SRA performance from the restrained ring test could be extended to slab geome-

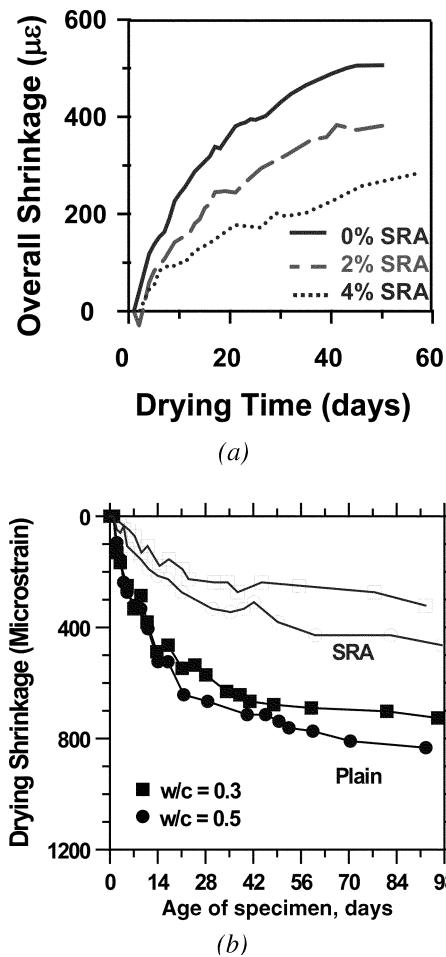


Fig. 5.10—(a) Influence of SRA on shrinkage in typical normal-strength concrete (Weiss 1999); and (b) influence of SRA on drying shrinkage with different w/cm (Weiss 1997).

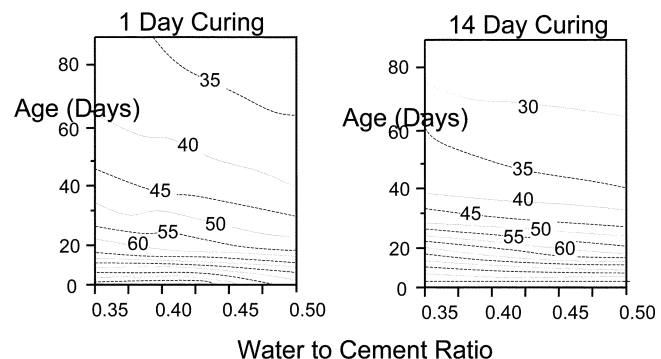


Fig. 5.11—Predicted percent reduction in shrinkage (contours represent percent reduction obtained using 2% SRA by mass of cement) (Berke et al. 1997).

tries. Shrinkage-reducing chemical admixtures were generally observed to delay the potential for cracking as well as the age of cracking, to decrease the width of cracks that develop, and to increase the spacing of the cracks (Lura et al. 2007).

The influence of less-than-perfect restraint has a significant influence on the potential for cracking. Shah et al. (1998) illustrated the role of SRA on the potential for

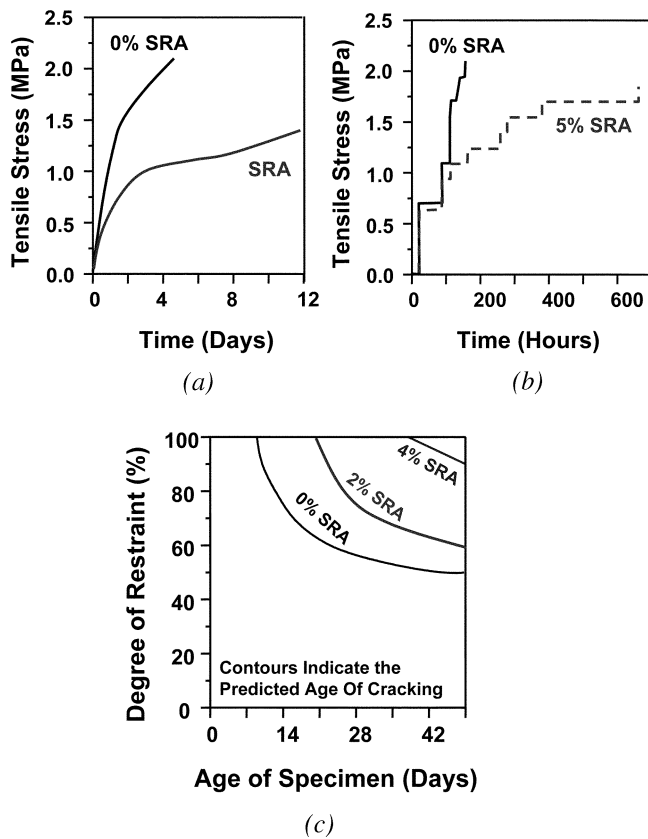


Fig. 5.12—Stress developed for 100% restraint: (a) (Brooks and Jiang 1994); (b) (Bentur et al. 2001); and (c) the influence of variable restraint on age of cracking (Shah et al. 1998). (Note: SRA is by mass of cement for (c); 145 psi = 1 MPa.)

cracking in structures with less-than-perfect restraint using a fracture-based approach with basic constant degree of restraint assumptions (Fig. 5.12(c)). Bentur et al. (2001) computed the actual levels of restraint for conventional steel bridge on steel sections, and reported values as low as 30% for the degree of restraint. That the degree of restraint, however, is not constant in field (or passively restrained) concrete elements; rather, it begins as nearly 100% during casting, and reduces as the concrete gains stiffness, thereby further complicating the analysis (Hossain and Weiss 2004; Moon and Weiss 2006).

A series of papers was written to relate free shrinkage to the probability of cracking when variability in material properties is considered (Radlinska et al. 2007). While the details of this analysis are beyond the scope of this review, a typical result of these simulations may be seen in Fig. 5.13. The Monte Carlo analysis approach was used to simulate the response of a restrained concrete element[†] (100% restraint) with long-term free shrinkage values of 670 and 480 $\mu\epsilon$ (that is, long-term free shrinkage may be thought of as the ASTM C157 shrinkage measured after set for 90 days or 1 year) (Radlinska et al. 2007). It may be seen that cracking for the

[†]This simulation was performed for one particular concrete; the results may change due to the constituent materials, mixture proportions, rate of strength gain, and specimen geometry. These simulations will vary depending upon the level of quality control that is assumed during batching and placement, as well as the environmental conditions at the time of placement.

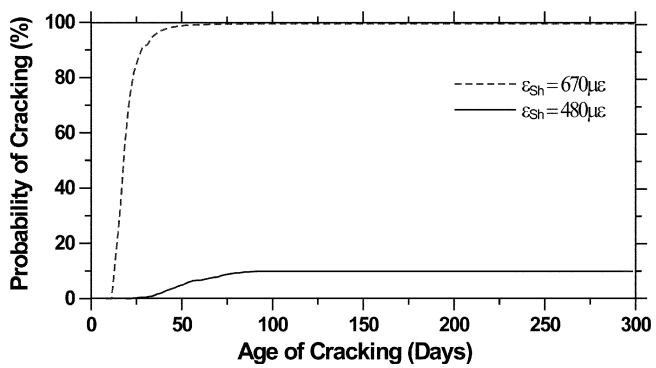


Fig. 5.13—Results of simulations showing how addition of SRA may decrease concrete shrinkage and reduce probability of cracking (Radlinska and Weiss 2006a).

plain concrete ($\epsilon_{sh} = 670 \mu\epsilon$) approaches nearly 100% probability of cracking at the age of 50 days, whereas the concrete with 28% less shrinkage ($\epsilon_{sh} = 480 \mu\epsilon$) has only a maximum 10% probability of cracking. This clearly shows the benefit of reducing shrinkage.

Figure 5.14(a) illustrates the relationship between the long-term free shrinkage and the probability of cracking (or the number of slabs that would crack if 100 slabs were cast). The relationship with the probability of cracking and free shrinkage is definitely not linear. This implies that even a small reduction in shrinkage may have a substantial benefit in reducing the potential for cracking.

Figure 5.14(b) illustrates how the concentration of one SRA may be related to the shrinkage that may be experienced in a concrete element. As the concentration of the SRA increases, the free shrinkage decreases. The reduction in shrinkage is not proportional to the concentration of the SRA, but rather to the surface tension (Fig. 5.4). Using diagrams like those in Fig. 5.14 may provide a powerful method to determine which concentration of SRA should be used for a particular application.[‡]

5.3.7 Influence of SRA on mechanical properties and durability—In addition to assessing its influence on shrinkage and cracking, it is crucial to understand the role that SRA plays on other material properties. Section 5.3.7.1 describes the role of SRA on mechanical property development and durability-related properties.

5.3.7.1 Mechanical properties of concrete containing SRA—A delay in initial set and an increase in the time between initial and final set is typically observed for mixtures containing SRA (Nmai et al. 1998; Weiss et al. 1999a; Folliard and Berke 1997). Figure 5.15 illustrates the results from one study. According to He et al. (2006), however, SRAs retard the hydration of portland cement under normal curing conditions, whereas under semi-adiabatic conditions, it seems that SRAs accelerate the hydration process. The temperature measurements by He et al. (2006) show that the additions of SRA (1.5 and 2%) slightly

[‡]This only considers cracking due to autogenous and drying shrinkage. To fully prevent cracking, thermal cracking and mechanical loading would also need to be considered.

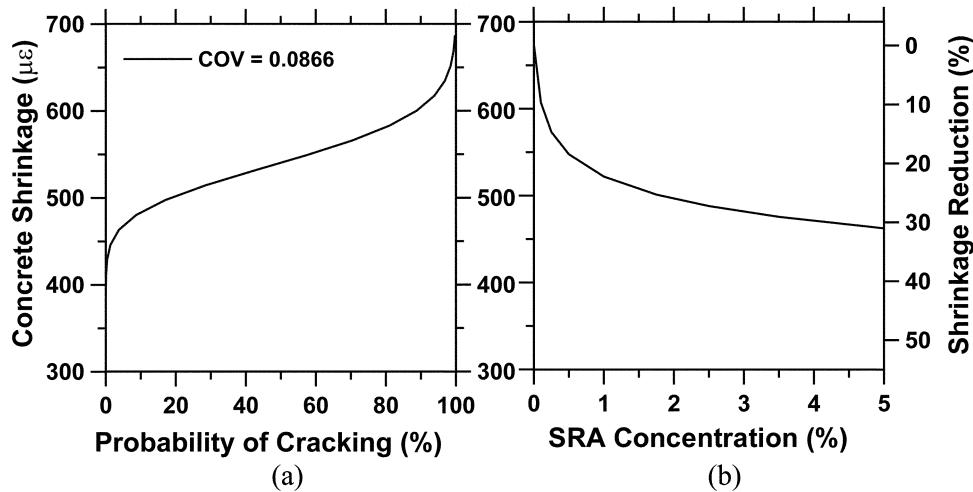


Fig. 5.14—The results of simulations showing how the addition of SRA may decrease the probability of cracking and to relate this to the concentration of SRA that may be used in mixture proportioning (Radlinska and Weiss 2006b).

increase the peak semi-adiabatic temperature for cement paste with a low w/cm (0.35). Conversely, lower temperature and later temperature development was observed by Weiss et al. (1999a) and Sant et al. (2006a,b).

The influences of SRA on the mechanical properties such as strength or stiffness have also been evaluated. Several researchers reported a reduction in strength and stiffness for water-cured specimens. For example, Brooks and Jiang (1994) reported a lower compressive strength (28%), tensile strength (30 to 40%), flexural strength (10 to 15%), and modulus of elasticity (38%) for specimens containing SRA. Cope and Ramey (2001) reported the compressive strength and elastic modulus were reduced by approximately 10%, while the splitting tensile strength was reduced by 8 to 34%. For concretes with and without silica fume, Folliard and Berke (1997) observed a 6 to 8% reduction in the 28-day strength for specimens.

Shah et al. (1992) reported that the influence of SRA on strength depended on the curing conditions, showing that poorly cured concrete (exposed to drying at 1 day) showed an increase in long-term strength and modulus with the addition of SRA, whereas water-cured specimens containing SRA showed a 5 to 10% reduction in strength, and no change in modulus. Bentz et al. (2001b) observed a slight increase in compressive strength after 28 days for low w/c mortars cured in sealed conditions. Weiss et al. (1998a) reported the reduction in strength and modulus in SRA mixtures was higher (15%) in a poorly cured low w/cm (0.29) specimen than it was in normal-strength concretes, which showed little effect of SRA (Fig. 5.16).

Few experimental investigations have been reported on the influence of SRAs on creep. In studies conducted by Brooks and Jiang (1994) using a propylene glycol ether SRA, a significant reduction in the creep of concrete was observed as shown in Fig. 5.17(a). Research by D'Ambrosia et al. (2001) reported a 17% reduction in the creep coefficient, as shown in Fig. 5.17(b). Although this reduction in creep would minimize

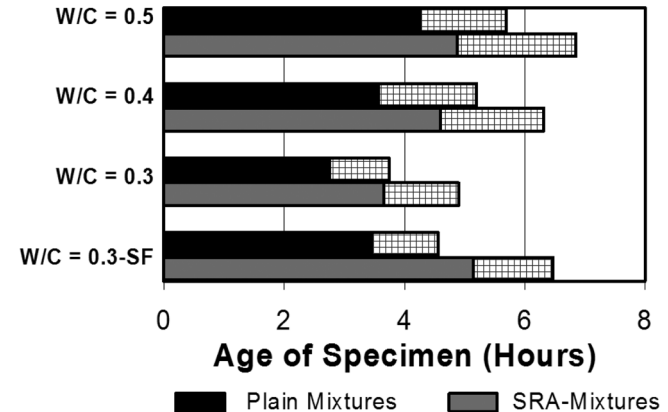


Fig. 5.15—Solid boxes denote time of initial set, while hatched boxes denote time of final set (Weiss et al 1999a). (Note: $w/c = w/cm$.)

vertical deflections or prestress losses, it may also increase residual stresses in a restrained shrinkage condition.

5.3.7.2 Durability properties of concrete containing SRA—The influence of SRA on fluid transport properties has been investigated by a few research groups. Cope and Ramey (2001) reported rapid chloride penetration (RCPT) values for concrete with and without SRA that were similar, while other researchers observed a slight reduction in RCPT values with SRA (Weiss et al. 1998a). Studies to determine the influence of SRA on corrosion indicated a beneficial effect in mixtures containing SRA (Berke et al. 1997).

The influence of SRA on fluid penetration was dramatically different between specimens with and without the SRA (Weiss 1999; Kehlem 1988). Specimens containing SRA show a slower fluid penetration, with the depth of fluid absorption being proportional to the square root of the surface tension/viscosity of the liquid. For a 4% SRA concentration, the surface tension would be reduced by 40%,

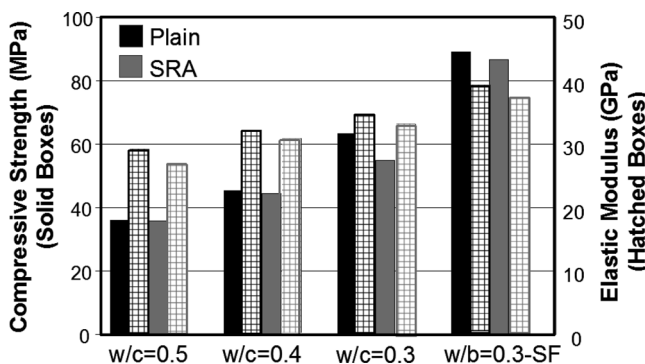


Fig. 5.16—Influence of SRA on strength and elastic modulus development (Weiss et al. 1999a). (Note: 145 psi = 1 MPa; 145,038 psi = 1 GPa.)

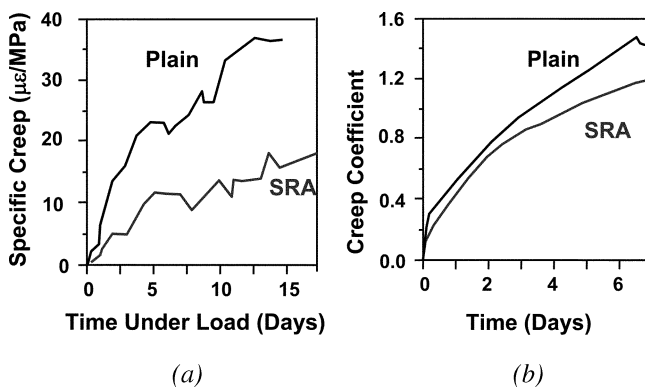


Fig. 5.17—(a) Specific tensile creep in concrete containing SRA (Brooks and Jiang 1994); and (b) the tensile creep coefficient with and without SRA (D'Ambrosia et al. 2001). (Note: 145 psi = 1 MPa.)

which corresponds with the reduction in capillary suction forces, sorptivity, and slower penetration.

One disadvantage of using an SRA is that it may destabilize the air void system. A proper air void system is essential to achieve good freezing-and-thawing resistance and durability performance. Some studies have indicated that proper air void structures may not always be obtained when SRAs are used (Cope and Ramey 2001), especially when changes in the admixtures and mixture proportions were not made to improve the quality of the air void system and increase strength. Other studies, however, have shown that acceptable air void systems are obtainable with glycol ether-based SRAs (Bae et al. 2002). Folliard and Berke (1997) found that air content and unit weight were not affected significantly by the use of an SRA. The ability to produce the air void system needed to achieve good freezing-and-thawing resistance is related to the proper choice of compatible admixtures, and it is recommended that a polycarboxylate-based high-range water-reducing admixture be used if a high-range water-reducing admixture is used. The ability to obtain a good air void system is significantly improved when the SRAs are used with a polycarboxylate high-range water-reducing admixture and tall, oil-based air entrainer (Lura et al. 2005). By saturating lightweight fine aggregates with an SRA

solution, as opposed to its conventional introduction via the mixing water, higher air content is achievable in fresh mortars (Bentz 2005b).

5.4—Internal curing

5.4.1 General—The term “internal curing” implies the introduction of a component into the concrete mixture that serves as a curing agent. Researchers suggested incorporating saturated porous aggregate such as lightweight aggregate or superabsorbent polymers (SAPs) to achieve some degree of internal curing (Philleo 1991; Bentz and Snyder 1999; Jensen and Hansen 2001). These porous materials act as internal reservoirs, providing an internal source of water necessary to replace that consumed by chemical shrinkage during hydration. As the cement hydrates, this extra water will be drawn from the relatively large pores in the curing agents into the much smaller ones in the cement paste. This process of internal curing will minimize the development of autogenous shrinkage and help avoid early-age cracking.

5.4.2 Lightweight aggregates—Because the autogenous stresses are inversely proportional to the diameter of the pores being emptied, for internal curing to do its job, the individual pores in the internal reservoirs should be much larger than the typical sizes of the capillary pores (inches [micrometers]) in the hydrating cement paste, and should also be well connected (percolated). During the hydration of the cement, the system of capillary pores in the three-dimensional paste microstructure is refined. The radii of these pores are generally smaller than the pores in the lightweight aggregate. As soon as the internal RH decreases (due to chemical shrinkage and self-desiccation), humidity gradient and capillary pressures develop.

With the lightweight aggregate acting as a water reservoir, the pores of the cement paste absorb the water from the lightweight aggregate via capillary suction (Hoff 2002). The capillary forces within the cement paste are large enough to transport water from the lightweight aggregate’s internal reservoirs to the drying/hydrating cement paste, where continuing hydration may then occur (Weber and Reinhardt 1999). The remaining unhydrated cement particles then have more free water available for hydration, and the capillary pores within the cement paste microstructure remain saturated. As new hydration products form, the capillary pores are further reduced in size, further increasing the capillary suction and drawing more water from the internal reservoirs (Weber and Reinhardt 1999). Water movement from the lightweight aggregate to the hydrating paste will stop only when all the cement is hydrated or when the RH within the lightweight aggregate’s internal reservoir is equivalent to that in the hydrating cement paste, eliminating the humidity (and capillary pressure) gradient (Weber and Reinhardt 1999).

5.4.3 Superabsorbent polymers—Superabsorbent polymers are chains of polymers interconnected with each other and have dissociated, ionic functional groups (Lam 2005). Early forms of SAPs were chemically modified starch and cellulose and other polymers like poly(vinyl alcohol) (PVA) and poly(ethylene oxide). Most of today’s SAPs are from partially

neutralized, lightly crosslinked poly(acrylic) acids (Buchholz and Graham 1998). With its high affinity for water, SAP will swell into a gel-like substance once in contact with water. The SAP will continue to swell until it has reached its threshold for absorption, which may vary from 20 to 2000 times its own mass in water (Jensen and Hansen 2001). When saturated SAP comes into contact with other ionic substances such as salt, the polymer releases the water due to the fact that the dissolved salt is electrically charged and attracts the water molecules from the SAP (Lam 2005). The absorption capacity of a SAP will, therefore, also depend on the ionic concentration of the pore solution in a concrete.

5.4.4 Mixture proportioning for internal curing—The effectiveness of lightweight aggregate as an internal curing agent depends primarily on four factors: 1) the amount of water in the lightweight aggregate; 2) the lightweight aggregate particle spacing factor; 3) the lightweight aggregate pore structure; and 4) the strength and shape of the lightweight aggregate (Mack 2006). The optimum amount of lightweight aggregate used to supply internal curing is a function of the type of lightweight aggregate used, the amount and size of that lightweight aggregate, the degree of moisture preconditioning the lightweight aggregate receives, the *w/cm* at mixing, the type and amount of binders used in the concrete mixture, and the extent and amount of external moist curing afforded to the concrete element (Hoff 2002). An equation to estimate the amount of lightweight aggregate needed for internal curing for any given concrete mixture was developed (Bentz et al. 2005)

$$M_{LWA} = \frac{C \times CS \times \alpha_{max}}{S \times \phi_{LWA}} \quad (5-3)$$

where

- M_{LWA} = mass of (dry) fine lightweight aggregate needed per unit volume of concrete (lb/yd^3 or kg/m^3);
- C = cement factor (content) for concrete mixture (lb/yd^3 or kg/m^3);
- CS = chemical shrinkage of cement (mass of water/mass of cement);
- α_{max} = maximum expected degree of hydration of cement (0 to 1);
- S = degree of saturation of aggregate (0 to 1); and
- ϕ_{LWA} = desorption of lightweight aggregate from saturation down to 93% RH (mass water/mass dry lightweight aggregate).

Scanning electron microscope images of mortar mixtures show that the mixture that contains lightweight sand may be easily distinguished from the control mixture due to its concentrated pores and voids within the lightweight sand particles, as shown in Fig. 5.18 (Lam 2005).

5.4.5 Water movement during internal curing (X-ray microtomography)—In low *w/cm* concretes (≤ 0.45), external curing has limited effectiveness beyond a few inches (millimeters) from the surface. The reason is that the capillary pores quickly become depercolated (disconnected) by the formation of hydration products, and water is no

longer able to penetrate into the concrete from the exposed surface at a rate sufficient to satisfy the demand of the ongoing hydration. Reasonable estimates based on balancing the water needed for the continuing hydration versus the water available from internal water reservoirs distributed uniformly throughout the concrete show the various distances that water will be expected to travel at different curing ages (Table 5.1) (Bentz et al. 2007). The early- and middle-age estimates are in good agreement with X-ray absorption analyses of mortars during curing.

For early age improvements of the characteristics of (high-performance) concrete, water availability for the hydration of the cement is especially critical. Without it, significant autogenous shrinkage and possibly cracking may occur. Strength is also impacted, because without hydration, strength gain does not occur. Water movement during the internal curing of a high-performance mortar was directly observed using three-dimensional X-ray microtomography with a voxel dimension of approximately 8×10^{-4} in. (20 μm) (Bentz et al. 2006a,b). With this technique, the emptying of individual pores within individual internal water reservoirs in the lightweight aggregate may be readily observed. The procedure shows that much of the reservoir water is removed during the first 24 hours of hydration at 86°F (30°C). The observations of water movement are in quantitative agreement with more conventional measures of performance, including degree of hydration and chemical shrinkage (Bentz et al. 2006b). In Fig. 5.19 and 5.20, the aqua regions show volumes and areas from the three- and two-dimensional microstructures, respectively, where the lightweight aggregate particles lost water to the surrounding hydrating cement paste (Bentz et al. 2006a).

5.4.6 Effect of internal curing on early-age shrinkage—Internal curing has been investigated intensively since the early 1990s as a means to reduce early-age shrinkage and self-induced stresses in high-performance concrete infrastructure by introducing a component into the concrete that serves as a curing agent (Philleo 1991; Weber and Reinhardt 1995; Vaysburd 1996; Jensen and Hansen 2001; Geiker et al. 2004). The generally used curing agents (water reservoirs) may be either presaturated lightweight aggregates or SAPs that act as internal reservoirs, providing an internal source of water necessary to replace that consumed by chemical shrinkage during hydration. Figure 5.21 shows the autogenous deformation of mortars at a curing temperature of 86°F (30°C) (Geiker et al. 2004). The reference mortar is designated fine silica fume (FSF) and contains 8% silica fume. For Mixtures LWA20 and LWA08, either 20 or 8%, respectively, of the sand by mass was replaced by saturated surface-dry lightweight aggregate smaller than 0.16 in. (4 mm). A 0.4% addition (mass fraction of cement) of SAP particles was used in mixture SAP. The results show that internal curing is highly effective in reducing autogenous shrinkage. The LWA20 mixture totally eliminated autogenous shrinkage, resulting in an autogenous expansion due to the extra curing water. According to Geiker et al. (2004), an additional benefit of internal curing is the increase of degree of hydration and, consequently, the compressive strength at later ages.

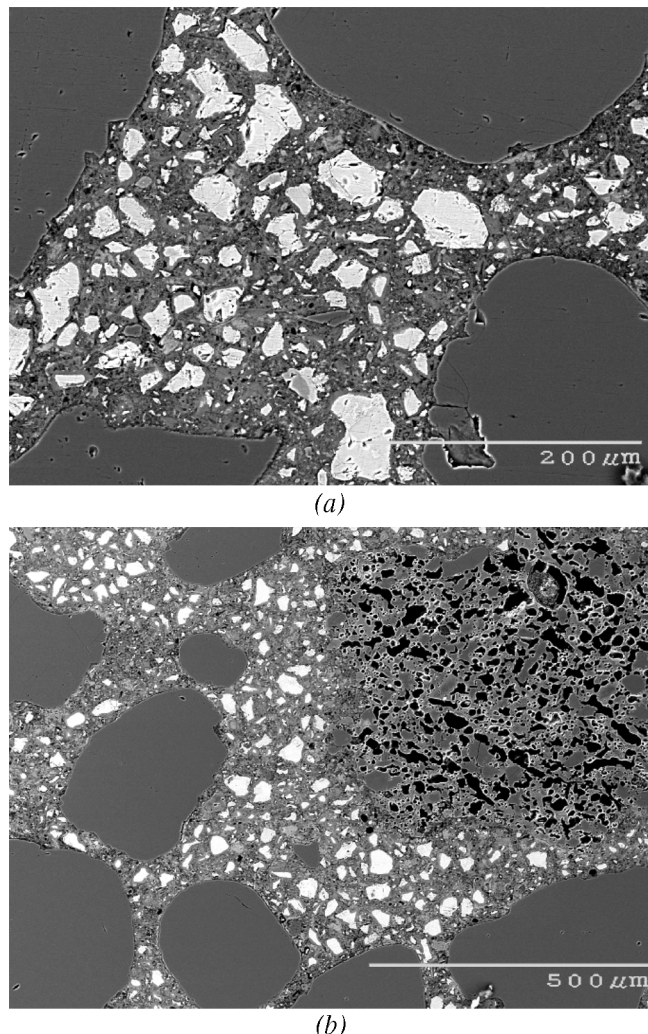


Fig. 5.18—Scanning electron image of mortar: (a) control mixture; and (b) mixture with lightweight sand replacement (Lam 2005); areas that appear bright gray to near white represent anhydrous portion, hydrated phases and quartz aggregate appear gray, and porosity appears dark. (Note: 3.94×10^{-5} in. = 1 μm .)

Table 5.1—Distance of water travel from surfaces of internal reservoirs (Bentz et al. 2007)

Hydration age	Estimate travel distance for water
Early (for example, <1 day)	0.79 in. (20 mm)
Middle (for example, 1 to 3 days)	0.20 in. (5 mm)
Late (for example, 3 to 7 days)	0.04 in. (1 mm)
Worst case (for example, >28 days)	0.001 in. (0.25 mm)

5.4.7 Effect of internal curing on early-age strength—As internal curing maintains saturation within the capillary pore system of the hydrating cement paste, it will also contribute to an enhancement in achieved hydration, particularly at later ages under sealed curing conditions. Depending on the strength characteristics of the internal reservoirs themselves, this increased hydration may translate into a strength gain for an internally cured mortar or concrete, relative to a control with no internal curing. Such a strength gain was observed

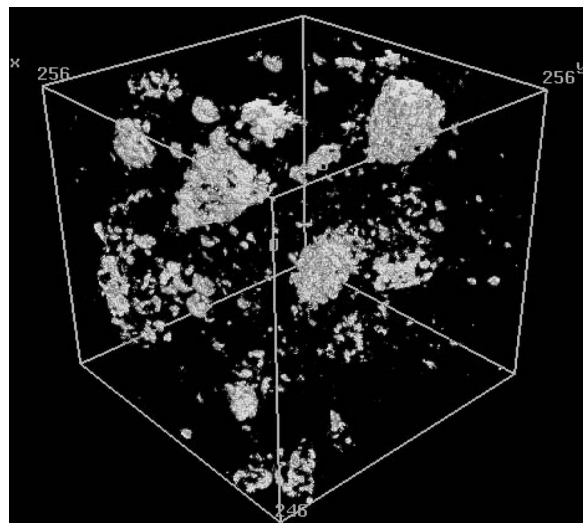


Fig. 5.19—Three-dimensional coded image of original X-ray microtomography data set subtracted from that obtained after 1 day of hydration for high-performance mortar with internal curing (Bentz et al. 2006a). Light gray volumes indicate regions where the LWA particles have lost water (to the surrounding hydrating cement paste). Three-dimensional volume is $0.181 \times 0.181 \times 0.185$ in. (4.6 x 4.6 x 4.7 mm).

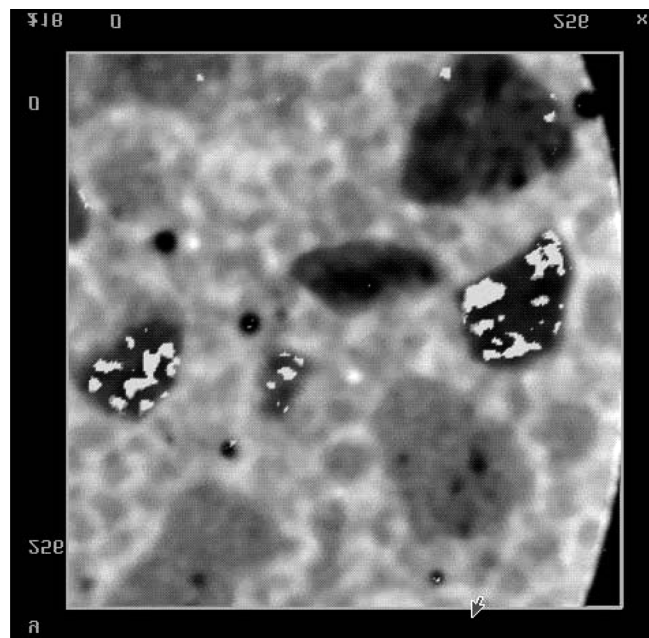


Fig. 5.20—Two-dimensional image (0.181×0.181 in. [4.6 x 4.6 mm]) of a portion of the original mortar microstructure with locations of evacuated water (in light gray) superimposed (Bentz et al. 2006a).

for the mortars with internal curing by Geiker et al. (2004), whose autogenous deformation measurements are presented in Fig. 5.21. The autogenous deformation and compressive strength development of a series of high-performance mortars based on blended cements were measured (Bentz 2007). The results summarized in Table 5.2 indicate that for each of the three blended cement high-performance mortars

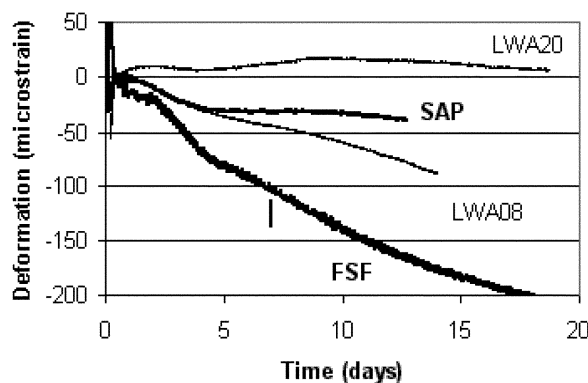


Fig. 5.21—Autogenous shrinkage (– is shrinkage) for mortars containing different internal curing agents, all cured at 86°F (30°C) (Geiker et al. 2004).

(silica fume, slag, and fly ash), internal curing results in approximately a 10% strength gain (relative to the control) at 28 days and beyond. These mortars were prepared with a $w/cm = 0.3$ and were cured under sealed conditions at 77°F (25°C) (Bentz 2007). In the internally cured mixtures, generally 0.08 extra mass units of water per unit mass of cement were added via the saturated lightweight aggregate. For the mortars using the silica fume blended cement, both 0.08 and 0.10 water additions via internal curing were investigated, as indicated by the designations IC(8) and IC(10) in Table 5.2.

Testing laboratory results have also indicated that early-age strength gains may be achieved by the incorporation of internal curing into high-performance concrete mixtures. For example, the results presented in Table 5.3 were obtained for a $w/cm = 0.395$, 2 in. (50 mm) slump concrete produced with only one chemical admixture (an air entrainer). At ages from 1 to 56 days, the mixture produced with internal curing exhibited strength gains over the control of as much as 44% at 3 days, to as little as 9% at 56 days. The original control mixture contained 1360 lb/yd³ (807 kg/m³) of normalweight sand and in the mixture with internal curing; 280 lb/yd³ (166 kg/m³) of this sand were replaced with 200 lb/yd³ (119 kg/m³) of saturated surface-dry lightweight aggregate sand. These concrete specimens were prepared and cured using conventional laboratory procedures, remaining in their molds for the first 24 hours and then being immersed in a tank of lime-saturated water throughout the remainder of their curing time (Roberts 2004).

For concretes for pavement applications, higher early-age flexural strength is desirable to get traffic on the road with minimal delay. Concrete mixtures with $w/cm = 0.433$ and internal curing at a level of 100 lb/yd³ (59 kg/m³) saturated lightweight aggregate replacement for natural sand have indicated that 74% of the 28-day flexural strength was achieved in 3 days, which is an improvement of 7% over the control mixture. The 3-day flexural strength of the internally cured mixture was 15% greater than that of the control. At 28 days, the flexural strength of the mixture with internal curing exceeded that of the control mixture by 8% (Roberts 2005).

If the internally cured sand is not saturated surface-dry (SSD), early-age strength improvements are delayed to a later

Table 5.2—Measured mortar cube compressive strengths for various mixtures* (Bentz 2007)

Mixture	3-day strength, psi (MPa)	8-day strength, psi (MPa)	28-day strength, psi (MPa)	56-day strength, psi (MPa)
SF – Control	9878 (68.1 [2.0]) [†]	11,665 (80.4 [3.0])	—	14,232 (98.0 [2.7])
SF – IC(8)	9843 (67.9 [4.6])	12,743 (87.9 [4.6])	—	15,312 (105.6 [6.9])
SF – IC(10)	9670 (66.7 [1.4])	12,327 (85.0 [2.9])	13,531 (93.3 [4.7])	—
SLAG – Control	8827 (60.9 [0.9])	10,376 (71.5 [2.0])	11,863 (81.8 [3.2])	12,226 (84.3 [5.7])
SLAG – IC	8581 (59.2 [4.2])	10,399 (71.7 [2.3])	12,873 (88.8 [3.9])	13,729 (94.6 [1.0])
FA – Control	8407 (58.0 [0.5])	10,224 (70.5 [3.3])	12,365 (85.3 [3.4])	13,827 (95.3 [4.0])
FA – IC	8324 (57.4 [2.3])	9794 (67.5 [3.5])	13,471 (92.9 [3.8])	14,665 (101.1 [2.9])

* SF = silica fume; FA = fly ash; and IC = internal curing.

[†]Numbers in parentheses indicate measured standard deviation, in MPa, for compressive strengths of three replicate cubes at each age for each mixture.

Table 5.3—Compressive strengths of $w/cm = 0.395$ concrete mixtures with and without internal curing (Roberts 2004)

Age, days	Control strength, psi (MPa)	Internal curing strength, psi (MPa)	Percent improvement with internal curing
1	2760 (19.0)	3210 (22.1)	16
3	3620 (25.0)	5320 (36.1)	44
7	4780 (33.0)	5410 (37.3)	13
28	5510 (38.0)	6160 (42.5)	12
56	6340 (43.7)	6900 (47.6)	9

time. For instance, at 62% of potential SSD, it takes time to adjust, as the lightweight aggregate first imbibes water in from the mixing water before it later starts to desorb. In this situation, strengths may still be above those of the control at 3 days. There are three reasons for this: 1) water is so fluid; 2) the capillary action within the hydrating cement paste is so strong; and 3) the water demand of the cement is so intense.

CHAPTER 6—REFERENCES

6.1—Referenced standards and reports

The standards and reports listed below were the latest editions at the time this document was prepared. Because these documents are revised frequently, the reader is advised to contact the proper sponsoring group if it is desired to refer to the latest version.

American Concrete Institute

- 207.1R Guide to Mass Concrete
- 207.2R Report on Thermal and Volume Change Effects on Cracking of Mass Concrete
- 209R Prediction of Creep, Shrinkage, and Temperature Effects in Concrete Structures

ASTM International

- C157 Standard Test Method for Length Change of Hardened Hydraulic-Cement Mortar and Concrete
- C1581 Standard Test Method for Determining Age at Cracking and Induced Tensile Stress Characteristics

- of Mortar and Concrete under Restrained Shrinkage
C1608 Standard Test Method for Chemical Shrinkage of Hydraulic Cement Paste

These publications may be obtained from these organizations:

American Concrete Institute
38800 Country Club Drive
Farmington Hills, MI 48331
www.concrete.org

ASTM International
100 Barr Harbor Drive
West Conshohocken, PA 19428
www.astm.org

6.2—Cited references

Acker, P., 2004, "Why Does Ultrahigh-Performance Concrete (UHPC) Exhibit Such Low Shrinkage and Such Low Creep?" *Autogenous Deformation of Concrete*, SP-220, O. M. Jensen, D. P. Bentz, and P. Lura, eds., American Concrete Institute, Farmington Hills, MI, pp. 141-154.

Adamson, A. W., 1990, *Physical Chemistry of Surfaces*, fifth edition, John Wiley and Sons, pp. 71, 777.

Ai, H., and Young, J. F., 1997, "Mechanisms of Shrinkage Reduction Using a Chemical Admixture," *Proceedings of the 10th International Congress on the Chemistry of Cement*, V. 3, H. Justnes, ed., Gothenburg, Sweden, 8 pp.

Altoubat, S. A., 2000, "Early Age Stresses and Creep-Shrinkage Interaction of Restrained Concrete," PhD dissertation, Department of Civil and Environmental Engineering, University of Illinois at Urbana-Champaign, Urbana, IL, 221 pp.

Altoubat, S. A., and Lange, D. A., 2002, "Grip-Specimen Interaction in Uniaxial Restrained Test," *Concrete: Material Science to Application—A Tribute to Surendra P. Shah*, SP-206, P. Balaguru, A. Naaman, and W. Weiss, eds., American Concrete Institute, Farmington Hills, MI, pp. 189-204.

Altoubat, S. A., and Lange, D. A., 2003, "Early Age Creep," *Early Age Cracking in Cementitious Systems*, RILEM Report 25, TC-181 EAS, A. Bentur, ed., pp. 57-62.

American Association of State Highway and Transportation Officials (AASHTO), 2004, *AASHTO Guide for Design of Pavement Structures*, Washington, DC, 640 pp.

American Association of State Highway and Transportation Officials (AASHTO), 2007, "Standard Test Method for Coefficient of Thermal Expansion of Hydraulic Cement Concrete," *AASHTO TP 60-00, 2007 AASHTO Provisional Standards*, Washington, DC, 8 pp.

Attiogbe, E. K.; See, H. T.; and Miltenberger, M. A., 2001, "Tensile Creep in Restrained Shrinkage, Creep, Shrinkage and Durability Mechanics of Concrete and Other Quasi-Brittle Materials," *Proceedings of the 6th International Conference CONCREP-6*, F. J. Ulm, Z. P. Bažant, and F. H. Wittmann, eds., Elsevier Science, pp. 651-656.

Attiogbe, E. K.; See, H. T.; and Miltenberger, M. A., 2003, "Cracking Potential of Concrete Under Restrained

Shrinkage," *Proceedings, Advances in Cement and Concrete: Volume Changes, Cracking, and Durability*, Engineering Conferences International, Copper Mountain, CO, pp. 191-200.

Attiogbe, E. K.; Weiss, W. J.; and See, H. T., 2004, "A Look at the Stress Rate Versus Time of Cracking Relationship Observed in The Restrained Ring Test," *Advances in Concrete Through Science and Engineering*, Northwestern University, Evanston, IL, 14 pp.

Bae, J.; Berke, N. S.; Hoopes, R. J.; and Malone, J., 2002, "Freezing and Thawing Resistance of Concretes with Shrinkage Reducing Admixtures," *Frost Resistance of Concrete: From Nano-Structure and Pore Solution to Macroscopic Behaviour and Testing*, PRO 24, RILEM, pp. 327-333.

Barde, A.; Parmaswaren, S.; Chariton, T.; Weiss, J.; Cohen, M.; and Newbolds, S., 2006, "Evaluation of Rapid Setting Cement-Based Materials for Patching and Repair," *Report to the Joint Transportation Research Board*, 155 pp.

Baroghel-Bouny, V., 1996, "Texture and Moisture Properties of Ordinary and High-Performance Cementitious Materials," *Proceedings of Séminaire RILEM*, 'Benton: du Matériaux à la Structure,' Sept., Arles, France, pp. 144-165.

Baroghel-Bouny, V., 1997, "Experimental Investigation of Self-Desiccation in High-Performance Materials—Comparison with Drying Behaviour in Self-Desiccation and its Importance in Concrete Technology," *Proceedings of the 1st International Seminar*, B. Persson and G. Fagerlund, eds., Lund University, Lund, pp. 72-87.

Bažant, Z. P., 1972, "Prediction of Concrete Creep Effects Using Age-Adjusted Effective Modulus Method," *ACI JOURNAL, Proceedings* V. 69, No. 4, Apr., pp. 212-217.

Bažant, Z. P., and Panula, L., 1978, "Practical Prediction of Time-Dependent Deformations of Concrete," *Material and Structures*, V. 11, pp. 307-328.

Bažant, Z. P., and Raftshol, W. J., 1982, "Effect of Cracking in Drying and Shrinkage Specimens," *Cement and Concrete Research*, V. 12, pp. 209-226.

Bentur, A., 2003, "Early Age Shrinkage Induced Stresses and Cracking in Cementitious Systems," *RILEM Technical Committee 191-EAS*, RILEM Publications, 337 pp.

Bentur, A.; Berke, N. S.; Dallaire, M. P.; and Durning, T., 2001, "Crack Mitigation Effects of Shrinkage Reducing Admixtures," *Design and Construction Practices to Mitigate Cracking*, SP-204, E. G. Nawy, F. G. Barth, and R. J. Frosch, eds., American Concrete Institute, Farmington Hills, MI, pp. 155-170.

Bentz, D. P., 2005a, "Curing with Shrinkage-Reducing Admixtures: Beyond Drying Shrinkage Reduction," *Concrete International*, V. 27, No. 10, Oct., pp. 55-60.

Bentz, D. P., 2005b, "Capitalizing on Self-Desiccation for Autogenous Distribution of Chemical Admixtures in Concrete," *Proceedings of the 4th International Seminar on Self-Desiccation and Its Importance in Concrete Technology*, Lund University, Lund, pp. 189-196.

Bentz, D. P., 2006, "Influence of Shrinkage-Reducing Admixtures on Drying, Autogenous Shrinkage, and Freezable

- Water Content of Cement Pastes at Early Ages," *Journal of Advanced Concrete Technology*, V. 4, No. 3, pp. 423-429.
- Bentz, D. P., 2007, "Internal Curing of High-Performance Blended Cement Mortars," *ACI Materials Journal*, V. 104, No. 4, July-Aug., pp. 408-414.
- Bentz, D. P., and Snyder, K. A., 1999, "Protected Paste Volume in Concrete: Extension to Internal Curing Using Saturated Lightweight Fine Aggregates," *Cement and Concrete Research*, V. 29, pp. 1863-1867.
- Bentz, D. P.; Jensen, O. M.; Hansen, K. K.; Oleson, J. F.; Stang, H.; and Haecker, C. J., 2001a, "Influence of Cement Particle Size Distribution on Early Age Autogenous Strains and Stresses in Cement-Based Materials," *Journal of the American Ceramic Society*, V. 84, No. 1, pp. 129-135.
- Bentz, D. P.; Hansen, K. H.; and Geiker, M. R., 2001b, "Shrinkage-Reducing Admixtures and Early Age Desiccation in Cement Pastes and Mortars," *Cement and Concrete Research*, V. 31, No. 7, pp. 1075-1085.
- Bentz, D. P.; Lura, P.; and Roberts, J., 2005, "Mixture Proportioning for Internal Curing," *Concrete International*, V. 27, No. 2, Feb., pp. 35-40.
- Bentz, D. P.; Halleck, P. M.; Grader, A. S.; and Roberts, J. W., 2006a, "Direct Observation of Water Movement during Internal Curing Using X-ray Microtomography," *Concrete International*, V. 28, No. 10, Oct., pp. 39-45.
- Bentz, D. P.; Halleck, P. M.; Grader, A. S.; and Roberts, J. W., 2006b, "Four-Dimensional X-Ray Microtomography Study of Water Movement During Internal Curing," *Proceedings of the International RILEM Conference—Volume Changes of Hardening Concrete: Testing and Mitigation*, O. M. Jensen, P. Lura, and K. Kovler, eds., RILEM Publications S.A.R.L., Bagneux, France, pp. 11-20.
- Bentz, D. P.; Koenders, E. A. B.; Mönnig, S.; Reinhardt, H. W.; van Breugel, K.; and Ye, G., 2007, "Materials Science-Based Models in Support of Internal Water Curing," *RILEM Report* 41, RILEM Publications SARL, pp. 29-43.
- Berke, N. S.; Dallaire, M. P.; Hicks, M. C.; and Kerkar, A., 1997, "New Developments in Shrinkage-Reducing Admixtures," *Superplasticizers and Other Chemical Admixtures in Concrete*, Proceedings of the Fifth CANMET/ACI International Conference, SP-173, V. M. Malhotra, ed., American Concrete Institute, Farmington Hills, MI, pp. 971-998.
- Bisschop J., 2002, "Drying Shrinkage Microcracking in Cement-Based Materials," PhD thesis, Delft University Press, Netherlands, 198 pp.
- Bjontegaard, Ø., 1999, "Thermal Dilation and Autogenous Deformation as Driving Forces to Self-Induced Stress in High Performance Concrete," Doctoral dissertation, Norwegian University of Science and Technology, 256 pp.
- Bloom, R., and Bentur, A. 1995, "Free and Restrained Shrinkage of Normal and High-Strength Concretes," *ACI Materials Journal*, V. 92, No. 2, Mar.-Apr., pp. 211-217.
- Boivin, S.; Acker, P.; Rigaud, S.; and Clavaud, B., 1999, "Experimental Assessment of Chemical Shrinkage of Hydrating Cement Paste," *Autogenous Shrinkage of Concrete*, E. Tazawa, ed., E&FN Spon, London, pp. 81-92.
- Breitenbücher, R., 1990, "Investigation of Thermal Cracking with the Cracking-Frame," *Materials and Structures*, V. 23, No. 135, pp. 172-177.
- Breitenbücher, R., and Mangold, M., 1994, Minimization of Thermal Cracking in Concrete at Early Ages, *RILEM Proceedings 25, Thermal Cracking in Concrete at Early Ages*, R. Springenschmid, ed., E&FN Spon, London, pp. 205-212.
- Brewer, H. W., and Burrows, R. W., 1951, "Coarse Ground Cement Makes More Durable Concrete," *ACI JOURNAL, Proceedings*, V. 47, No. 1, Jan., pp. 353-360.
- Brooks, J. J., and Jiang, X., 1994, "The Influence of Chemical Admixtures on Restrained Drying Shrinkage of Concrete," *Chemical Admixtures*, SP-173, American Concrete Institute, Farmington Hills, MI, pp. 249-265.
- Brown, K.; Brown, A. W.; Colpitts, B. G.; and Bremner, T. W., 2004, "The Mitigation of Measurement Inaccuracies of Brillouin Scattering Based Fiber Optic Sensors through Bonded Fiber Temperature Calibrations," *7th Cansmart Workshop: Smart Materials and Structures*, Montreal, QC, Canada, pp. 317-324.
- Buchholz, F. L., and Graham, A. T., 1998, *Modern Superabsorbent Polymer Technology*, John Wiley & Sons Inc., New York, 304 pp.
- Burnham, T., and Koubaa, A., 2001, "A New Approach to Estimate the In-Situ Thermal Coefficient and Drying Shrinkage for Jointed Concrete Pavement," *Proceedings of the 7th International Conference on Concrete Pavements*, Orlando, FL, 13 pp.
- Burrows, R. W., 1998, "The Visible and Invisible Cracking of Concrete," *Monograph No. 11*, American Concrete Institute, Farmington Hills, MI, 78 pp.
- Burrows, R. W.; Kepler, W. F.; Hurcomb, D.; Schaffer, J.; and Sellers, G., 2004, "Three Simple Tests for Selecting Low-Crack Cement," *Cement and Concrete Composites*, V. 26, No. 5, pp. 509-519.
- Byfors, J., 1980, "Plain Concrete at Early Ages," *Report* 3:80, Swedish Cement and Concrete Research Institute, 464 pp.
- Carlson, R. W., 1942, "Cracking of Concrete," *Boston Society of Civil Engineers*, V. 29, No. 2, pp. 98-109.
- Carlson R. W., 1988, "Model of Studying Shrinkage Cracking in Concrete Building Walls," *ACI Structural Journal*, V. 85, No. 4, July-Aug., pp. 395-404.
- Chariton, T., and Weiss, W. J., 2002, "Using Acoustic Emission to Monitor Damage Development in Mortars Restricted from Volumetric Changes," *Concrete: Material Science to Application—A Tribute to Surendra P. Shah*, SP-206, P. Balaguru, A. Naaman, and W. Weiss, eds., American Concrete Institute, Farmington Hills, MI, pp. 205-218.
- Cope, B. L., and Ramey, G. E., 2001, "Reducing Drying Shrinkage of Bridge Deck Concrete," *Concrete International*, V. 23, No. 8, Aug., pp. 76-82.
- Coutinho, A. S., 1959, "The Influence of the Type of Cement on its Cracking Tendency," *RILEM Bulletin*, V. 5, pp. 26-40.
- Cusson, D., and Hoogeveen, T., 2007, "New Test Method for Determining Coefficient of Thermal Expansion at Early Age in High-Performance Concrete," *12th International Conference on Chemistry of Cement*, Montreal, QC, Canada, pp. 1-12.

- D'Ambrosia, M. D.; Altoubat, S.; Park, C.; and Lange, D. A., 2001, "Early-Age Tensile Creep and Shrinkage of Concrete with Shrinkage Reducing Admixtures," *Creep, Shrinkage, and Durability Mechanics of Concrete and Other Quasi-Brittle Materials*, F. J. Ullm, Z. P. Bažant, and F. H. Wittman, eds., Elsevier, Cambridge, MA, pp. 645-651.
- Embong, M., 1989, "Thermal Stress in Concrete Structures at Early Ages," PhD thesis, Luleå University of Technology, Division of Structural Engineering, Luleå, Sweden, 285 pp.
- Embong, M., 1998, "Development of Mechanical Behavior at Early Ages," *Prevention of Thermal Cracking in Concrete at Early Ages*, RILEM Report 15, R. Springer-schmid, ed., E&FN Spon., London, pp. 76-148.
- Follard, K. J., and Berke, N. S., 1997, "Properties of High-Performance Concrete Containing Shrinkage-Reducing Admixture," *Cement and Concrete Research*, V. 27, No. 9, pp. 1357-1364.
- Geiker, M. R., and Knudsen, T., 1982, "Chemical Shrinkage of Portland Cement Pastes," *Cement and Concrete Research*, V. 12, pp. 603-610.
- Geiker, M. R.; Bentz, D. P.; and Jensen, O. M., 2004, "Mitigating Autogenous Shrinkage by Internal Curing," *High-Performance Structural Lightweight Concrete*, SP-218, J. P. Ries and T.A. Holm, eds., American Concrete Institute, Farmington Hills, MI, pp. 143-154.
- Gettu, R.; Roncero, J.; and Martin, M. A., 2007, "Study of the Behavior of Concrete with Shrinkage Reducing Admixtures Subjected to Long-Term Drying," *Concrete: Material Science to Application—A Tribute to Surendra P. Shah*, SP-206, P. Balaguru, A. Naaman, and W. Weiss, eds., American Concrete Institute, Farmington Hills, MI, pp. 157-166.
- Grasley, Z.; Lange, D. A.; and D'Ambrosia, M. D., 2006a, Internal Relative Humidity and Drying Stress Gradients in Concrete, *Materials and Structures*, V. 39, pp. 901-909.
- Grasley, Z. C.; Lange, D. A.; and Liu, Y.-S., 2006b, "Volume Change Mechanisms in Concrete: New Directions for Modeling," *Proceedings of the Knud Hojgaard Conference, Advanced Cement-Based Materials: Research and Teaching*, O. M. Jensen, M. Geiker, and H. Stang, eds., Technical University of Denmark, Lyngby, Denmark, pp. 77-87.
- Gryzbowski, M., and Shah, S. P., 1989, "Model to Predict Cracking in Fiber Reinforced Concrete Due to Restrained Shrinkage," *Magazine of Concrete Research*, V. 41, No. 8, pp. 125-135.
- Grzybowski, M., and Shah, S. P., 1990, "Shrinkage Cracking of Fiber Reinforced Concrete," *ACI Materials Journal*, V. 87, No. 2, Mar.-Apr., pp. 138-148.
- He, Z.; Li, Z.; Chen, M.; and Liang, W., 2006, "Properties of Shrinkage-Reducing Admixture-Modified Paste and Mortar," *Materials and Structures*, V. 39, pp. 445-453.
- Hedlund, H., 1996, "Stress in High Performance Concrete due to Temperature and Moisture Variations at Early Ages," Licentiate thesis, Sweden, 240 pp.
- Higgins, D. D., and Bailey, J. E., 1976, "A Microstructural Investigation of the Failure Behavior of Cement Paste," *Hydraulic Cement Pastes: Their Structure and Properties, Proceedings of an International Conference*, Sheffield, England, pp. 283-296.
- Hoff, G. C., 2002, *The Use of Lightweight Fines for the Internal Curing of Concrete*, Northeast Solite Corp., 44 pp.
- Holt, E., 2002, "Very Early Age Autogenous Shrinkage: Governed by Chemical Shrinkage or Self-Desiccation," *Proceedings of the Third International Research Seminar on the Importance of Self-Desiccation in Concrete*, B. Persson and G. Fagerlund, eds., Lund, pp. 1-26.
- Horai, K., 1971, "Thermal Conductivity of Rock-Forming Minerals," *Journal of Geophysical Research*, V. 76, No. 5, pp. 1278-1308.
- Hossain, A. B., and Weiss, W. J., 2004, "Assessing Residual Stress Development and Stress Relaxation in Restrained Concrete Ring Specimens," *Cement and Concrete Composites*, V. 26, pp. 531-540.
- Hossain, A. B.; Pease, B.; and Weiss, W. J., 2003, "Quantifying Early-Age Stress Development and Cracking in Low w/c Concrete Using the Restrained Ring Test with Acoustic Emission," *Transportation Research Record, Concrete Materials and Construction* 1834, pp. 24-33.
- Hossain, M.; Khanum, T.; Tanesi, J.; Schieber, G.; and Montney, R., 2006, "The PCC Coefficient of Thermal Expansion Input for the Mechanistic-Empirical Pavement Design Guide," *Paper No. 06-2573, Preprint CD-ROM of the 85th Annual Meeting of the Transportation Research Board*, Washington, DC, 21 pp.
- Hwang, C. L., and Young, J. F., 1984, "Drying Shrinkage of Portland Cement Pastes I. Microcracking during Drying," *Cement and Concrete Research*, V. 14, pp. 585-594.
- Israelachvili, J. N., 1991, *Intermolecular and Surface Forces*, second edition, Academic Press, London, 450 pp.
- Jeffery, G. B., 1921, "Plane Stress and Plane Strain in Bipolar Co-ordinates," *Philosophical Transactions of the Royal Society of London: Series A*, V. 221, pp. 265-293.
- Jensen, O. M., and Hansen, P. F., 1995, "A Dilatometer for Measuring Autogenous Deformation in Hardening Portland Cement Paste," *Materials and Structures*, V. 28, No. 181, pp. 406-409.
- Jensen, O. M., and Hansen, P. F., 1996, "Autogenous Deformation and Change of Relative Humidity in Silica Fume Modified Cement Paste," *ACI Materials Journal*, V. 93, No. 6, Nov.-Dec., pp. 539-543.
- Jensen, O. M., and Hansen, P. F., 2001, "Water-Entrained Cement-Based Materials: I. Principle and Theoretical Background," *Cement and Concrete Research*, V. 31, No. 4, pp. 647-654.
- Justnes, H.; Ardoullie, B.; Hendrix, E.; Sellevold, E. J.; and Gemert, D. V., 1998, "The Chemical Shrinkage of Pozzolanic Reaction Products," *Fourth CANMET/ACI/JCI Conference: Advances in Concrete Technology*, SP-179, American Concrete Institute, Farmington Hills, MI, pp. 191-205.
- Justnes, H.; Gemert, A. V.; Verboven, F.; and Sellevold, E., 1996, "Total and External Chemical Shrinkage of Low w/c Ratio Cement Pastes," *Advances in Cement Research*, V. 8, No. 31, pp. 121-126.
- Kehlem, S., 1988, "A Water Absorption Test for Concrete," *Magazine of Concrete Research*, V. 40, No. 143, pp. 106-110.

- Kim, K. H.; Jeon, S. E.; Kim, J. K.; and Yang, S., 2003, "An Experimental Study on Thermal Conductivity of Concrete," *Cement and Concrete Research*, V. 33, pp. 363-371.
- Koenders, E. A. B., and van Breugel, K., 2004, "Modeling Moisture Transport Processes in Cement Paste Systems," *The Challenge of Creativity*, FIB Symposium Proceedings, Avignon, Apr. 26-28. (CD-ROM)
- Kovler, K., 1994, "Testing System for Determining the Mechanical Behavior of Early-Age Concrete Under Restrained and Free Uniaxial Shrinkage," *Materials and Structures*, V. 27, No. 170, pp. 324-330.
- Kovler, K.; Sikuler, J.; and Bentur, A., 1993, "Restrained Shrinkage Tests of Fiber Reinforced Concrete Ring Specimens: Effect of Core Thermal Expansion," *Materials and Structures*, V. 26, pp. 231-237.
- Kovler, K.; Igarashi, S.; and Bentur, A., 1999, "Tensile Creep Behavior of High-Strength Concrete at Early Ages," *Materials and Structures*, V. 32, No. 219, pp. 383-387.
- Krauss, P. D.; Rogalla, E. A.; Sherman, M. R.; McDonald, D. B.; Osborn, A. E. N.; and Pfeifer, D.W., 1996, "Transverse Cracking in Newly Constructed Bridge Decks," *NCHRP Report 380*, Transportation Research Board, 91 pp.
- Krenchel, H., and Shah, S. P., 1987, "Restrained Shrinkage Tests with PP-Fiber Reinforced Concrete," *Fiber Reinforced Concrete*, SP-105, American Concrete Institute, Farmington Hills, MI, pp. 173-179.
- Lam, H., 2005, "Effects of Internal Curing Methods on Restrained Shrinkage and Permeability," PCA R&D Serial No. 2620, 134 pp.
- Lamond, J., and Pielert, J., 2006, *Significance of Tests and Properties of Concrete & Concrete-Making Materials*, STP-169D, ASTM International, West Conshohocken, PA.
- LeChatelier, H., 1904, *Recherches Expérimentales sur la Constitution des Mortiers Hydrauliques*, Dunod, Paris, 196 pp.
- L'Hermite, R. G., 1959, "What Do We Know About the Plastic Deformation and Creep of Concrete?" *RILEM Bulletin*, No. 1, Paris, France, pp. 21-51.
- L'Hermite, R. G., 1960, "Volume Changes of Concrete," *4th International Symposium on the Chemistry of Cement*, Washington D.C., 43 pp.
- Li, Q.; Yuan, L.; and Ansari, F., 2002, "Model for Measurement of Thermal Dilation Coefficient of Concrete by Fiber Optic Sensor," *International Journal of Solids and Structures*, V. 39, pp. 2927-2937.
- Lura, P., 2003, "Autogenous Deformation and Internal Curing of Concrete," PhD thesis, Delft University, Delft, The Netherlands, 180 pp.
- Lura, P., and Jensen, O. M., 2005, "Volumetric Measurement in Water Bath—An Inappropriate Method to Measure Autogenous Strain of Cement Paste," *PCA R&D Serial No. 2925*, Portland Cement Association, Skokie, IL, 25 pp.
- Lura, P.; Mazzotta, G.; Rajabipour, F.; and Weiss, W. J., 2005, "Evaporation, Settlement, Temperature Evolution, and Development of Plastic Shrinkage Cracks in Mortars with Shrinkage-Reducing Admixtures," *Concrete Durability and Service Life Planning (Concrete Life '06)*, K. Kovler, ed., Dead Sea, Israel, pp. 203-213.
- Lura, P.; Pease, B.; Mazzotta, G.; Rajabipour, F.; and Weiss, J., 2007, "Influence of Shrinkage-Reducing Admixtures on the Development of Plastic Shrinkage Cracks," *ACI Materials Journal*, V. 104, No. 2, Mar.-Apr., pp. 187-194.
- Mack, E. C., 2006, "Using Internal Curing to Prevent Concrete Bridge Deck Cracking," Master's thesis, Cleveland State University, Cleveland, OH, 105 pp.
- Malhotra, V. M., 1970, "Concrete Rings for Determining Tensile Strength of Concrete," *ACI JOURNAL, Proceedings* V. 67, No. 4, pp. 354-357.
- Mangold, M., 1994, "The Development of Restraint and Intrinsic Stresses in Concrete Members during Hydration," PhD thesis, Technical University of Munich.
- Mangold, M., 1998, "Methods for Experimental Determination of Thermal Stresses and Crack Sensitivity in the Laboratory," *Prevention of Thermal Cracking in Concrete at Early Ages*, RILEM Report 15, R. Springenschmid, ed., E&FN Spon, London, pp. 26-39.
- Meyers, S. L., 1950, "Thermal Expansion Characteristics of Hardened Cement Paste and of Concrete," *Proceedings of the Highway Research Board*, V. 30, 193 pp.
- Mindess, S., and Young, J. F., 1981, *Concrete*, Prentice-Hall, Englewood Cliffs, NJ, 671 pp.
- Mizobuchi, T.; Yokozeki, K.; and Nobuta, Y., 2000, "Experimental Estimation of Thermal Cracking using the Modified Temperature-Stress Testing Machine," *Control of Cracking in Early-Age Concrete*, pp. 153-162.
- Moon, J.-H., 2006, "Shrinkage, Residual Stress, and Cracking in Heterogeneous Materials," PhD thesis, Purdue University, West Lafayette, IN, 244 pp.
- Moon, J.-H., and Weiss, W. J., 2006, "Estimating Residual Stress in the Restrained Ring Test under Circumferential Drying," *Journal of Cement and Concrete Composite*, V. 28, pp. 486-496.
- Moon, J.-H.; Rajabipour, F.; and Weiss, W. J., 2004, "Incorporating Moisture Diffusion in the Analysis of the Restrained Ring Test," CONSEC (Concrete Under Severe Conditions—Environment and Loading), Seoul, Korea, pp. 1973-1980.
- Moon, J.-H.; Rajabipour, F.; Pease, B. J.; and Weiss, W. J., 2005, "Autogenous Shrinkage, Residual Stress, and Cracking in Cementitious Composites: The Influence of Internal and External Restraint," *Proceedings of the Fourth International Seminar on Self-desiccation and Its Importance in Concrete Technology*, B. Persson, D. Bentz, and L.-O. Nilsson, eds. Lund University, Lund, pp. 1-20.
- Moon, J.-H.; Rajabipour, F.; Pease, B. J.; and Weiss, W. J., 2006, "Quantifying the Influence of Specimen Geometry on the Results of the Restrained Ring Test," *Journal of ASTM International*, V. 3, No. 8, p. 14.
- Mukhopadhyay, A.; Siddharth, N.; and Zollinger, D., 2004, "New Mineralogical Approach to Predict Aggregate and Concrete Coefficient of Thermal Expansion (CoTE)," Preprint CD-ROM of the 83rd Annual Meeting of the Transportation Research Board, Washington, DC, 22 pp.
- Neville, A. M., 1981, *Properties of Concrete*, third edition, Pitman Publishing Ltd. London, 779 pp.

- Neville, A. M., 1996, *Properties of Concrete*, fourth edition, John Wiley & Sons, Inc., New York, 844 pp.
- Nielsen, C. V., and Berrig, A., 2005, "Temperature Calculations during Hardening," *Concrete International*, V. 27, No. 2, Feb., pp. 73-76.
- Nmai, C.; Tomita, R.; Hondo, F.; and Buffenbarger, J., 1998, "Shrinkage Reducing Admixtures," *Concrete International*, V. 20, No. 4, Apr., pp. 31-37.
- Pailiere, A. M.; Buil, M.; and Serrano, J. J., 1989, "Effect of Fiber Addition on the Autogenous Shrinkage of Silica Fume Concrete," *ACI Materials Journal*, V. 86, No. 2, Mar.-Apr., pp. 139-144.
- Paulini, P., 1992, "A Weighing Method for Cement Hydration," *9th International Congress on the Chemistry of Cement*, New Delhi, India, pp. 248-254.
- Pease, B. J., 2005, "The Role of Shrinkage Reducing Admixtures on Shrinkage, Stress Development, and Cracking," Master's thesis, Purdue University, West Lafayette, IN, 217 pp.
- Pease, B. J.; Shah, H. R.; and Weiss, W. J., 2005, "Shrinkage Behavior and Residual Stress Development in Mortar Containing Shrinkage Reducing Admixture (SRAs)," *Shrinkage and Creep of Concrete*, SP-227, N. J. Gardner and J. Weiss, eds., American Concrete Institute, Farmington Hills, MI, pp. 285-302.
- Philleo, R. E., 1991, "Concrete Science and Reality," *Materials Science of Concrete II*, J. Skalny and S. Mindess, ed., American Ceramic Society, Westerville, OH, pp. 1-8.
- Pickett, C., 1942, "The Effect of Change in Moisture Content on the Creep of Concrete under a Sustained Load," *ACI JOURNAL, Proceedings* V. 38, Feb., pp. 333-356.
- Polivka, M., and Wilson, C., 1973, "Properties of Shrinkage-Compensating Concrete Slabs," *Klein Symposium on Expansive Cement Concretes*, SP-38, American Concrete Institute, Farmington Hills, MI, pp. 227-238.
- Powers, T. C., and Brownyard, T. L., 1947, "Studies of the Physical Properties of Hardened Portland Cement Paste," *ACI JOURNAL, Proceedings* V. 43, pp. 101, 249, 469, 549, 669, 845, 993.
- Radlinska, A., and Weiss, J., 2006a, "Quantifying Variability in Assessing the Risk of Early-Age Cracking in Restrained Concrete Elements," *Eighth International Symposium on Brittle Matrix Composites*, Warsaw, Poland. pp. 331-342.
- Radlinska, A., and Weiss, J., 2006b, "Determining Early-Age Cracking Potential in Restrained Concrete Elements Using a Load and Resistance Factor Design (LRFD) Approach," *Conference Proceedings: Advances in Concrete through Science and Engineering*, Quebec City, QC, Canada, 13 pp.
- Radlinska, A.; Moon, J.-H.; Rajabipour, F.; and Weiss, W. J., 2006, "The Ring Test: History and Developments," *Volume Changes in Hardening Concrete: Testing and Mitigation*, O. Jensen, P. Lura, and K. Kovler, eds., Lyngby, Denmark, pp. 205-214.
- Radlinska, A.; Pease, B.; and Weiss, J., 2007, "A Preliminary Numerical Investigation on the Influence of Material Variability in the Early-Age Cracking Behavior of Restrained Concrete," *RILEM Materials and Structures*, V. 40, No. 4, pp. 375-386.
- Rajabipour, F.; Sant, G.; and Weiss, J., 2008, "Interactions between Shrinkage Reducing Admixtures and Cement Pastes Pore Solution," *Cement and Concrete Research*, V. 38, pp. 606-615.
- RILEM Committee 42-CEA, 1981, "Properties of Set Concrete at Early Ages: State of the Art Report," *Materials and Structures, Research and Testing*, V. 14, No. 84, pp. 399-450.
- RILEM Technical Committee 119, 1998, "Testing of the Cracking Tendency of Concrete at Early-Ages in the Cracking Frame Test," *Prevention of Thermal Cracking in Concrete at Early Ages*, RILEM Report 15, R. Springenschmid, ed., E&FN Spon, London, pp. 339-346.
- Roberts, J. W., 2004, "The 2004 Practice and Potential of Internal Curing of Concrete Using Lightweight Sand," *Advances in Concrete Through Science and Engineering*, Northwestern University, Evanston, IL, Mar. 22-24.
- Roberts, J. W., 2005, "Internal Curing in Pavements, Bridge Decks, and Parking Structures using Absorptive Aggregates to Provide Water to Hydrate Cement not Hydrated by Mixing Water," *TRB Committee A2E05, Concrete Materials and Placement Techniques, 83rd Annual Meeting*, TRB, Washington, DC., Jan. 11-15.
- Rongbing, B., and Jian, S., 2005, "Synthesis and Evaluation of Shrinkage-Reducing Admixture for Cementitious Materials," *Cement and Concrete Research*, V. 35, No. 3, pp. 445-448.
- Russell, H., and Larson, S.C., 1989, "Thirteen Years of Deformation in Water Tower Place," *ACI Structural Journal*, V. 86, No. 2, Mar.-Apr., pp. 182-191.
- Sant, G.; Rajabipour, F.; Lura, P.; and Weiss, J., 2006a, "Examining Time-Zero and Early Age Expansion in Pastes Containing Shrinkage Reducing Admixtures (SRAs)," *2nd RILEM Symposium on Advances in Concrete through Science and Engineering*, Quebec City, QC, Canada, 11 pp.
- Sant, G.; Rajabipour, F.; Fishman, P.; Lura, P.; and Weiss, J., 2006b, "Electrical Conductivity Measurements in Cement Paste at Early Ages," *International Conference on Advances in Testing of Fresh Cement-Based Materials*, Stuttgart, Germany, pp. 213-222.
- Sant, G.; Rajabipour, F.; Lura, P.; and Weiss, J., 2007a, "Volume Changes in Pastes Containing Shrinkage Reducing Admixtures under Autogenous and Drying Conditions," *12th International Congress on the Chemistry of Cement*, Montréal, QC, Canada, 12 pp.
- Sant, G.; Rajabipour, F.; Lura, P.; and Weiss, J., 2007b, "Examining Residual Stress Development in Cementitious Materials Experiencing an Early-Age Expansion," *Terence C. Holland Symposium on Advances in Concrete Technology*, G. C. Hoff, ed., pp. 515-530.
- Sant, G.; Dehdrai, M.; Bentz, D.; Lura, P.; Ferraris, C.; Bullard, J.; and Weiss, J., 2009, "Detecting the Fluid-to-Solid Transition in Cement Pastes," *Concrete International*, V. 31, No. 6, June, pp. 53-58.
- Sato, T.; Goto, T.; and Sakai, K., 1983, "Mechanism for Reducing Drying Shrinkage of Hardened Cement by Organic Additives," *CAJ Review*, V. 193, pp. 52-55.

- Schießl, A.; Weiss, W. J.; Shane, J. D.; Berke, N. S.; Mason, T. O.; and Shah, S. P., 2000, "Assessing the Moisture Profile of Drying Concrete Using Impedance Spectroscopy," *Concrete Science and Engineering*, V. 2, pp. 106-116.
- Schindler, A. K., and McCullough, B. F., 2002, "The Importance of Concrete Temperature Control during Concrete Pavement Construction in Hot Weather Conditions," *Journal of the Transportation Research Board* (TRR), No. 1813, pp. 3-10.
- Schoppel, K., 1994, "The Effect of Thermal Deformations, Chemical Shrinkage and Swelling on Restraint Stresses in Concrete from the Beginning of Hydration," *Proceedings of the International Symposium, Thermal Cracking of Concrete at Early Ages*, Munich, pp. 10-12.
- See, H. T.; Attiogbe, E. K.; and Miltenberger, M. A., 2003, "Shrinkage Cracking Characteristics of Concrete Using Ring Specimens," *ACI Materials Journal*, V. 100, No. 3, May-June, pp. 239-245.
- See, H. T.; Attiogbe, E. K.; and Miltenberger, M. A., 2004, "Potential for Restrained Shrinkage Cracking of Concrete and Mortar," *Cement, Concrete, and Aggregates*, V. 26, No. 2, pp. 123-130.
- Setter, N., and Roy, D. M., 1978, "Mechanical Features of Chemical Shrinkage of Cement Paste," *Cement and Concrete Research*, V. 8, No. 5, pp. 623-634.
- Shah, H. R., and Weiss, W. J., 2006, "Quantifying Shrinkage Cracking in Fiber Reinforced Concrete Using the Ring Test," *RILEM Materials and Structures*, V. 39, No. 9, pp. 887-899.
- Shah, S. P.; Karaguler, M. E.; and Sarigaphuti, M., 1992, "Effects of Shrinkage Reducing Admixture on Restrained Shrinkage Cracking of Concrete," *ACI Materials Journal*, V. 89, No. 3, May-June, pp. 289-295.
- Shah, S. P., and Weiss, W. J., 2000, "High Strength Concrete: Strength, Permeability, and Cracking," *Proceedings of the PCI/FHWA International Symposium on High Performance Concrete*, Orlando, FL, pp. 331-340.
- Shah, S. P.; Weiss, W. J.; and Yang, W., 1998, "Shrinkage Cracking—Can It Be Prevented?" *Concrete International*, V. 20, No. 4, Apr., pp. 51-55.
- Springenschmid, R., and Adam, G., 1980, "Mechanical Properties of Set Concrete at Early Ages: Test Methods," *Materials and Structures*, V. 13, No. 77, pp. 391-396.
- Springenschmid, R., and Breitenbücher, R., 1998, "Influence of Constituents, Mix Proportions and Temperature on Cracking Sensitivity of Concrete," *Prevention of Thermal Cracking in Concrete at Early Ages*, RILEM Report 15, R. Springenschmid, ed., E&FN Spon, London, pp. 40-50.
- Springenschmid, R., and Plannerer, M., 2001, "Experimental Research on the Test Methods for Surface Cracking of Concrete," Institute for Building Materials, Technical University Munich, Germany.
- Springenschmid, R.; Breitenbücher, R.; and Kussman, W., 1987, "Cracking Tendency of Concretes with Blast Furnace Slag Cements due to Outflow Heat of Hydration," *Concrete Precasting Plant Technology*, V. 53, No. 12, pp. 817-821.
- Springenschmid, R.; Breitenbücher, R.; and Mangold, M., 1994, "Development of the Cracking Frame and the Temperature-Stress Testing Machine," *Thermal Cracking in Concrete at Early Ages*, RILEM Proceedings 25, R. Springenschmid, ed., E&FN Spon, London, pp. 137-144.
- Springenschmid, R.; Gierlinger, E.; and Kernozycki, W., 1985, "Thermal Stress in Mass Concrete: A New Testing Method and the Influence of Different Cements," *Proceedings of the 15th International Congress for Large Dams*, Lausanne, pp. 57-72.
- Swamy, R. N., and Stavardes, H., 1979, "Influence of Fiber Reinforcement on Restrained Shrinkage Cracking," *ACI JOURNAL, Proceedings* V. 76, No. 3, May-June, pp. 443-460.
- Tazawa, E., 1999, *Autogenous Shrinkage of Concrete*, E&FN Spon, London, 406 pp.
- Tazawa, E., and Miyazawa, S., 1995, "Influence of Cement and Admixture on Autogenous Shrinkage of Cement Paste," *Cement and Concrete Research*, V. 25, No. 2, pp. 281-287.
- Tazawa, E.; Miyazawa, S.; and Kasai, T., 1995, "Chemical Shrinkage and Autogenous Shrinkage of Hydrating Cement Paste," *Cement and Concrete Research*, V. 25, No. 2, pp. 288-292.
- Texas Department of Transportation, 2001, "Test Procedure for Determining the Coefficient of Thermal Expansion of Concrete," Texas DOT, Construction Division, Austin, TX, Jan., 6 pp.
- Thomas, M. D. A., and Mukherjee, P. K., 1994, "The Effect of Slag on Thermal Cracking in Concrete," *Thermal Cracking in Concrete at Early Ages*, RILEM Proceedings 25, R. Springenschmid, ed., E&FN Spon, London, pp. 197-204.
- Timoshenko, S. P., and Goodier, J. N., 1987, *Theory of Elasticity*, McGraw-Hill Inc., New York, 567 pp.
- Toma, G.; Pigeon, M.; Marchand, J.; Bissonnette, B.; and Barcelo, L., 1999, "Early Age Restrained Shrinkage: Stress Build Up and Relaxation," *International Research Seminar: Self-Desiccation and Its Importance in Concrete Technology*, Lund, Sweden, pp. 61-71.
- Tomita, R.; Simoyama, Y.; and Inoue, K., 1986, "Properties of Hardened Concrete Impregnated with Cement Shrinkage Reducing Agent," *CAJ Review*, pp. 314-317.
- U.S. Army Corps of Engineers, 1981, "Test Method for Coefficient of Linear Thermal Expansion of Concrete," CRD C 39-81, 2 pp.
- Van Breugel, K.; Lura, P.; and Lokhorst, S. J., 2002, "Predicting Cracks in Hardening Concrete Using a Stress-Based Cracking Criterion," *Control of Cracking in Early Age Concrete*, pp. 317-324.
- Vaysburd, A. M., 1996, "Durability of Lightweight Concrete Bridges in Severe Environments," *Concrete International*, V. 18, No. 7, July, pp. 33-38.
- Verbeck, G. J., and Helmuth, R. H., 1968, "Structure and Physical Properties of Cement Paste," *Proceedings of 5th International Symposium on Chemistry of Cement*, Tokyo, Part III, pp. 1-32.
- Vosteen, H. D., and Schellschmidt, R., 2003, "Influence of Temperature on Thermal Conductivity, Thermal Capacity, and Thermal Diffusivity for Different Types of Rocks," *Physics and Chemistry of the Earth*, V. 28, pp. 499-509.

- Waller, V.; de Larrard, F.; and Roussel, P., 1996, "Modelling the Temperature Rise in Massive HPC Structures," *4th International Symposium on Utilization of High-Strength/High-Performance Concrete*, RILEM S.A.R.L., Paris, pp. 415-421.
- Weber, S., and Reinhardt, H. W., 1995, "A Blend of Aggregates to Support Curing of Concrete," *Proceedings of the International Symposium on Structural Lightweight Aggregate Concrete*, I. Holand, T. A. Hammer, and F. Fluge, eds., Sandefjord, Norway, pp. 662-671.
- Weber, S., and Reinhardt, H. W., 1999, "Manipulating the Water Content and Microstructure of High Performance Concrete Using Autogenous Curing," *Modern Concrete Materials: Binders, Additions, and Admixtures*, R. K. Dhir and T. D. Dyer, eds., Thomas Telford, pp. 567-577.
- Weiss, W. J., 1997, "Shrinkage Cracking in Restrained Concrete Slabs: Test Method, Material Compositions, Shrinkage Reducing Admixtures, and Theoretical Modeling," MS thesis, Northwestern University, Evanston, IL, 117 pp.
- Weiss, W. J., 1999, "Prediction of Early-Age Shrinkage Cracking in Concrete Elements," PhD dissertation, Northwestern University, Evanston, IL, 258 pp.
- Weiss, W. J., and Berke, N. S., 2002, "Admixtures for Reduction of Shrinkage and Cracking," *Early Age Cracking in Cementitious Systems—State of the Art Report*, A. Bentur, ed., RILEM, 15 pp.
- Weiss, W. J., and Ferguson, S., 2001, "Restrained Shrinkage Testing: The Impact of Specimen Geometry on Quality Control Testing for Material Performance Assessment," *Creep, Shrinkage and Durability Mechanics of Concrete and Other Quasi-Brittle Materials*, F. J. Ulm, Z. P. Bažant, and F. H. Wittmann, eds., Elsevier Science, pp. 645-650.
- Weiss, W. J., and Shah, S. P., 1997, "Recent Trends to Reduce Shrinkage Cracking In Concrete Pavements," *Aircraft/Pavement Technology: In the Midst of Change*, Seattle, WA, pp. 217-228.
- Weiss, W. J., and Shah, S. P., 2002, "Restrained Shrinkage Cracking: The Role of Shrinkage Reducing Admixtures and Specimen Geometry," *RILEM Materials and Structures*, V. 35, No. 246, pp. 386-395.
- Weiss, W. J.; Lura, P.; Rajabipour, F.; and Sant, G., 2007, "Performance of Shrinkage Reducing Admixtures at Different Humidities and at Early Ages," *ACI Materials Journal*, V. 105, No. 5, Sept.-Oct., pp. 478-486.
- Weiss, W. J.; Schießl, A.; Yang, W.; and Shah, S. P., 1998a, "Shrinkage Cracking Potential, Permeability, and Strength, for HPC: Influence of w/c, Silica Fume, Latex, and Shrinkage Reducing Admixtures," *International Symposium on High Performance and Reactive Powder Concrete*, Sherbrooke, Canada, pp. 349-364.
- Weiss, W. J.; Yang, W.; and Shah, S. P., 1998b, "Shrinkage Cracking of Restrained Concrete Slabs," *Journal of Engineering Mechanics*, ASCE, V. 124, pp. 765-774.
- Weiss, W. J.; Yang, W.; and Shah, S. P., 1999b, "Factors Influencing Durability and Early-Age Cracking in High Strength Concrete Structures," *High Performance Concrete: Research to Practice*, SP-189, American Concrete Institute, Farmington Hills, MI, pp. 387-409.
- Weiss, W. J.; Yang, W.; and Shah, S. P., 2000, "Influence of Specimen Size and Geometry on Shrinkage Cracking," *Journal of Engineering Mechanics*, ASCE, V. 126, No. 1, pp. 93-101.
- Westman, G., 1999, "Concrete Creep and Thermal Stresses," PhD thesis, Division of Structural Engineering, Lulea University of Technology, 301 pp.
- Willis, T. F., and DeReus, M. E., 1939, "Thermal Volume Change and Elasticity of Aggregates and Their Effect on Concrete," *Proceedings*, V. 39, ASTM International, West Conshohocken, PA, p. 919.
- Won, M., 2005, "Improvements of Testing Procedures for Concrete Coefficient of Thermal Expansion," Preprint CD-ROM of the 84th Annual Meeting of the Transportation Research Board, Washington, DC, 14 pp.
- Zoldner, N. G., 1971, "Thermal Properties of Concrete under Sustained Elevated Temperatures," *Temperature and Concrete*, SP-25, American Concrete Institute, Farmington Hills, MI, pp. 1-32.



American Concrete Institute®
Advancing concrete knowledge

As ACI begins its second century of advancing concrete knowledge, its original chartered purpose remains “to provide a comradeship in finding the best ways to do concrete work of all kinds and in spreading knowledge.” In keeping with this purpose, ACI supports the following activities:

- Technical committees that produce consensus reports, guides, specifications, and codes.
- Spring and fall conventions to facilitate the work of its committees.
- Educational seminars that disseminate reliable information on concrete.
- Certification programs for personnel employed within the concrete industry.
- Student programs such as scholarships, internships, and competitions.
- Sponsoring and co-sponsoring international conferences and symposia.
- Formal coordination with several international concrete related societies.
- Periodicals: the *ACI Structural Journal* and the *ACI Materials Journal*, and *Concrete International*.

Benefits of membership include a subscription to *Concrete International* and to an ACI Journal. ACI members receive discounts of up to 40% on all ACI products and services, including documents, seminars and convention registration fees.

As a member of ACI, you join thousands of practitioners and professionals worldwide who share a commitment to maintain the highest industry standards for concrete technology, construction, and practices. In addition, ACI chapters provide opportunities for interaction of professionals and practitioners at a local level.

American Concrete Institute

38800 Country Club Drive

Farmington Hills, MI 48331

U.S.A.

Phone: 248-848-3700

Fax: 248-848-3701

www.concrete.org

Report on Early-Age Cracking: Causes, Measurement, and Mitigation

The AMERICAN CONCRETE INSTITUTE

was founded in 1904 as a nonprofit membership organization dedicated to public service and representing the user interest in the field of concrete. ACI gathers and distributes information on the improvement of design, construction and maintenance of concrete products and structures. The work of ACI is conducted by individual ACI members and through volunteer committees composed of both members and non-members.

The committees, as well as ACI as a whole, operate under a consensus format, which assures all participants the right to have their views considered. Committee activities include the development of building codes and specifications; analysis of research and development results; presentation of construction and repair techniques; and education.

Individuals interested in the activities of ACI are encouraged to become a member. There are no educational or employment requirements. ACI's membership is composed of engineers, architects, scientists, contractors, educators, and representatives from a variety of companies and organizations.

Members are encouraged to participate in committee activities that relate to their specific areas of interest. For more information, contact ACI.

www.concrete.org



American Concrete Institute®
Advancing concrete knowledge